Universidade Federal de São Carlos

Center of Exact Sciences and Technology - Graduate Program in Physics

Optical and Transport properties of p-i-n GaAs/AlAs Resonant Tunneling Diode

Iram Taj Awan

Supervisor:
Prof. Dr. Yara Galvão Gobato

Co-supervisor:
Prof. Dr Maria Jose S. P. Brasil

Thesis submitted to the Postgraduate Program in Physics from Federal University of São Carlos, as a part of requirements for obtaining PhD title in Physics.

Sao Carlos, May 2014.

Ficha catalográfica elaborada pelo DePT da Biblioteca Comunitária/UFSCar

A964ot

Awan, Iram Taj.
Optical and transport properties of p-i-n GaAs/AlAs resonant tunneling diode / Iram Taj Awan. -- São Carlos : UFSCar, 2014.
85 f.

Tese (Doutorado) -- Universidade Federal de São Carlos, 2014.

1. Física da matéria condensada. 2. Semicondutores. 3. Propriedades óticas. 4. Diodos de tunelamento ressonante. I. Título.

CDD: 530.41 (20ª)

Iram Taj Awan

Tese de doutorado submetida à Coordenação do Programa de Pós-Graduação em Física, da Universidade Federal de São Carlos, como requisito parcial para a obtenção do título de doutor em ciências.

Aprovado em: 26 de maio de 2014

BANCA EXAMINADORA

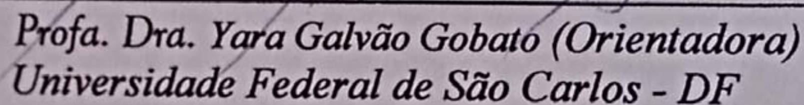

Profa. Dra. Yara Galvão Gobato (Orientadora)
Universidade Federal de São Carlos - DF

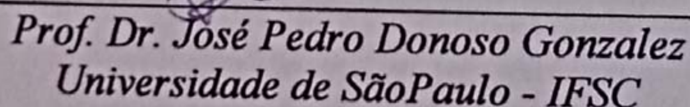

Prof. Dr. José Pedro Donoso Gonzalez
Universidade de SãoPaulo - IFSC

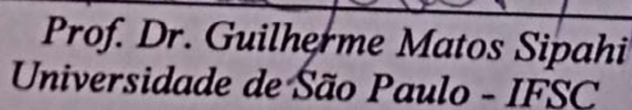

Prof. Dr. Guilherme Matos Sipahi
Universidade de São Paulo - IFSC

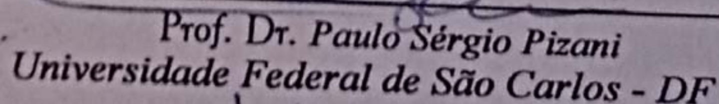

Prof. Dr. Paulo Sérgio Pizani
Universidade Federal de São Carlos - DF

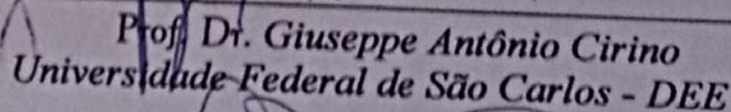

Prof. Dr. Giuseppe Antônio Cirino
Universidade Federal de São Carlos - DEE

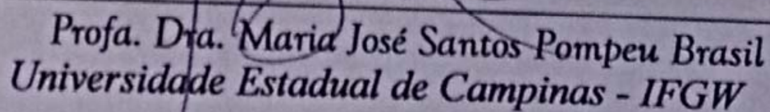

Profa. Dra. Maria José Santos Pompeu Brasil
Universidade Estadual de Campinas - IFGW

I Dedicate this work to my
beloved husband, Sarosh and
my parents.

Similarity between me and my sample is, we both are under discovery.

Iram

Do not go where the path may lead, go instead where there is no path and leave a trail.

Ralph Waldo Emerson

Acknowledgements

I am very grateful to have had the opportunity to undertake PhD research that has been enjoyable, challenging and worthwhile.

First and foremost I would like to express my sincere gratitude to my advisor Prof. Dr. Yara Galvao Gobato, who accepted me as a PhD student for her insightful guidance to my research and comprehensive support and encouragement on my thesis work. Without her help, my completion of doctoral degree is unreachable. Also I deeply appreciate my co-supervisor, Dr. Maria Jose S. P. Brasil for her help on developing my research skills, her intellectual suggestions and helpful discussions on project are worthy regarded. I am also particularly very grateful to Dr. Helder V. A. Galeti for his great support and fruitful contributions to this project.

Part of the experiments are performed at GPO (Group of Optical Properties) Lab at IFGW - UNICAMP. I also wish to express thanks to my PhD funding agency TWAS-CNPq and to the staff members and students of the GPO lab for their support and help. Special thanks to Miguel A.G. Balanta, Milton Tanabe (the lab technician) and Fernando Ikawa.

Thanks to Dr. Mohamed Henini, University of Nottingham (UK), for providing us high quality samples used in this study.

To the fellows of UFSCar Anibal, Jaldair, Leonilson, Dr. Lara, Dr. Marcio Peron, Dr. Márcio Daldin, Vanessa, Mariana, Anne for sharing of "academic pain" together by the many collaborations and friendships founded throughout this period.

Special thanks to my husband Sarosh Farjam for giving me moral support, care and encouragement all the time during my PhD. Same I address for my elder sister Dr. Almas T. Awan as well. Special thanks to Pouya (one of my dearest friends).

At last, I am deeply indebted to my parents Mr. Malik T. M. K. Awan and Mrs Zainab K. Awan along with other family members Kiran, Zeeshan, Masooma, Urooj. Their prayers, patience, support and unconditional love made me come up to this level.

Resumo

Neste trabalho, estudamos as propriedades óticas e de transporte de diodos de tunelamento ressonante de GaAs-AlAs do tipo p-i-n. Observamos duas emissões no poço quântico (QW) que foram associadas a recombinação e eletrons e buracos que tunelam no QW e que podem recombinar com os níveis confinados no QW ou com o nível de impureza aceitadora no QW. Foi observado que a intensidade relativa dessas bandas é bastante sensível a voltage aplicada. Em particular, a emissão ótica relativa a impureza mostrou ser mais eficiente na condição de voltagem que resulta em alta densidade de portadores no QW.

Estudamos também efeitos de spin nesses dispositivos na presença de altos campos magnéticos de até 15T. Observamos que polarização de spin de portadores é controlada por voltagem aplicada. Em particular, observamos que a polarização de spin apresenta fortes oscilações e variações abruptas dependendo da voltagem aplicada no dispositivo . Esse efeito foi associado a mudanças importantes de densidade de carga acumulada no QW em função da voltage aplicada. Foi também observado uma emissão fortemente dependente da voltagem na região dos contatos que foi associada a formação de uma gas bidimensional de eletrons (2DEG) com alto grau de polarização circular.

A polarização de spin no QW foi associada a presença de impurezas , efeitos de injeção de portadores spin polarizados no QW, variação de densidade de portadores no QW, processos de tunelamento de eletrons e buracos e etc.

Abstract

In this thesis, we have investigated the optical and transport properties of a p-i-n GaAs-AlAs resonant tunneling diode (RTD). The possibility of controlling and significantly varying the density of carriers accumulated at different layers of this structure simply by applying an external bias makes it very useful to investigate various fundamental issues. Furthermore, the process of tunneling that critically depends on the alignment from confined energy levels and the injection of carriers that attain quasi-equilibrium distribution at distinct accumulation layers makes this structure very special for analyzing optical properties in general, and in special, spin-polarization effects when an external magnetic field is applied to the RTD.

Particularly, two emission bands were observed for the quantum well (QW) of our structure and were associated to the recombination of electrons and holes that tunnel into the QW and may recombine either as an exciton involving the fundamental states of the QW or a transition involving an acceptor state in the QW. It was also observed that the relative intensity of these emission bands strongly depend on the applied bias voltage. The optical recombination involving acceptors states becomes relatively more efficient as compared to the excitonic recombination for higher densities of electrons in the QW. This effect was discussed considering how the electron carrier density depends on the applied voltage and other effects such the capture rate of holes by the acceptors and electron and hole differences concerning mobility, effective mass and tunneling processes.

We have also investigated spin properties of the tunneling carriers in our device by measuring the polarization-resolved electroluminescence from the quantum well (QW) and the contact layers under low temperatures and high magnetic fields, up to 15 T. Under these conditions, we have observed that the QW emission presents a large negative polarization degree which depends on the external applied bias voltage. The

QW spin polarization shows oscillations and abrupt changes at the electron resonant peak. The results are mainly attributed to the abrupt changes of intensity of the two QW emission lines. Furthermore, the contact-layer emission have also shown voltage dependent emission lines that were attributed to the two-dimensional electron gas formed at the accumulation layer under an applied bias. The contact-layer emission presents a large negative polarization degree which is also voltage dependent. The QW spin polarization degree was discussed considering different effects such as the presence of neutral acceptors in the QW, the voltage control of carrier densities in the device, hole and electron tunneling processes and the spin injection of spin polarized two-dimensional gases formed at the accumulation layers.

Table of Contents

Acknowledgements -- IV

Abstract --- V

List of Figures -- VIII

Introduction -- 1

Chapter 1- Theoretical Fundamentals -- 3

1.1 - Resonant Tunneling Diodes (RTDs) ----------------------- 3

1.2 - Simple Model for Carrier Transport in RTDs --------------- 6

1.3 – RTDs under Magnetic Fields -------------------------------- 12

1.3.1 - Atomic model --------------------------------- 12

1.3.2 - Landau Levels --------------------------------- 15

Chapter 2 - Materials and Experimental Techniques ------------------------------- 22

2.1 - Resonant Tunneling Diode Structure ----------------------- 22

2.2- Transport Measurements -- 24

2.3 Optical Measurements - Luminescence ----------------------- 26

2.3.1 p-i-n RTD -- 27

2.3.2 - Selection Rules for Optical Transitions in Semiconductors --- 31

2.4 - Experimental Techniques -- 33

2.4.1 Polarization-resolved Magneto Luminescence --------------- 33

2.4.2 Time-Resolved Photoluminescence (PLRT) --------------- 34

Chapter 3 - Transport and Optical Studies under zero magnetic field ---- 39

Chapter 4 - Time Resolved Photoluminescence in p-i-n RTD ---------------------- 51

Chapter 5 - Magneto-Transport and Magneto-Electroluminescence Studies in p-i-n resonant tunneling diodes -- 66

Conclusion -- 82

References --

Chapter 1 -- 20

Chapter 2 -- 38

Chapter 3 -- 50

Chapter 4 -- 65

Chapter 5 -- 81

List of Figures

Page

1 .	Figure	1-1	Band structure of bulk GaAs near the center of the Brillion Zone.	4
2 .	Figure	1-2	Schematic representation of a Resonant Tunneling diode (a) and its potential profile (b) showing the bottom of the conduction band and the top of the valence band along the growth direction.	5
3 .	Figure	1-3	Simplified schematic profile of the conduction band for five different applied voltages between collector and emitter (a) at V = 0 (b) V = V1 (c) V1 < V < V2 (d) V = V2. Adapted by (Mizuta, et al., 1995).	7
4 .	Figure	1-4	Characteristic ideal I (V) curve for RTD illustrating a triangular profile.	8
5 .	Figure	1-5	Fermi sphere in emitter region with intersection plane shown at three different voltage conditions, applied to RTD: (a) V = V1 (b) V1 < V < V2 and (c) V = V2.	9
6 .	Figure	1-6	Detail of the conduction band with 2D triangular potential well formed due to the presence of accumulation layer, case with thermalization of carriers in the states of triangular QW (2D-2D tunneling).	10
7 .	Figure	1-7	(a) Fermi sphere "sliced" due to the quantization in z direction with the intersection for a given voltage. (b) I(V) Curve showing three consecutive resonances.	11
8 .	Figure	1-8	In the presence of spin-orbit coupling, L and S are no longer separately preserved, they presses around the total angular momentum J.	14
9 .	Figure	1-9	Representation of the Fermi sphere in reciprocal space k: (a) 3D Fermi sphere without magnetic field, (b) with 2D space quantization along the z direction without magnetic field, (c) 2D system with magnetic field, the disks are broken down into concentric circles.	16
10 .	Figure	1-10	Effect of magnetic field in a 2D system. (a) Energy levels and density of states of a triangular well without magnetic field, (b) Energy levels and density of states with magnetic field (in red).	17
11 .	Figure	1-11	Density of states of Landau levels with and without disorder. The disorder leads to enlargement of landau energy levels through the localization of the wave functions of carriers (localized states).	18
12 .	Figure	2-1	Potential profile of a symmetric p-i-n GaAs- AlAs RTD without considering the built-in electric field due to the doped layers.	24

13 .	Figure	2-2	Schematic diagram of a DC circuit connected to p-i-n type RTD with symmetric barriers in a 4-wire mounting, showing the ammeter, the voltage source and the layers of diode.	25
14 .	Figure	2-3	Schematic potential profile of sample NU491, illustrating the transport and recombination of carriers in the structure as a function of bias (a) below flat band, (b) at flat band condition, (c) above flat band.	27
15 .	Figure	2-4	Diagram of potential profile of sample NU491, illustrating the photogeneration, transport and recombination of carriers in the structure as a function of bias (a) sample is biased below flat band, (b) biased at flat band, (c) biased above flat band.	30
16 .	Figure	2-5	(a) Band diagram of a GaAs QW at the center of the Brilloiun zone (b) Selection rules for optical transitions between the sublevels for a circularly polarized light in a GaAs QW, the numbers in purple indicate the relative transition intensities of both recombinations s+ and s- (Zutic, et al., 2004)	32
17 .	Figure	2-6	Schematic illustration of the mounting of main components used in CW magneto-luminescence experiments.	34
18 .	Figure	2-7	Schematic illustration of the set up of main components used in PLRT experiments.	35
19 .	Figure	2-8	(a) PL image taken at P = 15mW and T = 5K, (b) Integrated PL intensity in time versus wavelength (c) Integrated PL intensity in wavelength versus time.	36
20 .	Figure	3-1	(a) I(V) characteristics curve at 5K (b) for differential conductance dI/dV and (c) d2I/dV2 .	39
21 .	Figure	3-2	Schematic band diagram of the device for (a) voltages lower than flat band condition (b) at flat band condition and (c) for voltages higher that flat band condition.	40
22 .	Figure	3-3	Electroluminescence spectra of QW at 4K for different applied voltages.	41
23 .	Figure	3-4	(a) Color-coded map of EL intensity as a function of applied voltage and (b) Voltage dependence of the total QW EL integrated intensity.	43
24 .	Figure	3-5	I(V) characteristics curves under light excitation at T=2K.	44
25 .	Figure	3-6	Schematic band diagram of the device under light excitation for (a) voltages lower than flat band condition (b) at flat band condition and (c) for voltages higher than the flat band condition.	44
26 .	Figure	3-7	(a) Color-coded map of PL intensity as function of applied voltage for laser intensity of 60 mW at 2K.	45

27 .	Figure	3-8	(a) Color-coded map of PL intensity as function of applied voltage in the region of flat band condition for laser intensity of 60 mW.	46
28 .	Figure	3-9	Typical EL emission for the contact layers for different applied.	48
29 .	Figure	3-10	Color coded map of EL intensity as function of applied bias for the contact layers.	49
30 .	Figure	4-1	I(V) characteristics curve in dark and under different pulsed laser excitation powers at 5K. The flat-band condition and tunneling resonances are indicated on the graph. The photocurrent curve can be estimated by subtracting the current with and without laser excitation. Reversed bias data range is showed under a yellow background graph.	52
31 .	Figure	4-2	Integrated intensity of QW emission (a) in dark and under a 15 mW pulsed laser excitation at 5K for whole bias range. (b) Detail of emission intensity for reversed bias under pulsed laser excitation. The flat-band condition and tunneling resonances are indicated on the graph.	54
32 .	Figure	4-3	(a) PLRT Images at T = 5K and P = 15mW for different voltages below the VFB. (b) PL spectra obtained by integration of entire PLRT image and (c) PL spectra integrated obtained by integration of different time window at long and short times.	56
33 .	Figure	4-4	PL transient obtained by integrating the PL signal for a wavelength interval around each emission, correspond to the integrated intensity of the (a) lower energy (e1) and (b) higher energy (e2) of QW emission bands. A fitting of the PL transient was made to estimate the decay time values of each emission.	57
34 .	Figure	4-5	PL characteristic time obtained by fitting the PL transient of each correspondent emission, lower energy (e1) and higher energy (e2) of QW PL bands.	58
35 .	Figure	4-6	TR Images at T = 5K and P = 15mW for different voltages at V>VFB (a) in dark, where only to EL is present, and (b) with pulsed laser excitation. (c) PL spectra obtained by integration of entire TRPL image.	60
36 .	Figure	4-7	(a) TR Images obtained from subtraction of TR (EL) and TR (EL+PL) at T = 5K and P = 15mW, for different voltages at V>VFB. The color scale indicate the intensity of signal after the subtraction procedure, where the blue color indicate positive values and red color indicates negative values.(b) Transients obtained by integration of entire TRPL image.	60

37 .	Figure	4-8	(a) TR Images at T = 5K and P = 15mW for different voltages at V>VFB without (EL) and with (EL+PL) pulsed laser excitation. (b) PL transient obtained from the subtraction procedure explained in the text, by the wavelength integration for each QW emission (e1 and e2) and the correspondent exponential fitting of the transient decay.	61
38 .	Figure	4-9	(a) PLTR Images at T = 5K and P = 15mW for different voltages at V>VFB obtained from images under pulsed laser excitation subtracted from images without excitation (dark), here denominated Pure PL, where the blue color scale indicate positive, and red color, negative values of intensity. (b) Some critical bias transients close to e1 resonance that present a decrease of the total luminescence (pure PL negative), here showed in green when is add a constant (y0) in order to obtain the decay time.	62
39 .	Figure	4-10	PL decay time obtained by fitting the pure PL transient of each correspondent emission, lower energy (e1) and higher energy (e2) of QW PL bands, when the RTD is forward biased.	63
40 .	Figure	4-11	PL transients obtained from two characteristic biases where an abrupt variation of EL intensity is observed.	64
41 .	Figure	5-1	I(V) characteristic curves for different magnetic fields at temperature T = 2K. Each IV curve is shifted 0.2mA upward.	67
42 .	Figure	5-2	Polarization resolved EL spectra and taken at different voltages for both QW and contact regions at 15T 2K.	68
43 .	Figure	5-3	Color coded maps of polarization resolved EL emission due to recombination in the GaAs contact region as a function of applied bias for different values of magnetic field 8T(a, b) and 15T(d, e) at T=2K. Polarization resolved EL intensity as a function of bias (c, f).	70
44 .	Figure	5-4	(a) (b) are same results of figure 5-3 (d, e) in another color-coded scale and (c) Polarization resolved EL intensity as a function of bias.	71
45 .	Figure	5-5	Bias dependence of EL peak positions of contact emissions showing complex voltage dependent EL emission at contact layers under 15T at 2K.	73
46 .	Figure	5-6	I(V) characteristics curve and color coded maps of polarization resolved EL emission due to recombination in QW region as a function of applied bias for different values of magnetic field 8T (a, b) and 15T (d, e) at T=2K. Polarization resolved EL intensity as a function of bias (c, f).	74

47 .	Figure	5-7	Voltage dependence of the degree of circular polarization of EL for (a) the total QW emission and for the 2DEG-h emission under 8T 2K (b) Voltage dependence of polarization degree for the 2DEG-h emission, for the total QW emission and for recombination lines E1-A0 (red symbols) and E1-HH1 (green symbols) under 15T and 2K.	75
48 .	Figure	5-8	Bias voltage dependence of (a) QW peak positions (b) QW spin splitting energy (c) 2DEG-h peak positions (d) 2DEG-h spin splitting energy under 15T and 2K.	76
49 .	Figure	5-9	EL polarization resolved emission spectra from QW region at different voltages(a), (b), (c) under B = 8T and T = 2K.	78
50 .	Figure	5-10	EL polarization resolved emission spectra from QW region at different voltages (a), (b), (c), (d) under B = 15T and T = 2K.	79

Introduction

The control of the spin degree of freedom in addition to the charge of carriers is a major aspiration for semiconductor device development for spintronics. Long spin lifetimes and the possibility to transport spins coherently over large distances in semiconductors have motivated several studies for a new generation of microelectronic devices based on the spin degree of freedom. Several systems have been proposed for spin-based devices, including magnetic metal/semiconductor junctions, all metallic devices and all semiconductor systems (Ziese, et al.; Motsnyi, et al., 2003). Particularly, it was shown that the spin-polarization of carriers in Resonant tunneling Diodes (RTDs) can be voltage-selected, which makes this device very attractive for spintronic applications. The successful operation of semi-magnetic RTDs as a voltage-controlled electron-spin-polarized filter was first reported for structures based in II-VI semiconductor alloys with a magnetic ion (Slobodskyy, et al., 2003).

In the last years, our group has been investigating spin effects in III-V non-magnetic RTDs under high magnetic fields (Carvalho, et al., 2007; Dos Santos, et al., 2008; Galeti, et al., 2012). It has been shown that both the excitonic spin-splitting energy and the polarization of the QW emission from p-i-p non-magnetic RTDs under high magnetic fields present strong oscillations near resonant voltages (Carvalho, et al., 2006). It was also shown that the spin-splitting and circular polarization degree did not present a clear correlation, which implies that the spin polarization of carriers in the QW cannot be explained by a simple thermal occupation of the QW levels. Therefore, other effects such as spin-conservation along the resonant tunneling through spin-split levels and the spin-polarization of the carriers accumulated at the contact layers should also be considered in order to explain the spin-polarized emission from these devices.

In this thesis, we have investigated optical, transport and spin properties of a non-magnetic p-i-n type GaAs/AlAs RTD. We have measured the current-voltage characteristics curves I(V), electroluminescence (EL), photoluminescence (PL), time-resolved photoluminescence (PLRT) and magneto-electroluminescence of our structure as a function of the applied voltage in low temperatures and high magnetic fields.

Chapter I presents a brief review of the basic concepts involved in this work. Chapter II presents information about the design of the sample and about the experimental techniques that were used. Chapter III presents the experimental results from transport, electroluminescence and photoluminescence measurements. Chapter IV presents the experimental results of time-resolved photoluminescence. Chapter V presents the magneto-electroluminescence results under high magnetic fields, up to 15T.

Chapter 1 - Theoretical Fundamentals

In this chapter, we discuss some theoretical concepts used in our work. We present the structure of the double-barrier diode also known as the resonant tunneling diode (RTD). We discuss the fundamental physics involved on transport, optical properties and spin effects related to this structure when an external voltage is applied to the structure.

1.1 - Resonant Tunneling Diodes (RTDs):

The sample studied in this thesis is a RTD composed of GaAs and AlAs layers. Both GaAs and AlAs are III-V zinc-blend semiconductors with similar lattice parameters, so that the strain developed on GaAs/AlAs heterostructures is negligible.

Thick semiconductor layers are usually called bulk or 3D. Figure 1-1 shows a simple diagram for the energy dispersion in reciprocal space for bulk GaAs around the center of the Brillouin zone (k=0) known as the Γ point. GaAs is a direct material, i.e., the maximum of the valence band and the maximum of the valence band and the minimum of conduction band are both at the Γ point. The p-orbitals of the valence band are degenerate, giving rise to the so-called heavy-hole (hh) and light-holes (lh) bands (with $m_j = \pm 3/2$ and $m_j = \pm 1/2$, respectively) and to the doubly degenerate split-off band (SO). In the case of GaAs, the SO band is separated from the hh and lh bands by a relatively large energy ($\Delta_o \sim 340$meV) and can be disregarded on simple models. AlAs is an indirect band gap material, but it only enters in our structure as a thin barrier.

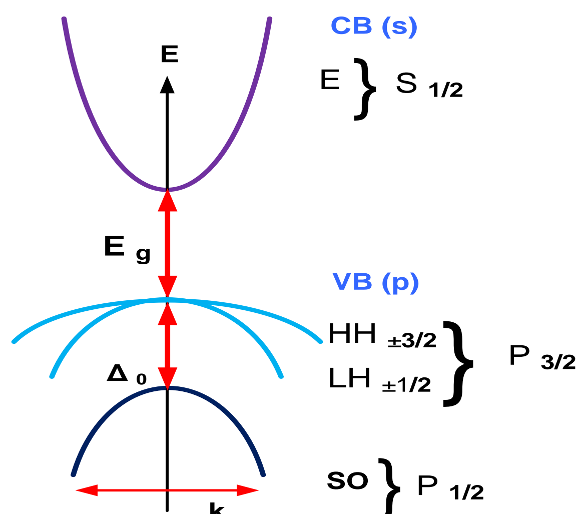

Figure 1-1 - Band structure of bulk GaAs near the center of the Brillion Zone. Figure modified from (Fabian, et al., 2007).

The growth of RTDs is done primarily through epitaxial growth techniques such as MBE (Molecular-Beam Epitaxy). This technique allows a controlled deposition, layer by layer, of a high-purity material. Thus, thicknesses of the components of the structure are precisely controlled. The active region of the RTD consists of a quantum well (QW) confined by two barriers connected to high-doped contact layers, known as emitter and collector. The barriers and the QW are composed of thin layers of suitable semiconductor materials with different band gap energies E_g (energy difference between the bottom of the conduction band and the top of the valence band). Figure 1-2 (a) illustrates a typical AlAs/GaAs/AlAs RTD processed as a small diode with metalized contacts. In our case, the upper contact has the form of a ring with an opened window in order to allow optical excitation and detection. Figure 1-2 (b) shows the profile of the bottom of the conduction band and top of the valence band along the growth direction of the RTD heterostructure.

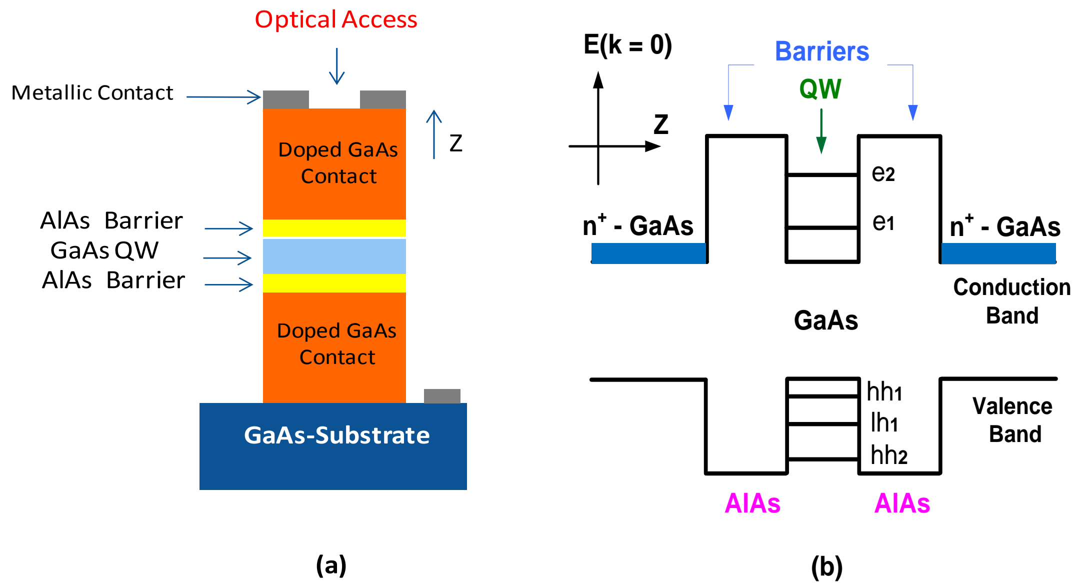

Figure 1-2 - Schematic representation of a n-i-n Resonant Tunneling diode (a) and its potential profile (b) showing the bottom of the conduction band and the top of the valence band along the growth direction (Mizuta, et al., 1995).

The emitter and collector materials are usually made of the same material as the QW, but they are heavily doped (n or p) in order to make it possible to create ohmic contacts to the structure. Figure 1-2 (b) shows as an example a RTD where both contacts are n-type doped. In this case, we say the RTD to be a n-i-n structure. In this work we investigated a p-i-n structure that will be discussed in detail later on. In order to minimize the effects of doping impurities on the transport properties of the RTD, usually an undoped spacer-layer can be inserted between the doped emitter/collector layers and the barriers (Tsuchiya, et al., 1986). When an external voltage is applied between the RTD contacts, carriers from the doped layers are accelerated along the structure, tunneling into the quantum well, where they might remain for some time before escaping by tunneling towards the collector region or recombining with other carriers.

In ideal structures with no roughness at the interfaces that might scatter the wave-function of the carriers coupling the transverse modes with the perpendicular one, we can separate the transverse variables (x, y) from the perpendicular solution (z) for

each of the components of the heterostructure. Thus, in a parabolic-band approximation the total energy of a carrier with isotropic effective mass m* can be expressed as:

$$E = E_z + \frac{\hbar^2(k_x^2 + k_y^2)}{2m^*} \qquad (1.1)$$

The spatial localization of the wave-functions of the carriers in the QW of the RTD structure give rise to quasi-stationary states with discrete energies. Therefore, the z-component of the energy corresponds to discrete states for the conduction band (e_1, e_2, ...) and the valence band (hh_1, lh_1, hh_2, ...), which, in the context of RTD, are usually called resonant states. Notice that the quantum confinement breaks the degeneracy of the valence band top, separating the sub-bands of light- and heavy-holes. The ground-state for holes corresponds to the hh_1 state as the effective mass of heavy-holes is larger than that of the light-holes.

1.2 - Simple Model for Carrier Transport in RTDs:

Transport in a RTD is governed by the phenomenon of resonant tunneling from emitter into the QW through the first barrier. For V=0, there is no current in the device (figure 1-3 (a)). The current starts to flow when the fundamental state of the QW (E_R) aligns with the Fermi level of the emitter (E_F^L) as shown in figure 1-3 (b). The current increases and attains its maximum when the level aligns with the conduction band edge (figure 1-3 (c) and (d)). As soon as E_R goes below the conduction band edge, the current is abruptly reduced as coherent tunneling becomes no longer possible for this configuration, remaining approximately zero for larger voltages (figure 1-3 (d)). This behavior gives rise to the typical triangular peak in the current vs voltage (I(V)) curve from a RTD structure (figure 1-4). The abrupt decrease of current is usually known as negative differential resistance (NDR). In a real RTD structure, the I(V) curve should present a series of triangular peaks associated to the various electron and hole QW confined levels that should reach a resonant condition with increasing applied voltages.

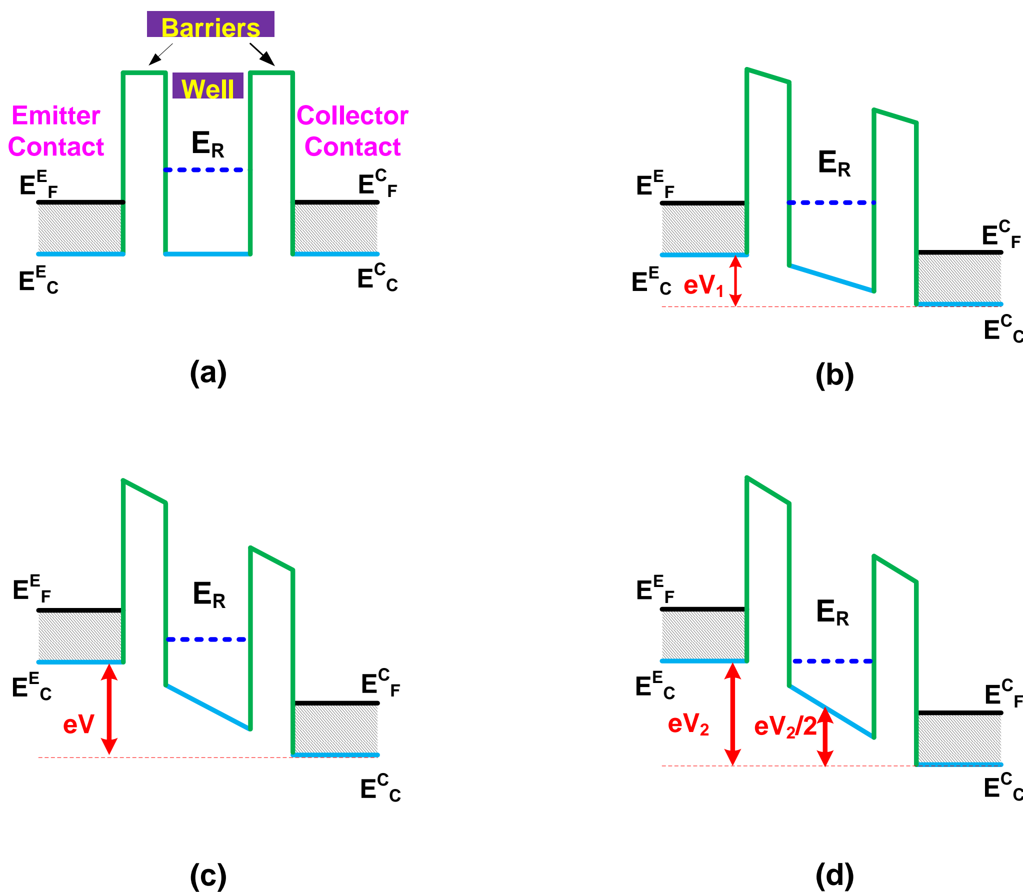

Figure 1-3 - Simplified schematic profile of the conduction band for five different applied voltages between collector and emitter (a) at V = 0 (b) V = V1 (c) V1 < V < V2 (d) V = V2. Adapted by (Mizuta, et al., 1995).

A detailed description of the transport through a RTD requires the calculation of the transmission probability T(E) for a given structure. However, we can infer some general points on the I(V) properties based on simple considerations. For T ~ 0 K, the carriers from the doped contacts occupy the states inside the Fermi sphere of radius k_F (figure 1-5). Let´s consider in this example the tunneling of electrons, even though this model can be applied for both, electrons and holes.

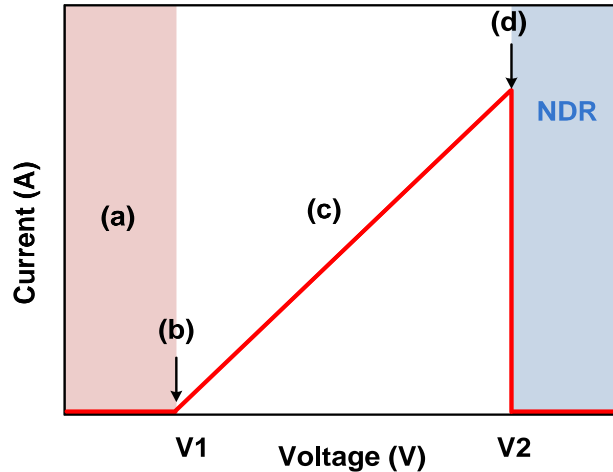

Figure 1-4 - Characteristic ideal I (V) curve for RTD illustrating a triangular profile

For ideal interfaces, the electrons must retain the lateral components of their momentum (k_x and k_y) and vertical energy component E_z. Thus, the electronic states participating in the tunneling process can be represented by the intersection of the plane $k_z = q_R$ with the Fermi sphere (figure 1-5), where q_R is the wave number associated with the resonant energy state (E_R) related to energy of the bottom of the conduction band (E_C^E):

$$q_R = \sqrt{\frac{2m^*(E_R - E_C^E)}{\hbar}} \qquad (1.2)$$

As we increase the applied voltage, we vary the value of E_R as shown in figure 1-3, thus varying the value of q_R. Figure 1-5 illustrates three different situations corresponding to voltages defined in figure 1-3.

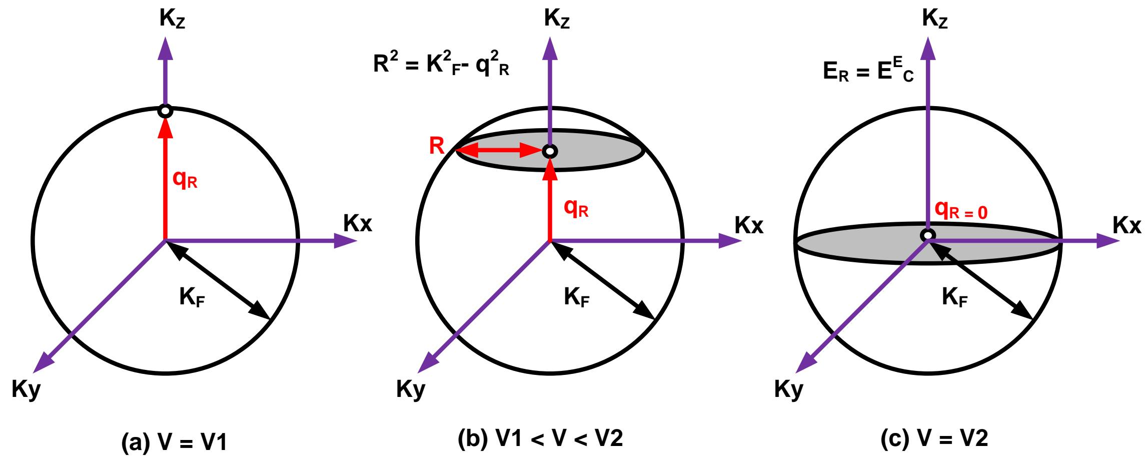

Figure 1-5 - Fermi sphere in emitter region with intersection plane $k_z = q_R$ shown at three different voltage conditions, applied to RTD: (a) V = V1 (b) V1 < V < V2 and (c) V = V2.

The current density through the RTD should be proportional to the density of states indicated by the circle of intersection marked in grey in figure 1-5. Assuming that the tunneling probability is approximately constant for the carriers which satisfy the conditions of conservation of momentum and energy in the voltage range considered, the tunneling current density can thus be expressed as:

$$J \propto (k_F^2 - q_R^2) \propto (E_F^E - E_R) \qquad (1.3)$$

In real cases, besides the coherent tunneling described above, carriers can also perform incoherent tunneling involving impurities, interface roughness. In those cases there is no more momentum conservation along the tunneling. These processes increase the line width of the states involved, so that the I (V) curve loses its linear characteristics, the current peak becomes less abrupt and the current after the resonance does not go to zero. Furthermore, in our simple model, we assumed that electrons in both the emitter and the collector, occupy 3D–like states. This consideration no longer applies for RTD structures with undoped spacer layers adjacent to the barriers. In such case there is a voltage drop along these undoped regions, leading to formation of triangular-like potential wells (Goldman, et al., 1987), as shown in figure 1-6

(a). Due to the buildup of charge in the triangular well, these regions are called as accumulation layers.

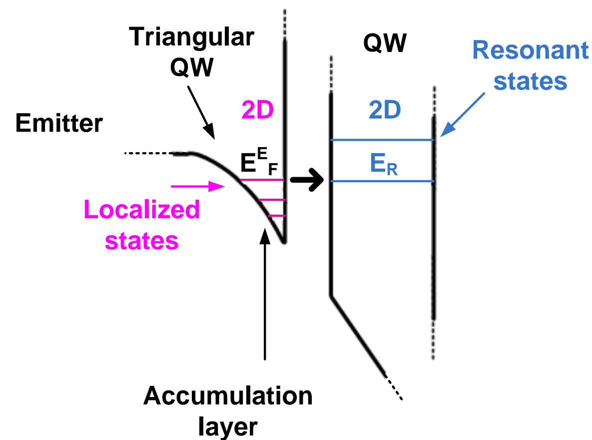

Figure 1-6 - Detail of the conduction band with 2D triangular potential well formed due to the presence of accumulation layer, case with thermalization of carriers in the states of triangular QW (2D-2D tunneling).

The lower energy states of the triangular well correspond to localized states close to the interfaces with a quasi-2D character, while the higher-energy states are more extended and quasi-3D. Injected carriers from the doped layers by an applied voltage quickly thermalize to the lower energy states of the triangular well forming a 2D-gas. Even though those carriers eventually tunnel into the QW, they can be considered to follow a quasi-equilibrium distribution, which allows us to define a quasi-Fermi level associated with this distribution. In this condition, electrons occupy discrete energy levels along the direction perpendicular to the barriers and tunneling becomes 2D-2D (figure 1-6).

The representation of the Fermi surface in k space considering the 2D states of the triangular potential well is shown in figure 1-7. As a consequence of space quantization along the z direction, the Fermi surface is "sliced" into concentric disks along the z direction. Here again, for coherent tunneling, the lateral components of the momentum (k_x, k_y) and the energy Ez must be conserved. Thus, the electronic states participating in the tunneling process are represented solely by the intersection of the plane $k_z = q_R$ with the discs of the Fermi surface Figure 1-7 (a). Based in this model, the I(V) curves should thus consist in a series of symmetrical narrow peaks with

intensities proportional to the areas of the disk. However, as discussed before, the real I(V) curves are broadened by scattering processes. In practice, the introduction of the undoped spacer layers results in a I(V) curve with better defined triangular-like peaks and NDR features as compared to structures without undoped spacer layers.

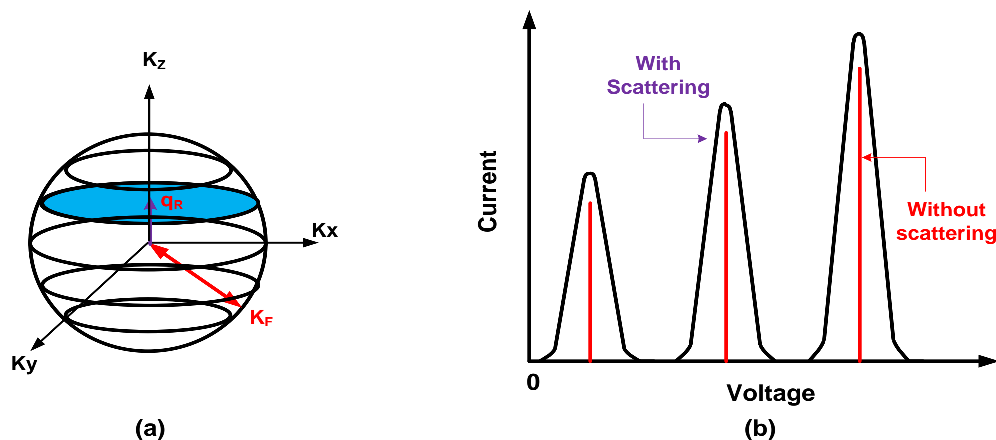

Figure 1-7 - (a) Fermi sphere "sliced" due to the quantization in z direction with the intersection $k_z = q_R$ for a given voltage. (b) I(V) Curve showing three consecutive resonances.

We remark that RTD structures allows us to select the resonant states through which the transport is performed through an applied voltage to the contacts. Therefore, if the spin degeneracy of the resonant states is broken, it opens the interesting possibility of adjusting the applied voltage so transport occurs preferentially through a level with a specific spin character, i.e. selecting the desired spin of the injected carrier. Spin degeneracy can be broken directly by applying an external magnetic field to the RTD due to the Zeeman Effect, or indirectly, through the spin-orbit coupling. The degeneracy of energy levels is directly related to the spatial symmetries experienced by the carriers. Therefore, the degeneracy of the RTD levels can be broken by an symmetry of the system, including an asymmetry of the crystal structure such as the Dresselhaus Effect (Dresselhaus, 1995) or due to the presence of intrinsic or extrinsic electric fields, such as the Bychkov - Rashba Effect (Bychkov, et al., 1984).

Another important effect to be considered for RTDs is the spin injection from the 2D gas formed in contact region which presents high g-factors and therefore is highly spin polarized under magnetic fields. As we will discuss in the next chapters this 2D gases formed at the accumulation layers can inject spin polarized carriers into the QW.

In this work, we have performed some measurements under a high magnetic field in order to analyze spin effects on the RTD structure by using the Zeeman effect to break the spin degeneracy of the resonant states.

1.3 – RTDs under Magnetic Fields:

We now discuss in more details the effects of a magnetic field on the properties of the RTD structures.

1.3.1 - Atomic model

In order to give a physical insight of the problem, we first present a brief description of the effects of a magnetic field on a hydrogen atom, which in fact, presents certain similarities with excitons, usually related to the optical emission in semiconductor structures. Let us first consider a particle of mass m_e and charge q =-e, without spin, submitted to a scalar potential V(R).The Hamiltonian, using the Coulomb gauge is given by:

$$H = \frac{1}{2m_e}[P + eA\,(R)]^2 + V(R) \qquad (1.4)$$

Where A(R) is the vector potential associated to the magnetic field $B = \nabla \times A(R)$. Considering that B is uniform, the vector potential can be expressed as:

$$A = \frac{1}{2} r \times B \qquad (1.5)$$

Substituting in (1.4) we can calculate the term.

$$[P + eA\,(R)]^2 = P^2 - \frac{e}{2}[P.(R\times B) + (R\times B).P] + \frac{e^2}{4}(R\times B)^2 \qquad (1.6)$$

Where B is actually a constant and not an operator. Therefore all the observables commute with B, so that we can obtain:

$$[P + eA(R)]^2 = P^2 - \frac{e}{2}[B.(P\times R) + (R\times P).B] + \frac{e^2}{4}(R\times B)^2 \qquad (1.7)$$

Considering that:

$$L = (R\times P) = -(P\times R) \qquad (1.8)$$

We can write the total Hamiltonian of the particle as:

$$H = H_o + H_Z + H_D \qquad (1.9)$$

where H_0, H_D and H_z are defined by:

$$H_o = \frac{[P]^2}{2m_e} + V(R) \qquad (1.10a)$$

$$H_D = \frac{e^2B^2}{8m_e}R_\perp^2 \qquad (1.10b)$$

$$H_Z = \frac{\mu_B}{\hbar}\,B.L \qquad (1.10c)$$

μ_B is the Bohr Magneton ($\mu_B = \frac{e\hbar}{2m_e} = 5.788\times10^{-5}\,\frac{eV}{T}$) and is the projection of R in the plane perpendicular to B that becomes:

$$R_\perp^2 = X^2 + Y^2 \qquad (1.11)$$

if we choose an orthogonal axis xyz where B is parallel to the z axis.

H_0 is the Hamiltonian without the presence of a magnetic field. H_D presents a quadratic dependence with the magnetic field and is known as the diamagnetic term. From (1.11), we observe that the diamagnetic shift is directly proportional to the mean

squared extension of the wave function of particle in the plane perpendicular to B (Walck, et al., 1998; Reynolds, et al., 1987). The term $\mathrm{H_Z}$ is called the Zeeman effect.

Let us now include the intrinsic magnetic moment of the particle (spin) simply by substituting **L** → **L**+2**S** in (1.14c). The factor 2 in front of S reflects the fact that the g-factor of electron in vacuum is 2. $\mathrm{H_Z}$, then becomes:

$$\mathrm{H_Z} = \frac{\mu_B}{\hbar}\,\mathrm{B.(L + 2S)} \qquad (1.12)$$

The nature of the Zeeman effect depends critically on the magnitude of the external magnetic field compared with the actual internal field generated by the spin-orbit interaction. For $B_{ext} \ll B_{int}$, the fine structure corrections dominate and $\mathrm{H_Z}$ can be treated as a perturbation. In this case, the energy correction term is given in the first order of approximation, by:

$$\mathrm{E_Z^1} = \frac{\mu_B}{\hbar}\,\mathrm{B.(L + 2S)} \qquad (1.13)$$

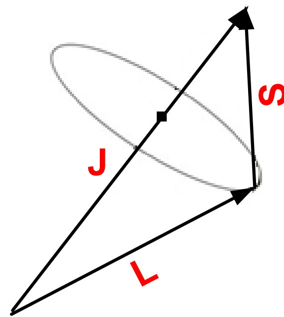

Figure 1-8 - In the presence of spin-orbit coupling, L and S are no longer separately preserved, they presses around the total angular momentum J.

We do not know the expected values of **S**, but the total angular momentum **J=L+S** is a constant (figure 1-8). **L** and **S** rotate around **J**, so that the average **S** is actually its projection on **J**:

$$\mathrm{S}_{med} = \frac{\mathrm{S\,.\,J}}{\mathrm{J}^2}\mathrm{J} \qquad (1.14)$$

But **L** = **J** - **S**, then $L^2 = J^2 + S^2 - 2\boldsymbol{S}.\boldsymbol{J}$ and therefore,

$$\boldsymbol{S}.\boldsymbol{J} = \frac{1}{2}(J^2 + S^2 - L^2) = \frac{\hbar^2}{2}[j(j+1) + s(s+1) - l(l+1)] \qquad (1.15)$$

Using s = 1 / 2, it follows that:

$$< L + 2S > = < 1 + \frac{\mathrm{S.J}}{J^2}J > = \left[1 + \frac{\mathrm{j(j+1) - l(l+1) + \frac{3}{4}}}{\mathrm{2j(j+1)}}\right] < J > \qquad (1.16)$$

The term in brackets is the Lande g-factor in vacuum of an electron in an atom:

$$\mathrm{g_j} = 1 + \frac{\mathrm{j(j+1) - l(l+1) + \frac{3}{4}}}{\mathrm{2j(j+1)}} \qquad (1.17)$$

Thus in first order, the Zeeman term is given by:

$$E_Z^1 = \mathrm{m_j g_j \mu}_B \mathrm{B} \qquad (1.18)$$

If the atom is not in vacuum, the Lande g-factor is no longer given by (1.17) and depends on the environment in which the measurements are performed, but the form of energy given by (1.18) can still be described by a similar expression.

In brief, the presence of an external magnetic field on the hydrogen atom can be described by two basic components: the diamagnetic effect and the Zeeman effect, that is responsible for breaking the spin degeneracy of the quantum states.

1.3.2 - Landau Levels (Pereira, 2001)**:**

We now discuss the effects of a magnetic field in a free particle, which is a adequate model for the carriers of a 2D gas. Classically, the effect of a magnetic field on the movement of free carriers is to force them to perform circular cyclotron orbits of radius $\mathrm{R}_C = \mathrm{mv\,/\,eB}$ and cyclotron frequency $\omega_\mathrm{C} = \mathrm{eB/m}$. However, quantum mechanics predicts the quantization of the allowed orbits of the carriers with energies given by:

$$E_N = (N + 1/2)\hbar\omega_C \, ,$$

where N = 0, 1, 2, 3, ... and $\omega_C = \frac{eB}{m}$. The quantized states are known as the Landau levels.

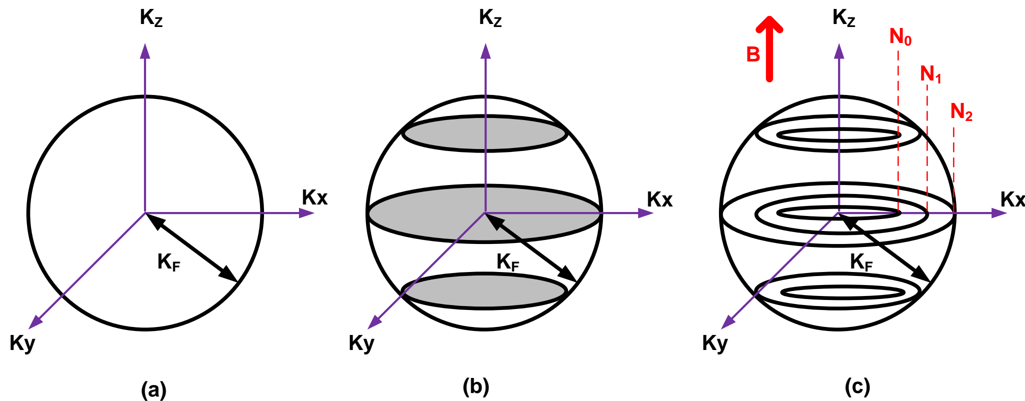

Figure 1-9 - Representation of the Fermi sphere in reciprocal space k: (a) 3D Fermi sphere without magnetic field, (b) with 2D space quantization along the z direction without magnetic field, (c) 2D system with magnetic field, the disks are broken down into concentric circles.

The quantization of the motion of carriers in the direction perpendicular to the magnetic field is equivalent to an additional spatial confinement, so that in the presence of perpendicular magnetic fields, 2D systems such as a triangular QW becomes a 0D system, as shown in figure 1-9.

The Landau levels have a singular density of states (Dirac Delta function-like) with a degeneracy given by eB/m. Figure 1-10 shows the density of states and energy levels for a triangular well without magnetic field (figure 1-10 (a)) and with magnetic field (figure 1-10 (b)). Increasing magnetic fields results in an increasing degeneracy, so that the number of states that fit into each Landau level increases with B. Therefore, for sufficiently high magnetic fields, all carriers may be fallen in the first Landau level.

An important remark is that the energy separation all Landau levels is given by: $\Delta E_L = \hbar\omega_C = \hbar eB/m^*$. We point out that for a given value of the magnetic field, ΔE_L is inversely proportional to the effective mass (m *) of the carrier.

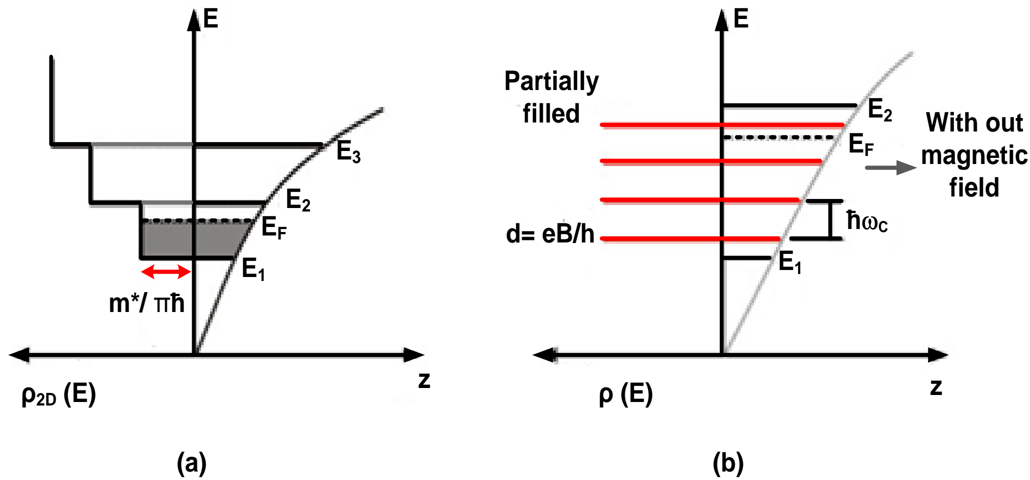

Figure 1-10 - Effect of magnetic field in a 2D system. (a) Energy levels and density of states of a triangular well without magnetic field, (b) Energy levels and density of states with magnetic field (in red).

Let´s now consider the effect of a magnetic field in (z) direction on the free carriers of a RTD structure. The presence of magnetic field, quantizes the lateral movement of carriers in both the emitter and the QW states. The kinetic energy of the carriers in the xy plane ($\hbar^2 k_\parallel^2/2m^*$) should then be replaced by the Landau levels, so that the energy of a resonant state shall be expressed as:

$$E_{R,N} = E_R(V) + (N + \tfrac{1}{2})\hbar\omega_C \qquad (1.19)$$

Once more, the components of wave-vector in the xy plane must be conserved. In this case, the Landau quantum number (N) should therefore be conserved during tunneling. Quantization into Landau levels reduces the dimensionality of the system to 0D-0D, so that the resonance peaks in the I(V) curve are symmetrical and narrow, each

relating to a given level and their different resonant Landau levels. However, as discussed before, the presence of scattering processes associated to system disorders (interfaces roughness, impurities, ...) should lead to the broadening of the Landau levels. The concept of carrier localization and Landau levels broadening into bands was first introduced by PW Anderson (Anderson, 1958), figure 1-11. In this simple view, the states in the center of the Landau bands are extended states that contributes to transport, while the states in the tails of the bands are localized and thus does not contribute to transport.

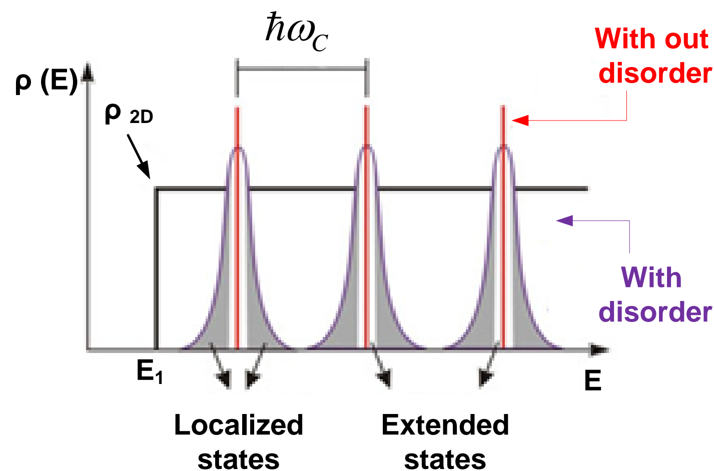

Figure 1-11 - Density of states of Landau levels with and without disorder. The disorder leads to enlargement of Landau energy levels through the localization of the wave functions of carriers (localized states).

If we now consider the spin degree of freedom from the free carriers, they should also give rise to a Zeeman-like interaction. Considering a similar approach used for the atomic case, the full expression for the energy of a free carrier in a 2D-like state can thus be expressed as:

$$E_{R,N} = E_R(V) + \left(N + \frac{1}{2}\right)\hbar\omega_C \pm g^*\mu_B B \qquad (1.20)$$

where ω_C is the cyclotron frequency eB/m^*, $g^*\mu_B B$ is the magnetic energy of spin, g^* is the Lande g-factor of the effective medium and E_R is the energy associated with movement of the carriers in z-direction.

In conclusion, the application of an external magnetic field affect the states of the carriers that accumulate as 2D gases at the QW and the accumulation layers of a RTD structure, giving rise to a series of Landau levels. This phenomenon was clearly observed in systems which have electronic transport (Goodings, et al., 1994). In the case of holes, the experimental results are not so evident due to their relatively larger effective masses, so that Landau levels for holes are usually less resolved ($\Delta E_L = \hbar\omega_C = \hbar eB/m^*$), which makes them difficult to be observed.

References

- Anderson, P W. "Absence of Diffusion in Certain Random Lattices." *Phys. Rev.* 109.1492 (1958).
- Bychkov, Yu A and E I Rashba. "Oscillatory effects and the magnetic susceptibility of carriers in inversion layers." *J. Phys. C: Solid State Phys.* 17.6039 (1984).
- Carvalho, H B de, et al. "Voltage controlled hole spin injection in non mangentic GaAs,AlAs RTD." *Physical Review B* 73 (2006).
- Carvalho, H B, et al. "Circular polarization from a non magnetic p-i-n resonant tunnelling diode." *Applied Physics Letters* 90.062120 (2007).
- Dos Santos, L F, et al. "Polarization resolved luminescence in asymmetric n-type GaAs/AlGaAs." *Appl. Phys. Lett.* 92 (2008).
- Dresselhaus, G. "Spin-Orbit Coupling Effects in Zinc Blende Structures." *Phys. Rev.* 100 (1995).
- Fabian, Jaroslav, et al. "SEMICONDUCTOR SPINTRONICS." 2007.
- Galeti, H V A, et al. "Magneto-optical investigation of two-dimensional gases in n-type resonant tunneling diodes." *Semiconduc. Sci. Technol* 27 (2012). <stacks.iop.org/SST/27/015018>.
- Goldman, V J, D C Tsui and J E Cunningham. "Observation of intrinsic bistability in resonant tunneling structures." *Phys. Rev. Lett* 58 (1987).
- Goodings, C J, H Mizuta and J R. A Cleaver. "Electrical studies of charge build-up and phonon-assisted tunneling in double-barrier materials with very thick spacer layers." *J. Appl. Phys.* 75.363 (1994).
- Mizuta, Hiroshi and Tomonori Tanoue. *the physics and applications of resonant tunnelling diodes*. Cambridge university press, 1995.
- Motsnyi, V F, et al. "Optical investigation of electrical spin injection into semiconductors." *Phys. Rev. B* 68 (2003).
- Pereira, Ana Luiza Cardoso. *Levitações de Estados Estendidos em Sistemas que Apresentam Efeito*. 2001.
- Reynolds, D C, et al. "Magneto-optical studies of GaAs-As multi-quantum-well structures grown by molecular-beam epitaxy." *Phys. Rev. B* 35 (1987).
- Slobodskyy, A, et al. "Voltage-Controlled Spin Selection in a Magnetic Resonant Tunneling Diode." *Phys. Rev. Lett* 90 (2003).

- Tsuchiya, Masahiro and Hiroyuki Sakaki. "Dependence of resonant tunneling current on well widths in AlAs/GaAs/AlAs double barrier diode structures." *Appl. Phys. Lett.* 49 (1986).
- Walck, S N and L T Reinecke. "Exciton diamagnetic shift in semiconductor nanostructures." *Phys. Rev. B* 57.9088 (1998).
- Ziese, Michael and Martin J Thornton. *Spin electronics*. springer, n.d.

Chapter 2 - Materials and Experimental Techniques

In this chapter we will briefly present the sample as well as the experimental techniques and methodologies used during our studies.

2.1 - Resonant Tunneling Diode Structure

This work is based on the study of a resonant tunneling diode (RTD) composed of III-V semiconductor materials with layers of GaAs and AlAs. An undoped quantum-well (QW) of GaAs with thin barriers of AlAs is grown around GaAs n- and p-type doped contacts. This structure is usually known as GaAs/AlAs a p-i-n RTD. The sample was432

grown by Prof. Mohamed Henini from the University of Nottingham (UK), using the |||

Molecular Beam Epitaxy (MBE) technique within a scientific collaboration with his group. Using this technique, it is possible to grow crystalline layers of semiconductor materials with excellent control of thicknesses and impurity concentrations and therefore obtain heterostructures of high crystalline quality, which is reflected by their optical and transport properties. The layers of GaAs and AlAs were deposited on a (100) substrate of GaAs. The impurities used for doping the GaAs contact layers were Be and Si , for acceptors (p-type) and donors (n-type), respectively. The layers that compose the sample from top to bottom (substrate) are detailed in table 2.1 below.

Under forward bias, the p-i-n structure allows for the simultaneous injection of electrons and holes into the quantum well and the investigation of the subsequent radiative recombination (Maude, et al., 1994). Figure 2-1 illustrates the schematic potential profile of our RTD structure along the growth direction (z) for k = 0 without considering the built-in electric field due to the doped layers. The undoped accumulation

layers of GaAs, adjacent to the barriers of AlAs are required to reduce the diffusion of carriers from the doped contacts into the QW (Fabian, et al., 2007; Tsuchiya, et al., 1985; Shewchuk, et al., 1985). The structure was processed on 400μm diameter mesas with a 20 μm thick top metallic contact with the shape of a ring in order to allow optical access to the structure while applying an external voltage. The other metallic contact was made in layer at the p-type GaAs layer and is thus called the bottom contact.

<table>
<tr><th>Material</th><th>Layer size</th><th>Dopant</th><th>Sample region</th></tr>
<tr><td>GaAs</td><td>25nm</td><td>n = 2×10^{18}</td><td rowspan="4">Superior Contact Region</td></tr>
<tr><td>$Al_{0.33}Ga_{0.67}As$</td><td>1μm</td><td>n = 1.33×10^{18}</td></tr>
<tr><td>GaAs</td><td>51nm</td><td>n = 2×10^{18}</td></tr>
<tr><td>GaAs</td><td>35nm</td><td>n = 1×10^{16}</td></tr>
<tr><td>GaAs</td><td>7.6nm</td><td>Undoped</td><td>Space layer</td></tr>
<tr><td>AlAs</td><td>5nm</td><td>Undoped</td><td>Barrier</td></tr>
<tr><td>GaAs</td><td>6 nm</td><td>Undoped</td><td>QW</td></tr>
<tr><td>AlAs</td><td>5nm</td><td>Undoped</td><td>Barrier</td></tr>
<tr><td>GaAs</td><td>5nm</td><td>Undoped</td><td>Space layer</td></tr>
<tr><td>GaAs</td><td>100nm</td><td>p = 5×10^{17}</td><td rowspan="3">Inferior Contact Region</td></tr>
<tr><td>GaAs</td><td>100nm</td><td>p = 1×10^{18}</td></tr>
<tr><td>GaAs</td><td>3μm</td><td>p = 3×10^{18}</td></tr>
<tr><td colspan="4">GaAs Substrate n-type, $n = 2 \times 10^{18}$</td></tr>
<tr><td colspan="4">Table 2.1 - Description of the growth of sample</td></tr>
</table>

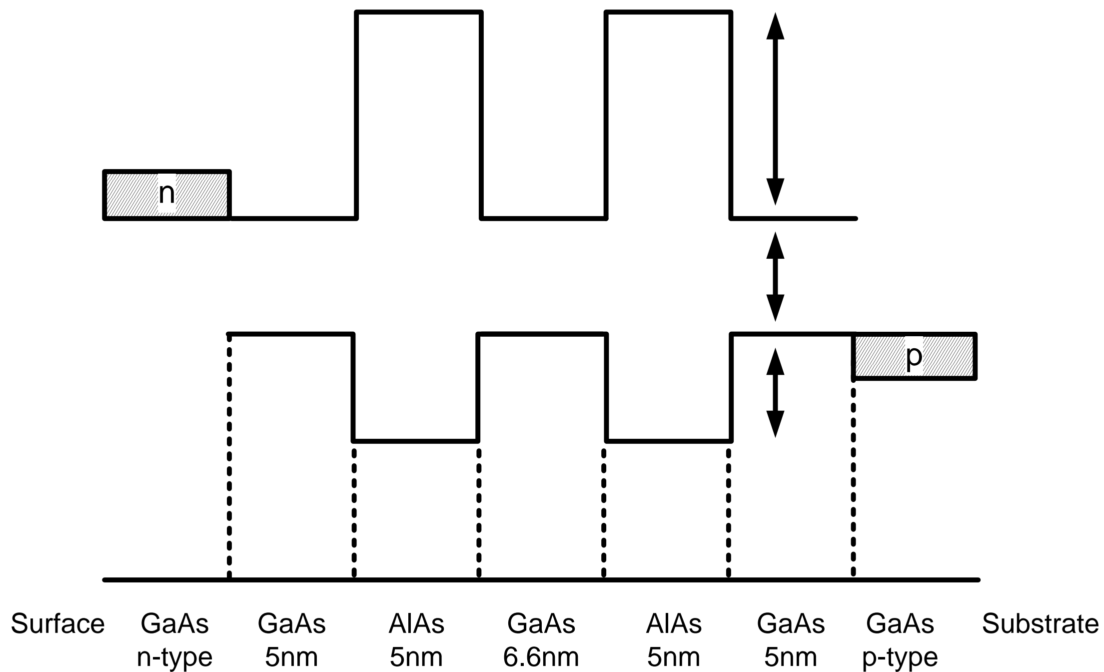

Figure 2-1 - Potential profile of a symmetric p-i-n GaAs- AlAs RTD without considering the built-in electric field due to the doped layers.

2.2 - Transport Measurements

The current-voltage characteristic curves I(V) are usually used to characterize electronic devices such as RTDs. In the case of an RTD as studied here, we do not expect a linear relationship between current and voltage. In fact, the I(V) function for a RTD structure is characterized by peaks that arise at certain voltages due to resonant tunneling through confined states in the QW. The confined states through which the carriers can efficiently tunnel the double-barrier structure at certain voltages are called the resonant voltages.

To measure the I(V) curves, the structure was connected to a DC circuit (figure 2-2) that makes it possible to apply an external voltage between the top and the bottom RTD contacts and read the current flowing through the diode. In this work, we have used a voltage source (Yokogawa - Model 7651 Programmable Voltage Source) and an multimeter (Keithley - Model 197A Auto ranging Multimeter DMM) operated remotely through an acquisition software. During measurements, the sample was kept within a

Helium super-fluid immersion cryostat at a temperature of 2 K. Figure 2-2 shows the layout of the circuit connected to the RTD.

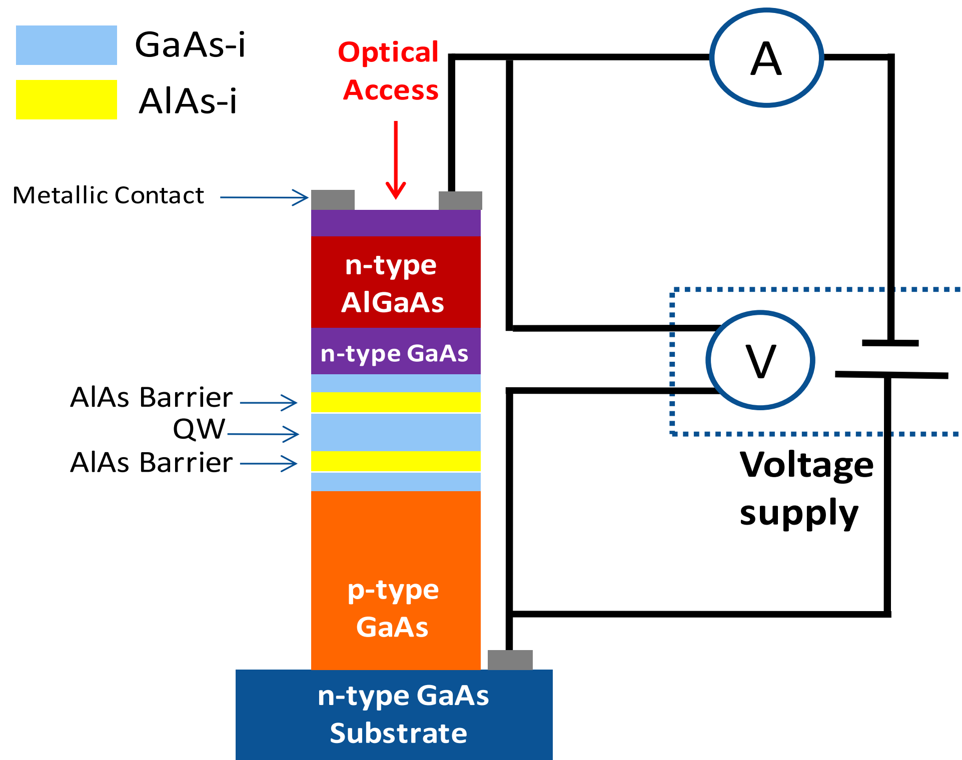

Figure 2-2 - Schematic diagram of a DC circuit connected to p-i-n type RTD with symmetric barriers in a 4-wire mounting, showing the ammeter, the voltage source and the layers of diode.

Since the sample is a p-i-n type RTD, resonances of both, holes and electrons can be observed in the I(V) curves by the procedure described above when the diode is forward biased. Resonant states can be clearly observed in the I (V) curves. In all experiments, we applied a positive voltage to the bottom contact relative to the top contact, which is called a positive bias in our convention. This kind of bias acts as to accelerate the majority charge carriers (electrons/holes) from the upper/bottom contact through the QW, which is conventionally known in the literature as a forward bias voltage. In this work, we have also studied the photocurrent by measuring the I(V) characteristics curves in dark and under light excitation.

2.3 - Optical Measurements - Luminescence:

Although various aspects of RTDs can be observed by transport measurements, the optical study allows further exploration of the transport properties and the interactions between different carriers. We briefly discuss the physical phenomena related to the optical measurements performed in our RTD structure, including photoluminescence and electroluminescence. Both phenomena have their origin in the recombination of an electron and hole, but the way these carriers are generated, distinguish these two process.

In the fundamental state of an undoped semiconductor at T= 0 K, the conduction band is completely empty of electrons and the valence band is completely filled with electrons. If this semiconductor illuminated with light of appropriated energy, it can promote an electron from the valence band to the conduction band, leaving a hole in the valence band. For this to occur, the photon must have an energy equal or greater than the energy difference between the bottom of the conduction band and the top of the valence band ($\mathrm{E_{Photon}} > \mathrm{E_g}$), where "$\mathrm{E_g}$" is the band gap. In the conduction/valence band, this electron/hole quickly relaxes to the bottom/top of the band, which is normally called the thermalization process. Thereafter, the electron can recombine with the hole left in the valence band by emitting a photon, that is called the luminescence. In this case, the pairs of electrons and holes that recombine emitting luminescence were generated by an optical excitation. Therefore, we call this luminescence as photoluminescence (PL).

In more complex structures we can have carriers (electrons or/and holes) already available in the structure, as it is the case of our RTD structure. Devices with only one type of doping (n-type or p-type), cannot generate optical recombination, unless it is illuminated by an external light, as for undoped structures. However, devices that have both, n- and p-type doping can generate an optical emission without the need of any illumination, when the majority carriers created by the two types of doping are injected towards each other and overlap in a given spatial region. For this to occur, the action of an electric field is necessary and so in this case, the emission is called Electroluminescence (EL) .

Let us now discuss the processes described above for the specific case of a p-i-n RTD. To represent the dynamics of the carriers, we will use schematic band diagrams. In these representations we will use the signal convention for the applied bias as a voltage applied to the lower contact (close to the substrate) relative to the upper contact, as discussed before. Furthermore, we will always draw the top contact to the left and the bottom contact to the right of the figure.

2.3.1- p-i-n RTD

The different doping of the contacts in a p-i-n RTD introduces an intrinsic electric field in the structure that bends the conduction and valence bands even without an external voltage applied to the RTD. Consider first the case where the voltage is applied to the RTD without illumination.

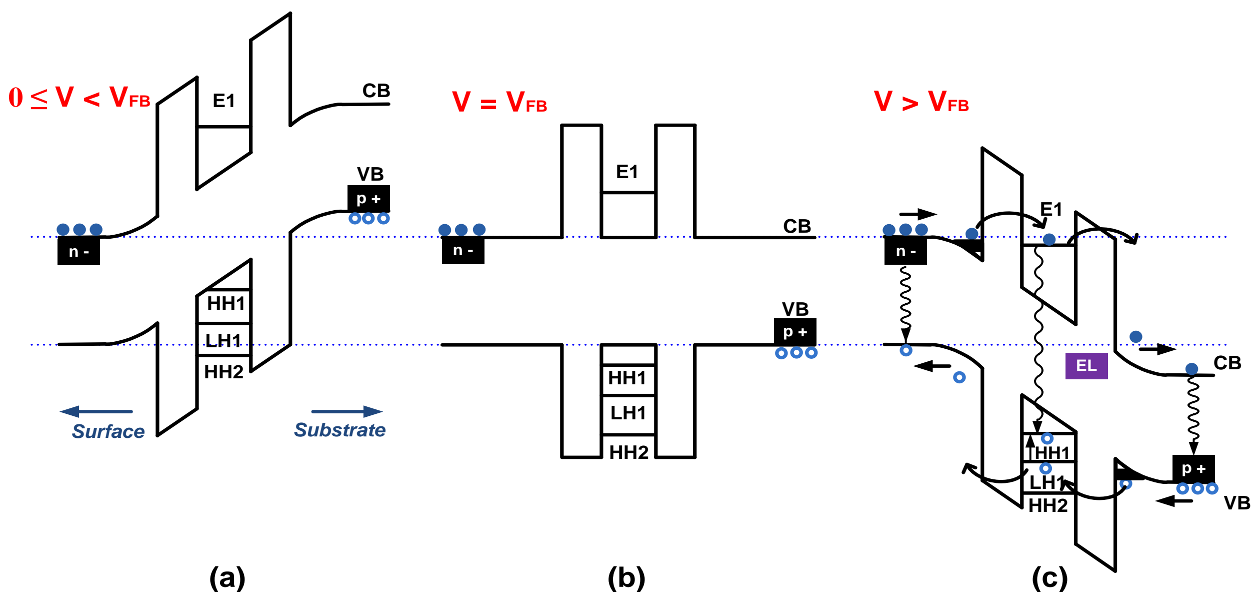

Figure 2-3 - Schematic potential profile of sample NU491, illustrating the transport and recombination of carriers in the structure as a function of bias (a) below flat band, (b) at flat band condition, (c) above flat band.

Figure 2-3 illustrates the dynamics of carriers as a function of voltage, using the convention defined above. Figure 2-3 (a) shows the intrinsic internal electric field which

opposes the flow of electrons and holes towards the QW, resulting in a zero EL signal. Figure 2-3 (b) represents the RTD under an positive voltage (forward biased), so that the intrinsic field is exactly compensated by the external bias, resulting in a flat band condition. In this situation, it is still not possible to observe electroluminescence.

In the case of Figure 2-3 (c), the electrons present in the upper contact are at a higher electric potential, and therefore, are driven by the electric field towards the QW. In the same way, the holes are driven from the top contact towards the QW. Driven electrons and holes tend to accumulate at the undoped layers close to the barriers at what is called accumulation layers, forming two-dimensional (2D) gases. Carriers from the accumulation layers may tunnel into the quantum well. As we discussed in previous chapter, tunneling into the well may include two types of tunneling limits: ballistic (3D-2D) or through the accumulation layer (2D-2D). Inside the well, we emphasize on the possible processes: injected carriers on excited QW levels can relax to fundamental levels, (as shown by the $\mathrm{hh}_2 \rightarrow \mathrm{hh}_1$ transition in figure 2.3 (c), experience radiative recombination, emitting photons (EL), and tunnel out of the well through the second barrier contributing to the current through the RTD. Furthermore, carriers tunneling through the second barrier can still recombine at the GaAs contacts with opposite majority carrier.

We will now discuss the photoluminescence process in our structure. When we illuminate the RTD, we create pairs of electrons and holes. Figure 2-4 illustrates the schematic layout of the sample profile of NU491 under three different conditions of voltage, with incident light on both the top (n-type) and the bottom (substrate) contacts. We remark that, even though, as we focus the laser at the measured diode so that most of the photons should be absorbed mostly at the top contact, a smaller part of the photons may penetrate up to the lower contact and/or be directly absorbed at the bottom contact since the laser beam diameter can be larger than the diode. Only the fundamental levels of the electrons/holes energy levels at the triangular potential wells formed on each side of the device are shown in figure 2.4. Under this condition, PL emission can be observed for all bias conditions, i.e., for reverse, flat-band and forward biases. We will discuss the optical generation of carriers in these three bias conditions.

In case of figure 2-4(a) the device is forward biased below flat band (reverse biased). In this bias range, photogenerated holes at the n-type contact of the sample may recombine at this layer or be accelerated towards the p-contact, while photogenerated electrons at the p-type contact can also recombine at this layer or be accelerate towards the n-contact. Therefore, the minority carriers photogenerated at each contact layer tend to accumulate close to the barriers, from where they may tunnel into the QW. However, under this condition the majority carriers do not contribute to the current and they are not injected into the QW.

Once again, injected photogenerated carriers can relax to fundamental energy levels and experience radiative recombination, emitting photons (PL), or tunnel out of the well through the second barrier, thus contributing to the current through the RTD. Finally, photo created carriers tunneling through the second barrier can also recombine at the contacts with the opposite majority carriers in each contact.

In figure 2-4 (b) the device is forward biased at flat band condition. Under this condition neither the intrinsic nor the photogenerated carriers would tunnel into the QW and therefore the resulting current should be zero. This is actually the main characteristic that allow us to identify the bias that gives rise to the flat band condition. In the p-i-n sample studied here, the flat-band condition is achieved for an applied voltage of ~1.5 V.

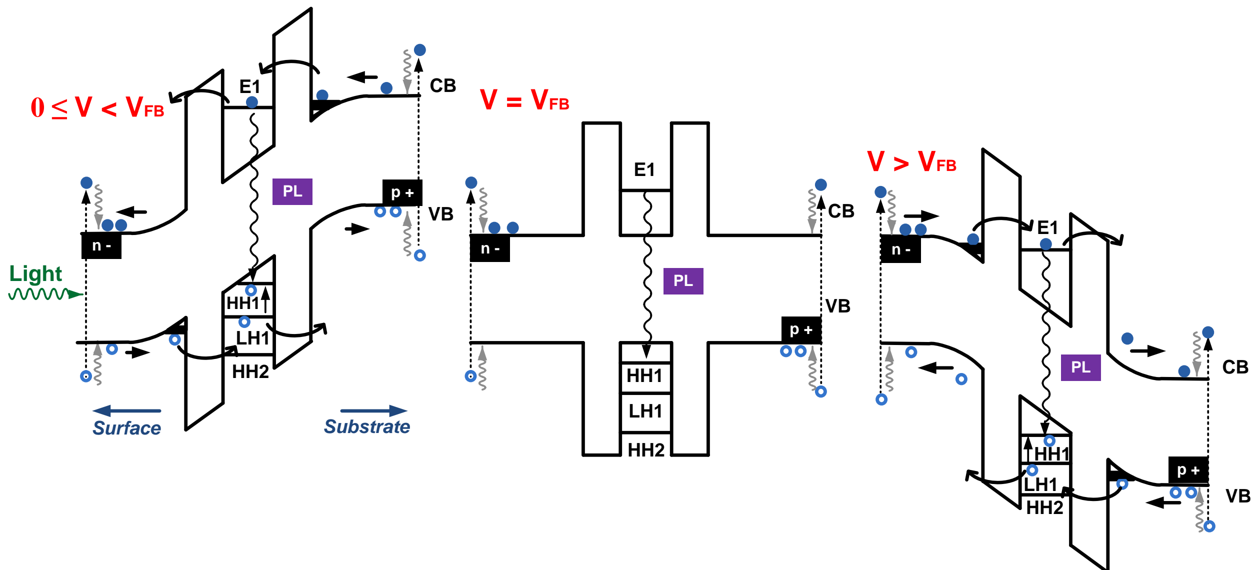

Figure 2-4 - Diagram of potential profile of sample NU491, illustrating the photogeneration, transport and recombination of carriers in the structure as a function of bias (a) sample is biased below flat band, (b) biased at flat band, (c) biased above flat band.

For voltages greater than 1.5V, the device is forward biased beyond flat band as shown in figure 2-4 (c). In this situation, both intrinsic and photogenerated electrons in the upper contact and intrinsic and photogenerated carriers from the bottom contact are pushed against the QW and tend to accumulate generating 2D gases next to the AlAs barriers. These carriers tunnel into the quantum well, where they can relax to the fundamental energy levels and recombine emitting a EL+PL signal or tunnel out of the QW, contributing to the current through the RTD. Once more, the carriers that traverse the double barrier can also recombine at the contacts, emitting a luminescence signal.

For all three cases discussed above, we applied a positive voltage to the substrate relative to the top contact. When a negative voltage is applied to the substrate, the RTD is even further reverse biased.

In this work, we investigated the PL and EL emission as a function of the applied bias, including time-resolved PL and EL measurements under high magnetic fields. We observe that under a magnetic field, the spin degeneracy of the resonant states of the localized states at the triangular wells and inside the QW are broken. On those measurements, we analyzed the circular polarization of the luminescence, that gives

information on the spin polarization of the carriers involved on each recombination band.

2.3.2 - Selection Rules for Optical Transitions in Semiconductors

Optical transition, including absorption and recombination, must obey the fundamental laws of energy and angular momentum conservation. Photons of right or left polarized light have a projection of the angular momentum on the direction of their propagation equal to +1 or −1, respectively (in units of ħ). When a circularly polarized photon is absorbed, this angular momentum must be distributed between the photo-excited electron and hole according to the selection rules determined by the band structure of the semiconductor. Although the complex nature of the semiconductor bands, the momentum conservation result is equivalent to optical transitions between atomic states with j = 3/2, mj = −3/2, −1/2, +1/2, +3/2 (valence bands of light- and heavy-holes) and j = 1/2, mj = −1/2, +1/2 (conduction band).

Possible transitions between these bands, as well as those involving the split-off (SO), for a zinc-blende bulk semiconductor such as GaAs are represented in figure 2.5. Optical absorption/emission occurs for electron-hole pairs or its bounded state (excitons) in such a way that:

$$\mathrm{m}_{\mathrm{electron}} + \mathrm{m}_{\mathrm{hole}} = \mathrm{m}_{\mathrm{exciton}} = \mathrm{m}_{\mathrm{photon}} ,$$

where $\mathrm{m}_{\mathrm{exciton}}$, $\mathrm{m}_{\mathrm{electron}}$, $\mathrm{m}_{\mathrm{hole}}$ and $\mathrm{m}_{\mathrm{photon}}$ are the components of angular momentum in the direction of the magnetic field of the exciton, electron, hole and photon respectively, and $\mathrm{m}_{\mathrm{lh}} = \pm 1 / 2$ (light-hole) and $\mathrm{m}_{\mathrm{hh}} = \pm 3 / 2$ (heavy-holes). It is important to point out that for the valence band, $\mathrm{m}_{\mathrm{hole}} = -\mathrm{m}_{\mathrm{electron}}$. Only transitions with $\mathrm{m}_{\mathrm{photon}}$ = +1 (right-circularly polarized) and -1 (left-circularly polarized) are optically permitted. Optical transitions associated to angular momenta $0 \text{ and } \pm 2$ are prohibited, and so are known as dark states.

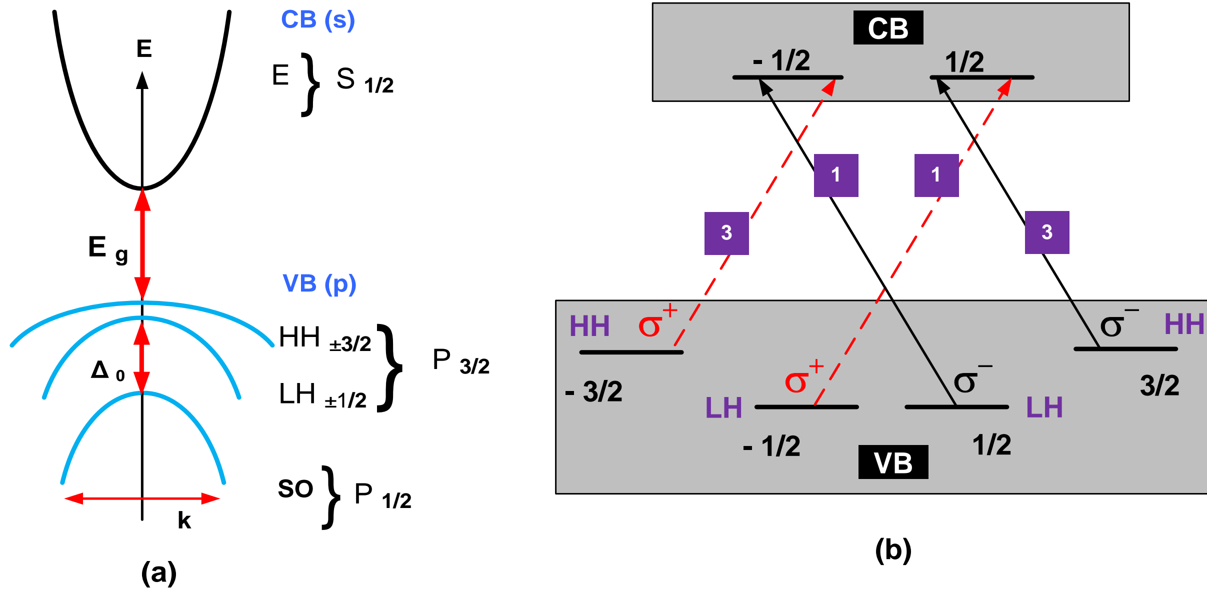

Figure 2-5 - (a) Band diagram of a GaAs QW at the center of the Brilloiun zone (b) Selection rules for optical transitions between the m_j sublevels for a circularly polarized light in a GaAs QW, the numbers in purple indicate the relative transition intensities of both recombinations σ+ and σ- (Zutic, et al., 2004)

In the case of the a quantum well, the confinement of holes with different effective masses results in the splitting of light- and heavy- holes sub-bands, as shown in figure 2-5 (a). Therefore, by selecting the energy and the circular polarization of the excitation/emission from a QW it is possible to select the transition of carriers with a specific composition of angular momenta, i.e., spin polarization. We remark that in our case, even when the holes are injected into excited states, the recombination always occur through the recombination of the fundamental e1-hh1 states. (Miller).

The circular degree of polarization of the luminescence is thus defined as:

$$P = \frac{I^+ - I^-}{I^+ + I^-} \qquad (2.1)$$

where I^+ and I^- are the intensities of left and right circularly-polarized light, respectively.

2.4 - Experimental Techniques

The main techniques used to investigate our RTD system in this thesis was the luminescence, including photo (PL) and electro (EL) luminescence, with the possibility of the application of an external magnetic field (magneto-luminescence) and time-resolved measurements (PL-RT). Two excitation sources for PL were used in our experiments. For measurements of magneto-PL, continuous-wave excitation (CW) by means of a solid-state laser with emission at 532 nm (Nd: YAG - Laser line) was used. For pulsed excitation, in PLRT measurements, we have used a titanium-sapphire laser (Spectra Physics - Tsunami Model).

2.4.1 - Polarization-resolved Magneto Luminescence

The CW EL and PL were performed in the laboratory of transport and luminescence of the Department of Physics at UFSCar. The experimental setup is sketched in Figure 2-6. In all CW measurements, the luminescence signal was collected by a convergent lens and focused into a monochromator, which was coupled to a Si CCD (Andor) detector.

The sample was placed inside a superconducting magneto cryostat (Oxford Instruments) for measurements under different magnetic fields. The magnet reaches fields up to 15T and temperatures ranging from 2 to 300K. The cryostat has windows that allows optical excitation and collection of luminescence, and provides electrical contacts for the RTD structures. For EL measurements, a bias voltage was supplied by a programmable Voltage Source (Yokogawa - Model 7651. The optical emission was analyzed by using a $\lambda/4$ retarder (Thorlabs), and a linear polarizer (Newport) to separate the circularly polarized $\sigma+$ and $\sigma-$ components. Appropriate band-pass optical filters were also used to eliminate detection of scattered and reflected laser.

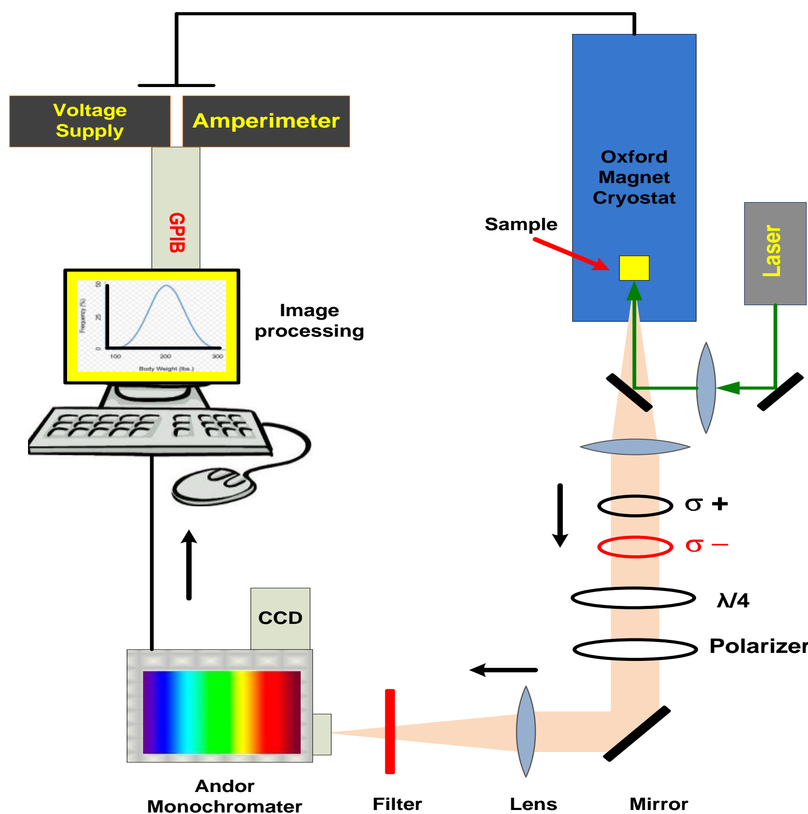

Figure 2-6 - Schematic illustration of the mounting of main components used in CW magneto-luminescence experiments.

2.4.2 - Time-Resolved Photoluminescence (TR-PL)

TR-PL measurements were performed in the Group of Optical Properties (GPO) at the Institute of Physics “Gleb Watagin” (IFGW) UNICAMP, in collaboration with Prof. Dr. Maria José Pompeu Santos Brasil using a system based in a Streak-Camera (Hamamatsu) and a Ti-Sa pulsed laser pumped by a 10 W solid-state Millenia laser (Spectra Physics). The Ti:Sa laser was tuned at 810 nm and doubled using a LiO_2 non-linear crystal in order to obtain a higher excitation energy (405 nm). The laser pulse has a frequency of 82 MHz and temporal width of about 3 ps. The estimated time between two consecutive pulses is thus of ~ 12 ns, which is therefore the maximum time window to analyze a PL transient for this system. A home-made autocorrelator, provided a qualitative view of the laser pulse during measurements,

The sample was placed in a He immersion cryostat and measurements were performed at ~10 K under He gas. The cryostat has quartz windows used to illuminate the sample with the laser beam and collect the luminescence.

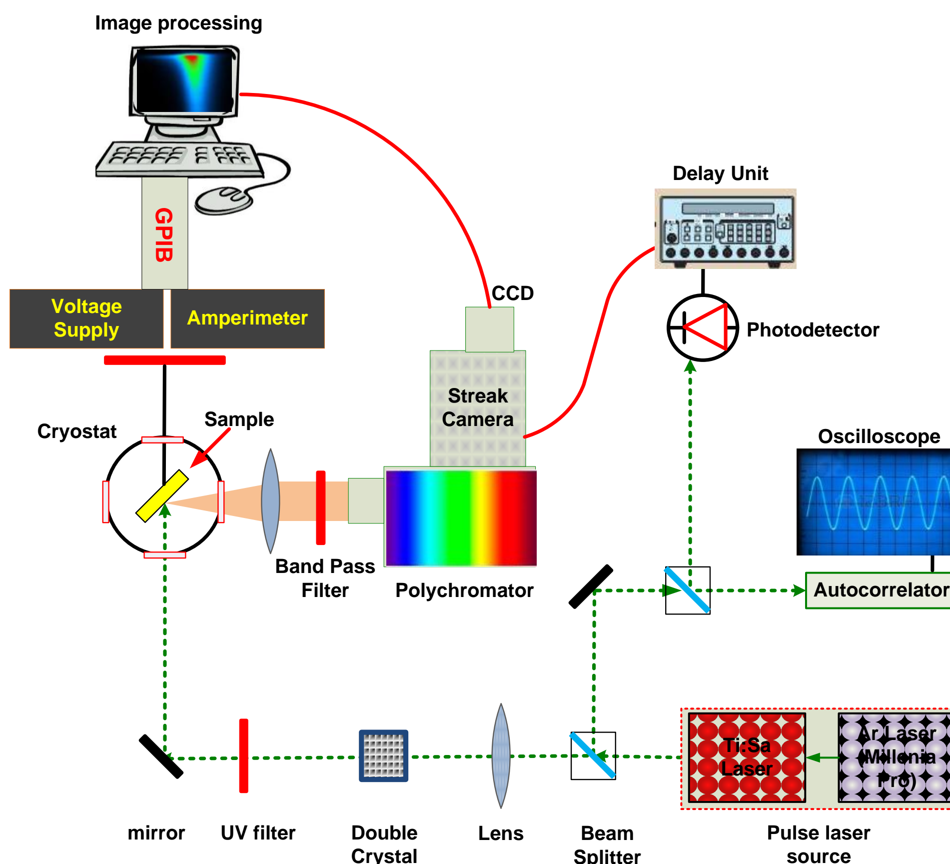

Figure 2-7 - Schematic illustration of the set up of main components used in PLRT experiments.

Linearly-polarized beam was used, which does not favor any selectivity of spin from the photogenerated carrier. The luminescence emitted by the RTD was collected by an assembly of quartz lens and focused on the spectrometer coupled to the streak-camera fast detector system. We have used a diffraction grating with 300 lines per mm. The layout of the experimental assembly of TRPL measurements performed in the laboratory of GPO is represented in Figure 2-7. Note in this illustration a beam-splitter is placed in the path of incident laser beam between the laser Ti: Sa and the cryostat. In

order to divided into two light beams. One beam is sent to the autocorrelator connected to an oscilloscope to observe the stability of the pulse, and the other beam is used to excite the sample. The laser trigger can be delayed by a system of resistors, so that we can adjust the start time of the reading window of the streak camera for an appropriate moment of time relative to the laser repetition rate.

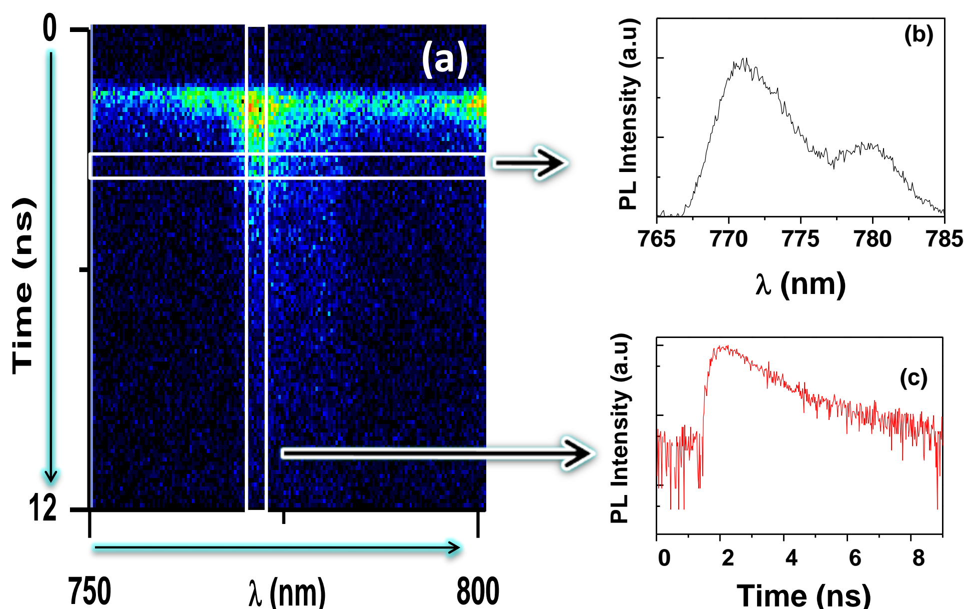

Figure 2-8 - (a) PL image taken at P = 15mW and T = 5K, (b) Integrated PL intensity in time versus wavelength (c) Integrated PL intensity in wavelength versus time.

The images provided by the streak camera system are processed by a suitable software(HPD-TA) for capturing images. Figure 2-8 (a) shows as an illustration, an image obtained by the streak camera from the TRPL measurement system. The measurement was performed using a 15 mW pulsed laser power. The horizontal axis corresponds to the wavelength of the detected light, and the vertical axis to the time. The emission intensity is represented on a scale of colors, ranging in order of increasing intensity from black to red. From this image, we can make two type of graphs: spectra, by integrating the emission intensity for a given time interval relative to the instant that the laser strikes the sample as a function of wavelength (figure 2-8 (b)) corresponding to the horizontal rectangle on the image) and transients, by integrating the emission

intensity for a given interval of wavelengths as a function of time (figure 2-8 (c) corresponding to the vertical rectangle on the image).

Streak images were also obtained in the absence of excitation by the pulsed laser, we call them ELRT, even though they are not strictly time-resolved measurements since there is not a pulsed excitation in this case. This was done as a calibration procedure, so that we could subtract the stationary component of the EL emission for a given bias situation from the PL measurement under the same bias, in order to analyze only the transient component due to the pulsed laser.

References:

- Fabian, Jaroslav, et al. "SEMICONDUCTOR SPINTRONICS." 2007.
- Maude, D K, et al. "Electroluminescence and magneto transport studies of a p-i-n superlattice double barrier resonant tunnelling structure." 4.9 (1994).
- Miller, David A. B. "Optical Physics of Quantum Wells." n.d.
- Shewchuk, T J, et al. "Stable and unstable current-voltage measurements of a resonant tunneling heterostructure oscillator." *Appl. Phys. Lett.* 47 (1985).
- Tsuchiya, Masahiro, Hiroyuki Sakaki and Junji Yoshino. "Room Temperature Observation of Differential Negative Resistance in an AlAs/GaAs/AlAs Resonant Tunneling Diode." *Jpn. J. Appl. Phys* 24 (1985).
- Zutic, I, J Fabian and S Das Sarma. "Spintronics: Fundamentals and applications." *Rev. Mod. Phys.* 76 (2004): 323.

Chapter 3 - Transport and Optical Studies under zero magnetic field

In this chapter, we have investigated transport and optical properties (electroluminescence and photoluminescence) of p-i-n GaAs-AlAs resonant tunneling diodes (RTD) under zero magnetic field.

Figure 3-1 shows the typical I(V) characteristics curve of our p-i-n RTD obtained at low temperature (T=5K). It shows pronounced electron and hole related resonant peaks in the current-voltage characteristics, I(V). Particularly, three clear peaks are observed, corresponding to resonant tunneling through LH1, E1 and HH2 states of the quantum well. In addition, a weak HH1 shoulder is observed at lower bias for the differential conductance of the I(V) characteristic curve (figure 3-1 (b) and (c)). The flat band condition is obtained when the p-i-n diode is forward biased with ~1.51V (labeled V_{FB}).

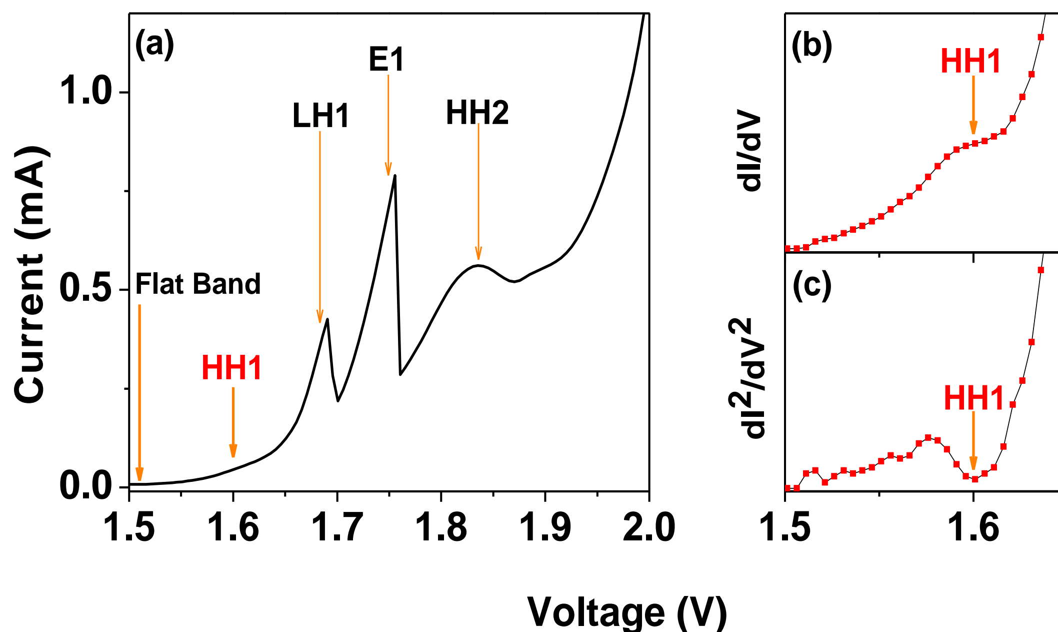

Figure 3-1 - (a) I(V) characteristics curve at 5K (b) for differential conductance dI/dV and (c) d^2I/dV^2
.

Figure 3-2 shows a schematic band diagram of our structure for (a) voltages lower than the flat band condition (V < V_{FB}), (b) for the flat band condition (V_{FB}) and (c) under a forward bias larger than V_{FB}. As will be discussed in Figure 3-5, under lower voltages (V ≤ V_{FB}), it is observed a negligible current flowing in our device. Under a forward bias larger than V_{FB}, current flows through the structure and electroluminescence (EL) signal is observed from both the GaAs quantum well (QW) and the contact layers.

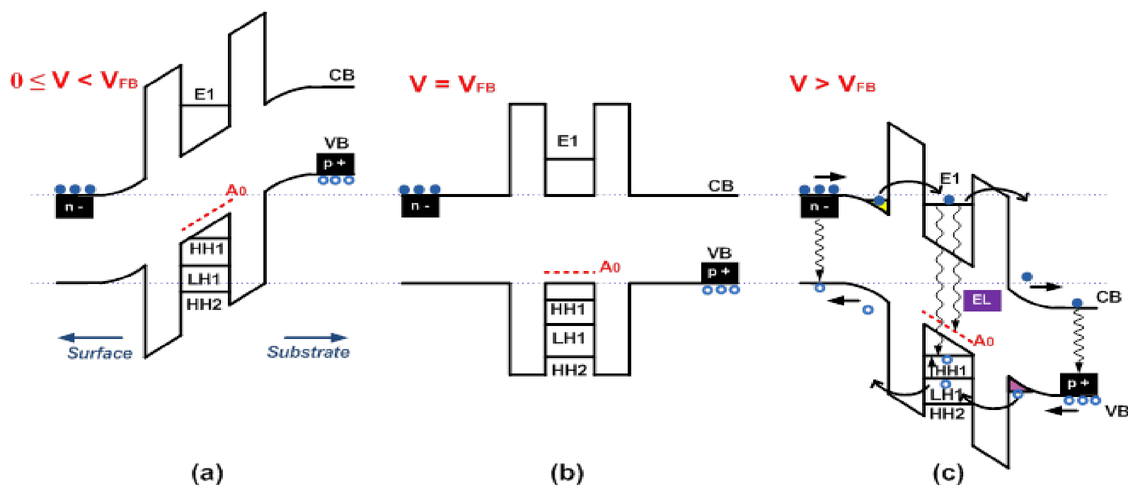

Figure 3-2 - Schematic band diagram of the device for (a) voltages lower than flat band condition (b) at flat band condition and (c) for voltages higher that flat band condition.

Typical QW EL spectra at various bias voltages are presented in Figure 3-3. Two clear EL peaks were observed : a 'hot' line which shows a peak around 1.607 eV and a 'cold' line with a peak around 1.586 eV. The terms hot and cold are assigned to the energy lines according to their high and low energies. These lines are separated by about 21 meV and both lines present a red shift with increasing applied bias voltage due to the Stark effect (Miller, et al., 1985).

Figure 3-4 (a) presents the color-coded map of the EL intensity as function of applied voltage and the voltage dependence of the total QW integrated EL intensity

(figure 3-4 (b)) which includes both bands. The total QW integrated EL presents a good correlation to the I(V) characteristics curve. Figure 3-4 (a) shows that the intensity of the cold line presents a maximum at the peak of the E1 resonance in the I(V) characteristics curve. In addition, we have observed the hot line is more intense for the LH1 and HH2 resonances. We also observe an abrupt change of these emission lines at critical voltages associated to the onset of electron resonant tunneling and to the resonant peak E1.

The observed hot line was previously observed for a similar device and associated to the excitonic recombination between fundamental confined states in the QW (labeled E1 - HH1) (Evans, et al., 1994).

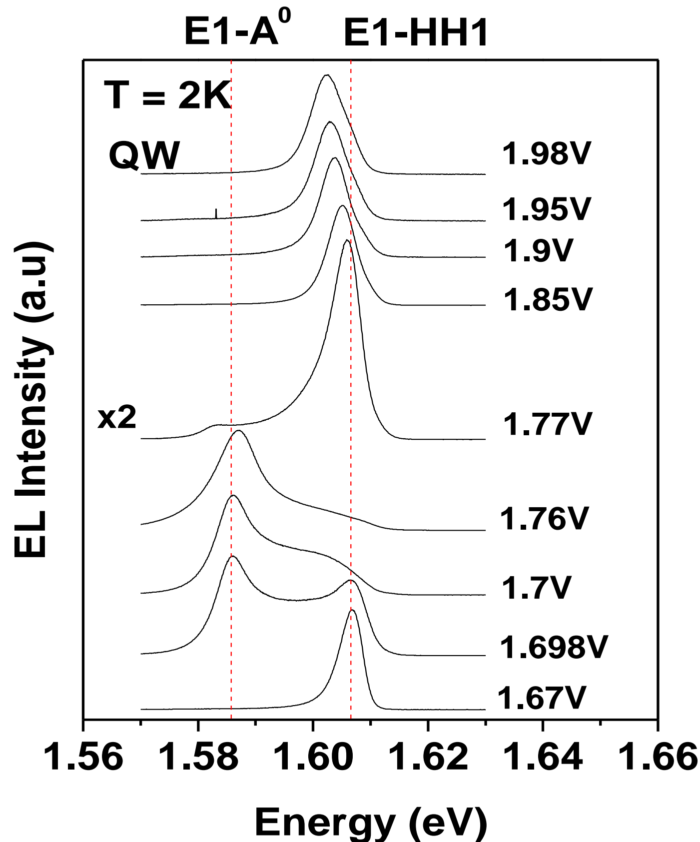

Figure 3-3 - Electroluminescence spectra of QW at 4K for different applied voltages which shows cold and hot energy emission due to the recombination of E1-A0 and E1-HH1.

Therefore, the observed lower-energy emission (cold line) should involve recombination of electrons with holes in which one of the particles are bound in a lower-

energy state of the QW. This cold emission was previously studied for similar RTD devices grown with different space layer thickness, growth temperatures and for devices grown with different Be delta doping density in the QW (Evans, et al., 1994). It was shown that depending on the thickness of space layers, the Be acceptors can diffuse into the QW during growth process (Dellow, et al., 1992) from the doped p-type contact layers which results in the observation of the cold line. In fact, it was shown previously that the relative intensity of the cold line and hot line is very sensitive to spacer layer thickness on the p-doped side and/or to the presence of intentional Be delta doping in the QW. Particularly, it was shown that increasing the spacer layer thickness between the p-doping region and the tunnel barriers greatly reduces the intensity of the cold line. In addition, it was also shown that the presence of delta doping strongly enhances the relative intensity of the cold line. Therefore, we have associated the cold EL line from the QW emission to the recombination of tunneling electrons with holes bound to neutral acceptors. This emission was labeled E1-A0 recombination. The energy difference between these EL emission lines is about 21 meV and would then correspond to the difference between the mean acceptor binding energy in the QW (about 30 meV) (Holtz, et al., 1989) and the exciton binding energy (about 9 meV) (Potemski, et al., 1990). We remark that that the binding energy of a donor state in the quantum well which is about 12 meV (Greene, et al., 1985) which is too close to the exciton binding to account for the observed 21 meV EL peak separation. It was also observed that the E1 – A0 recombination process seems to be relatively inefficient as compared with excitonic E1 - HH1 recombination when holes predominate in the QW (such as at hole resonances), probably due to the slow capture rate of holes on the acceptors at low temperatures as will be discussed below. It was also previously shown that the relative intensity of the cold line increases with temperature probably due to the increase of the hole mobility (Evans, et al., 1993; Skolnick, et al., 1986). The increase of E1-A0 EL intensity at the E1 resonance may be due to the highly increase of electron density as will be discussed below.

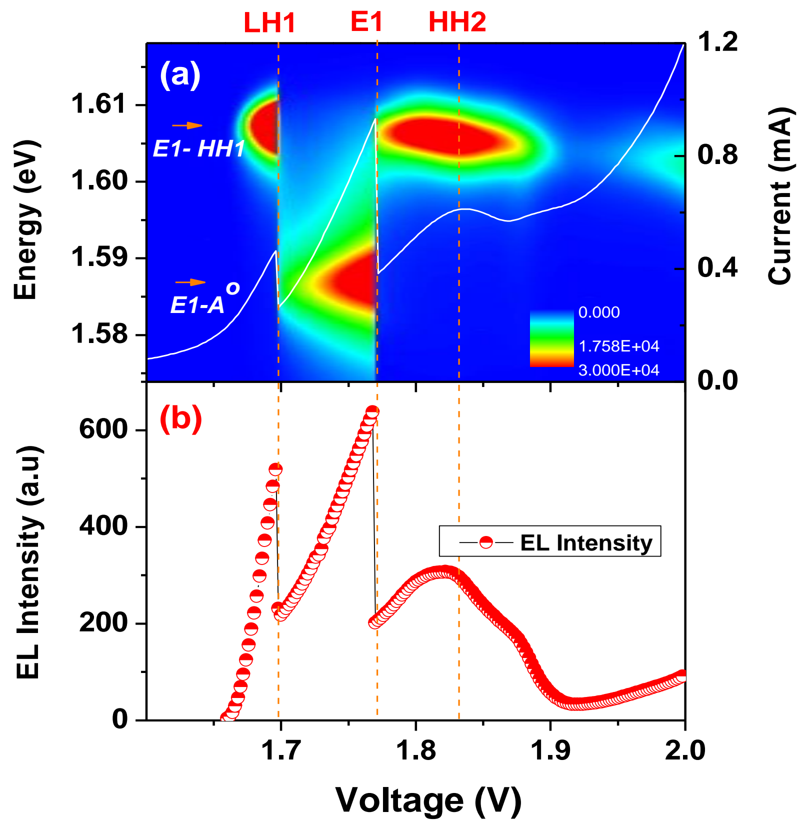

Figure 3-4 - (a) Color-coded map of EL intensity as a function of applied voltage and (b) Voltage dependence of the total QW EL integrated intensity.

We have also studied the I(V) characteristics under light excitation at low temperatures. Figure 3-5 shows the I(V) characteristic curves for several values of laser intensities before and after the flat band condition. The laser excitation results in a negative current flowing through the structure. Since the dark current is negligible for $V \leq V_{FB}$, the current measured under light excitation is due to the photo-created carriers tunneling through the barriers. As holes are created in n-type side and electrons in the p-type side, both carriers can tunnel through the structure which results in a negative photocurrent. Figure 3-6 shows a schematic potential profile under light excitation for voltages (a) lower than the flat band condition, (b) at flat band condition and (c) higher than flat band condition. Under higher laser intensities, two clear peaks are observed for $V < V_{FB}$. We associated these two peaks to resonant tunneling of photogenerated

carriers though E1 and LH1 states of the conduction and valence band confined states in the QW.

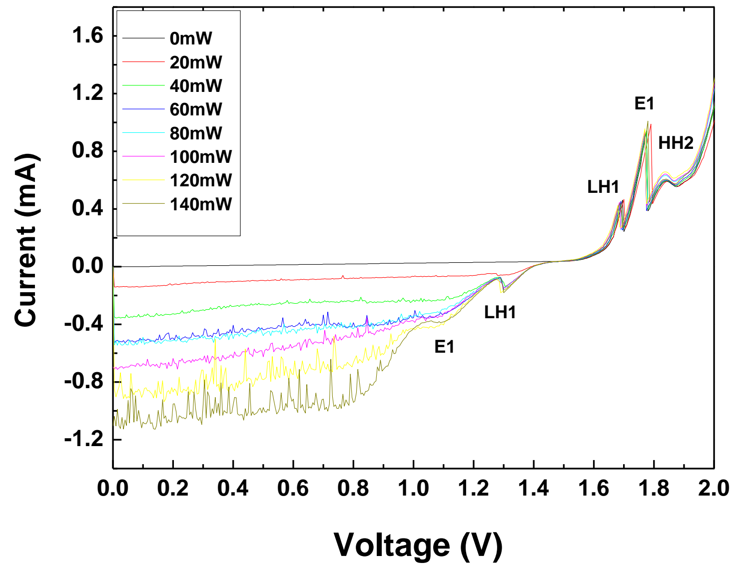

Figure 3-5 - I(V) characteristics curves under light excitation at T=2K.

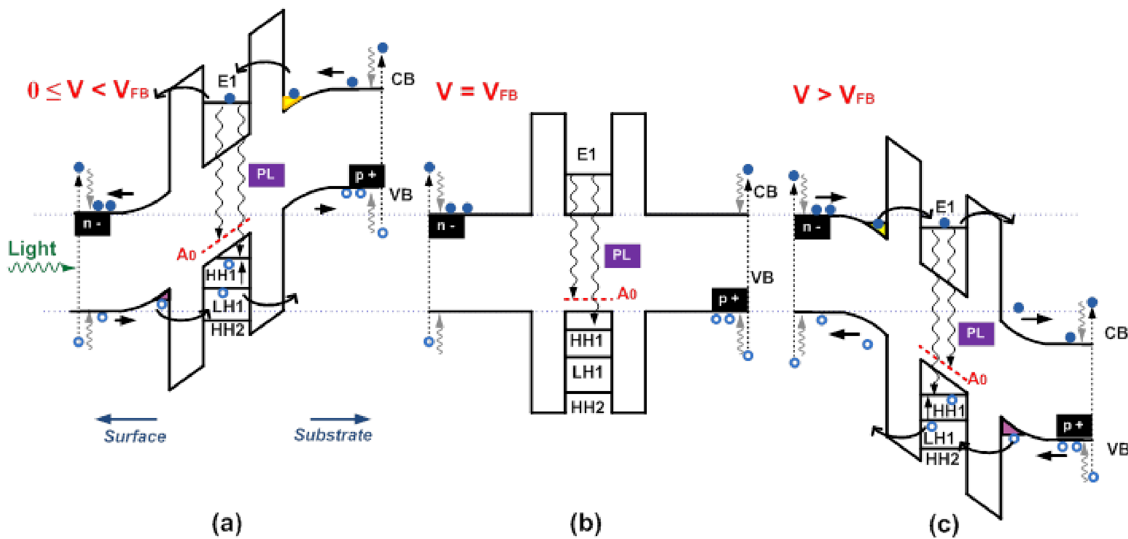

Figure 3-6 - Schematic band diagram of the device under light excitation for (a) voltages lower than flat band condition (b) at flat band condition and (c) for voltages higher than the flat band condition.

In this work, we have also investigated the photoluminescence (PL) from the p-i-n device. We observed that PL and EL spectra effect for $V \geq V_{FB}$ are similar. However, interesting features can be observed for $V \leq V_{FB}$. We remark that the cold line are only observed for some critical voltage regions. In the following , we will focus on the behavior of PL for voltages around the flat band condition V_{FB} and for $V < V_{FB}$.

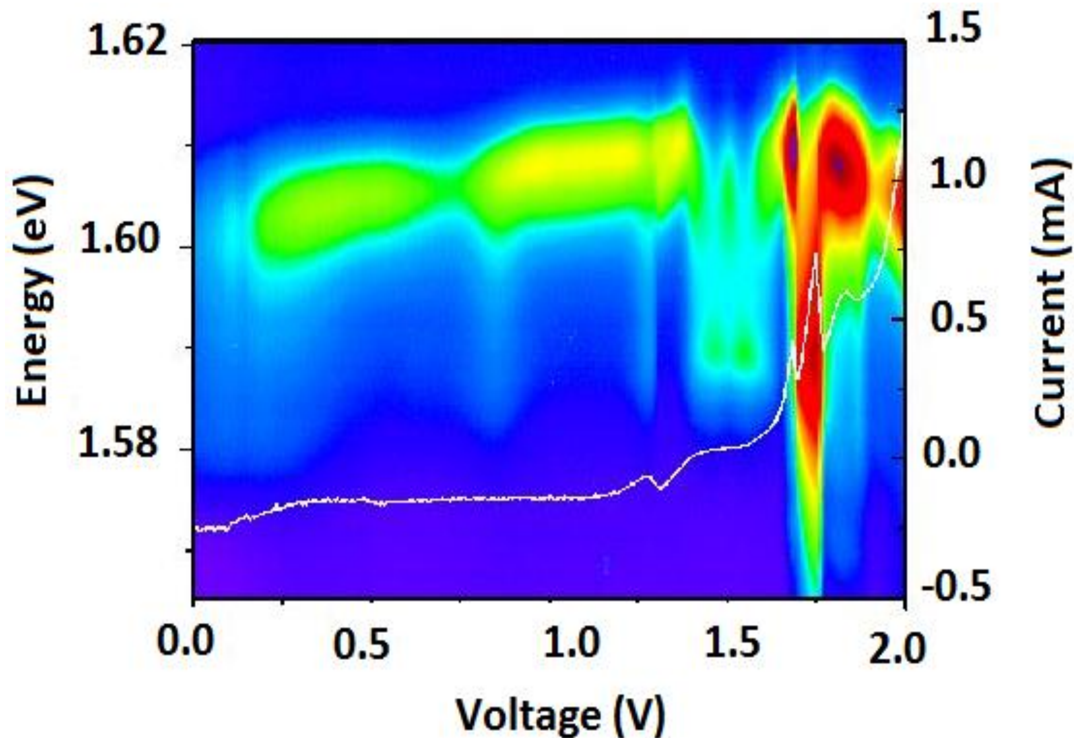

Figure 3-7 - (a) Color-coded map of PL intensity as function of applied voltage for laser intensity of 60 mW at 2K.

Figure 3-7 shows the color-coded map of the QW PL intensity as function of applied bias. We observe that the emissions of cold line to hot line are very sensitive to applied voltages and presents abrupt changes for specific voltage regions. We have observed that the PL is dominated by the hot line excepted by the region of electron resonance that results in an important increase of electron density. In general, the recombination between electron and holes bound to acceptors is only observed in bulk because the mobility of holes is higher and it would be easier for electrons to capture holes from the impurities. For QWs, the mobility is probably lower which should reduce

considerably the probably to observe the recombination between electrons and holes from acceptor levels. However, if we increase the electron density at the QW the localized states can be fully occupied and carriers occupy extend states which should increase the probability of electrons to recombine with holes bound to impurities. At this condition, the probability of recombination of electrons and acceptors (E1-A0) is actually enhanced as can be observed at the electron resonant condition.

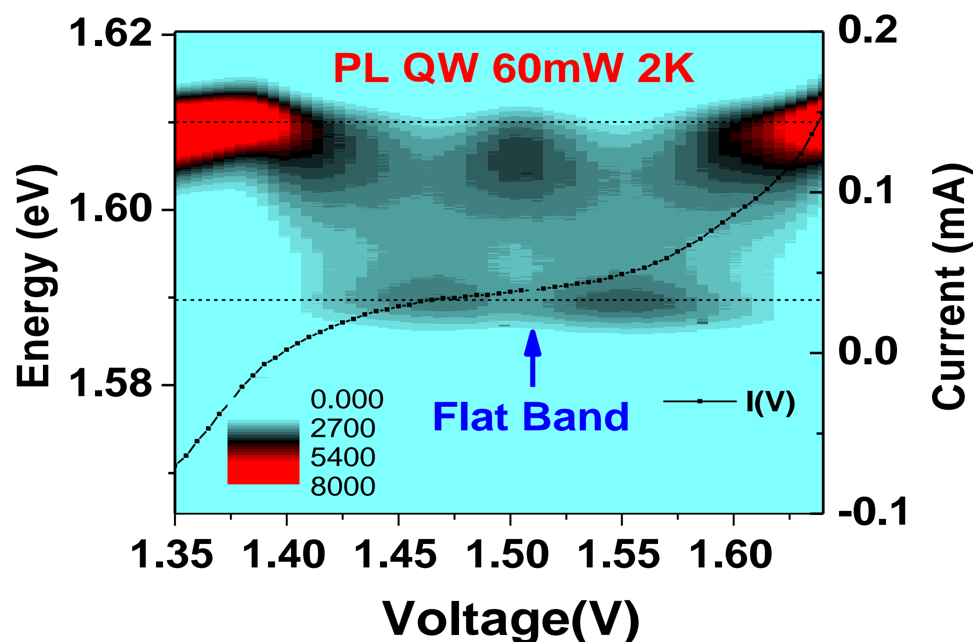

Figure 3-8 - (a) Color-coded map of PL intensity as function of applied voltage in the region of flat band condition for laser intensity of 60 mW.

Figure 3-8 shows the color-coded map for PL intensity around flat band condition. In this case, carriers are generated directly in the QW. At this condition, there is negligible current in the device and therefore the injection of carriers in the QW is negligible. The density of photogenerated electron and holes should be the same. Therefore, the PL at V_{FB} condition should be mainly due to the hot line associated to the excitonic recombination (E1-HH1). If we increase the applied voltage next to the flat band condition (V~ > V_{FB}), the injection and the carrier generation in the QW are both

negligible. However, we remark that the PL is mainly due to the cold line (E1-A0 recombination). We have observed previously that the cold line was only observed at electron resonance due to the important increase of electron density in the QW at this condition. The observance of this line at V~ > V_{FB} indicates that the density of electrons, when compared to the density of holes, should be higher at this condition. This effect could be explained by an increase of the electron concentration due to an increase of donor ionization in contact layers at lower temperatures as they have lower activation energy (about 5meV) (Gilliland, 1997) if compared with the acceptor activation energy (about 30meV) (Holtz, et al., 1989). In addition, the electron probability of non- resonant tunneling should be higher than for holes due to its lower effective mass and higher mobility which probably increase the relative electron-hole concentration in the QW.

For V~ < V_{FB} the photocurrent is an important issue. The direct generation of carrier in the QW is negligible as compared to the injection of carriers due to the photocurrent. In this region, the PL is dominated by the cold line (E1-A0). The increase density of electrons in this region is probably due to the higher probability of non-resonant electron tunneling probably due to its lower effective mass and higher mobility and also by the illumination of the substrate region.

For higher voltages (V > V_{FB}) the injection of photogenerated carriers and the direct generation in the QW are both negligible. In general, the PL is mainly dominated by the hot line excepted by the region of electron resonances which results in an important increase of electron density in the QW as shown in figure 3-7.

Figure 3-9 shows typical EL emission for the contact layers for different applied voltages. We observe two emission bands attributed, respectively to the donor- (~1.521 eV) (Carvalho, et al., 2007) and acceptor- (~1.50 eV) related bulk GaAs emission. We remark that the relative intensity of both emissions are voltage dependent as will be discussed below.

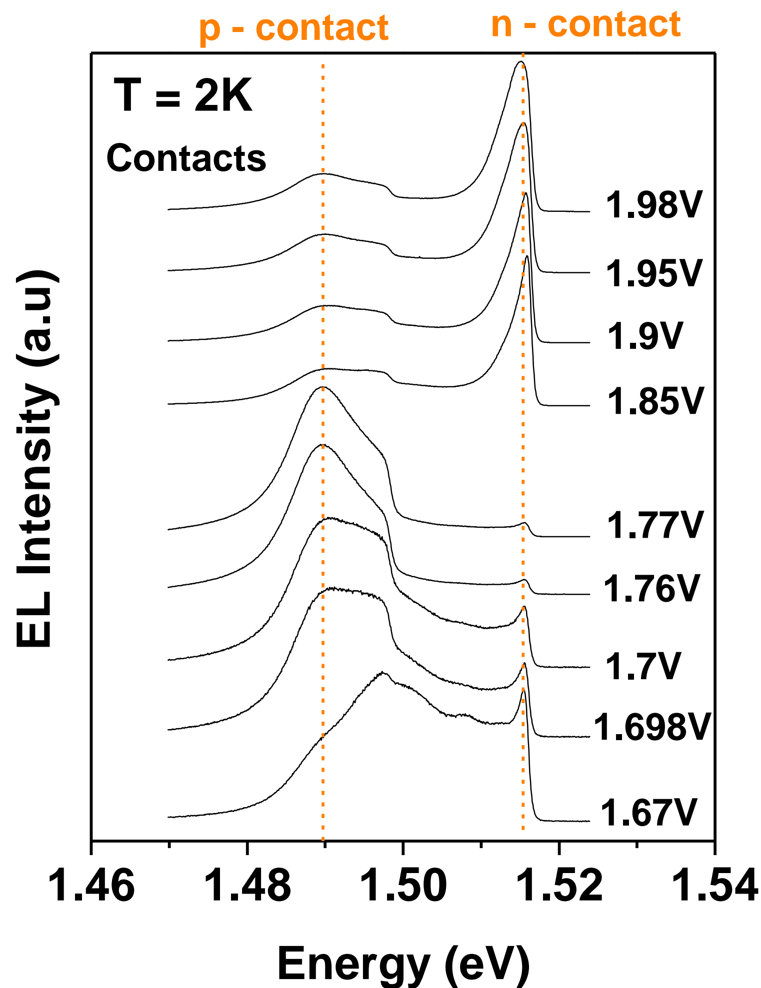

Figure 3-9 - Typical EL emission for the contact layers for different applied voltages .

Figure 3-10 shows the (a) color coded map of EL intensity as function of applied bias for the contact layers and the (b) total EL intensity including both bands versus applied voltages. We observe that the total EL shows a good correlation with the I(V) characteristics curve. We remark that the EL bands present distinct dependences on the applied bias reflecting the resonant conditions for electrons and holes. The intensity of the acceptor-related band (p-GaAs) shows no important correlation with the LH1 resonance but it does have a strong maximum around the E1 resonance when the injection of electrons from the n- towards the p-contact is maximized. On the other hand, the donor-related band (n-GaAs) shows an abrupt reduction of intensity at E1

resonant tunneling condition. For bias larger than E1, the EL intensity from both bulk GaAs emission bands increase and presents a mixture of resonant conditions for both carriers. We can therefore unambiguously associate the acceptor- (donor-) related EL band with the emission from the p- (n-) contact layer and with electrons (holes) that have tunneled through the RTD structure.

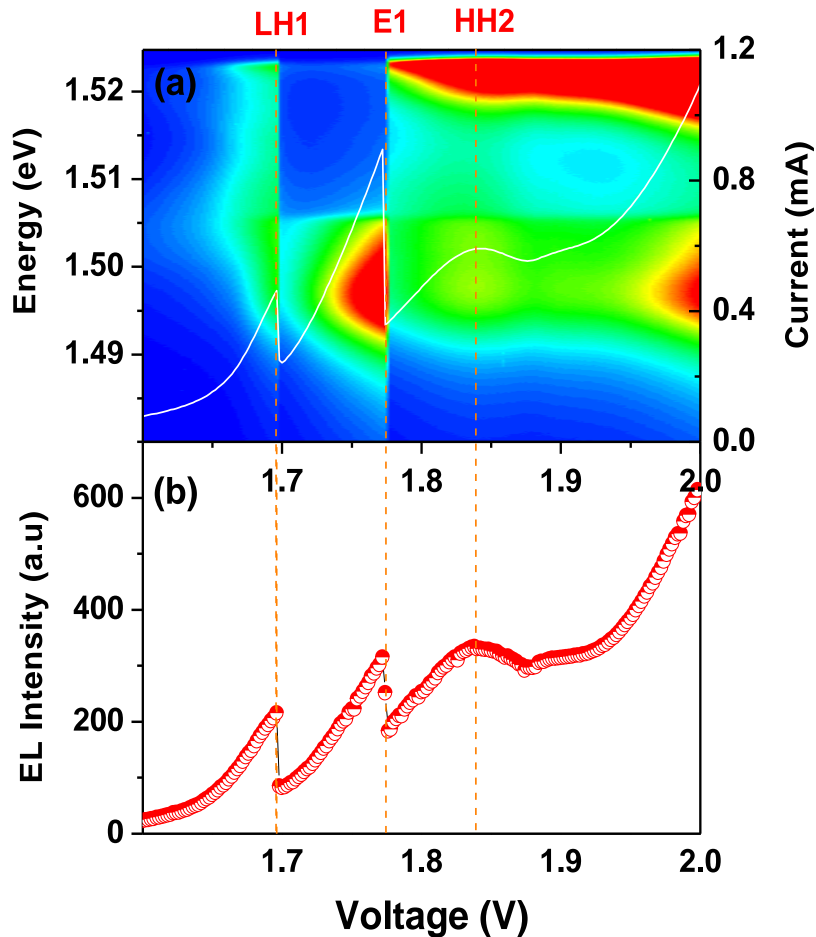

Figure 3-10 - Color coded map of EL intensity as function of applied bias for the contact layers.

References:

- Carvalho, H B, et al. "Circular polarization from a non magnetic p-i-n resonant tunnelling diode." *Applied Physics Letters* 90.062120 (2007).
- Dellow, M W, et al. "Resonant tunneling through the bound states of a single donor atom in a quantum well." *Phys. Rev. Lett* 68 (1992).
- Evans, H B, et al. "Quantum well luminescence by resonant tunneling injection of electrons and holes." A.Pinczuk, D.J.Lockwood and. *Optical phenomena in semiconductor structures of reduced dimensions*. Kluwer Academic Publishers, 1993. 387-399.
- Evans, H B, L Eaves and M Henini. "Quantum well luminescence at acceptors in the p-i-n resonant tunneling diodes." 9 (1994).
- Gilliland, G D. "Photoluminescence spectroscopy of crystalline semiconductors." 1997.
- Greene, Ronald L and K K Bajaj. "Effect of magnetic field on the energy levels of a hydrogenic impurity center in GaAs/Ga1-xAlxAs quantum-well structures." *Phys. Rev. B* 31 (1985).
- Holtz, P O, et al. "Observation of the acceptor-bound exciton confined in narrow GaAs/AlxGa1-xAs quantum wells in photoluminescence excitation." *Phys. Rev. B* 40.10021 (1989).
- Miller, D A. B., et al. "Electric field dependence of optical absorption near the band gap of quantum-well structures." *Phys. Rev. B* 32 (1985).
- Potemski, M, et al. "Exchange splitting of the heavy hole exciton ground state in GaAs-GaAlAs quantum wells." *Surface Science* 229.1-3 (1990): 151-154.
- Skolnick, M S, et al. "Investigation of InGaAs-InP quantum wells by optical spectroscopy." *Semicond. Sci. Technol.* 1 (1986).

Chapter 4 – Time Resolved Photoluminescence in p-i-n RTD

This chapter is dedicated to study the dynamic of tunneling of carriers along the RTD structure by analyzing the optical recombination from our structure by time-resolved photoluminescence (TRPL) under different applied voltages.

For RTD doped solely with one kind of impurity (n-i-n and p-i-p structures), the application of an external bias gives rise to a current and a quasi-stationary charge distribution along the structure with the accumulation of majority carriers inside the QW. However, optical emission from the QW is only observed if the RTD is submitted to an optical excitation in order to generate a significant density of minority carriers that may tunnel into the QW and recombine with the majority carriers. In this case, the dynamics of the minority carrier along the RTD structure can be followed using a pulsed excitation and analyzing the TRPL emission.

For a p-i-n RTD, the situation is different. Under forward polarization, both electrons and holes give rise to current through the structure and can simultaneously reach the QW, where they may recombine giving rise to EL signal. In this situation, a pulsed optical excitation should only give rise to a transient increase of the optical emission superposed on the time-independent EL signal. In contrast, when a p-i-n RTD is reversed biased, there is no injection of majority carriers from their respective emitter regions into the QW, so that the current remains close to zero, as well as the optical emission from the QW. In this case, the pulsed optical excitation may give rise to a transient optical signal, since only photo-created minority carriers would contribute to both the QW emission. However, for p-i-n RTDs, the analysis of time-resolved QW emission using a pulsed laser is rather complex as it may involve the transient of both, electrons and holes, photocreated by optical excitation and injected into the QW.

Figure 4-1 shows the I(V) characteristics when the RTD is in dark and illuminated by a pulsed laser with different intensities. The I(V) curves show similar resonance

peaks as discussed in the previous chapters. Under dark, we only observe I(V) peaks under forward biases (>V_{FB}) and they attribute to the resonance of majority holes and electrons. Under light excitation, we observe the development of additional peaks for reverse biases (<V_{FB} , yellow region in figure 4-1) that originate from the tunneling of optically created minority carriers. The peak at 1.30 V is attributed to the LH1 resonance and the more undefined feature around 1.20 V, may be related to the E1 resonance or to the saturation of photocreated carriers. We point out that even for the larger laser power excitation used, the current under reverse condition remains always significantly smaller than its counterpart for forward condition, i.e., under an equivalent electric potential difference between the contacts. Furthermore, the current tends to saturate for voltages smaller than ~1.2 V, indicating an exhaustion of carriers associated to the limitation of photo-created carriers.

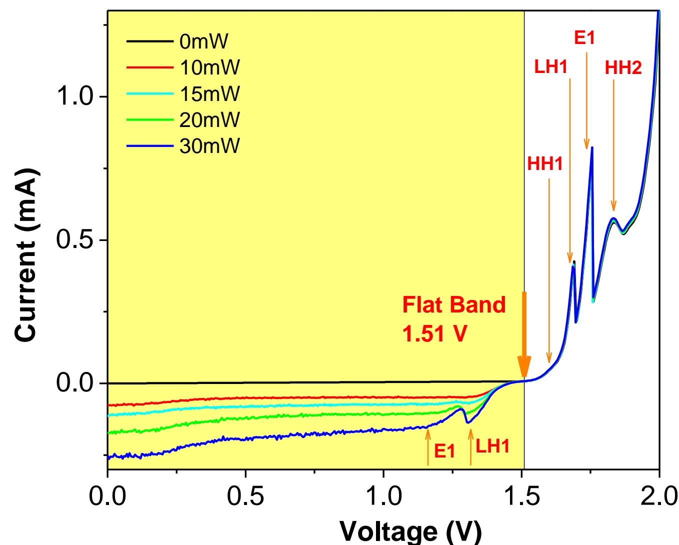

Figure 4-1 - I(V) characteristics curve in dark and under different pulsed laser excitation powers at 5K. The flat-band condition and tunneling resonances are indicated on the graph. The photocurrent curve can be estimated by subtracting the current with and without laser excitation. Reversed bias data range is showed under a yellow background graph.

As discussed in chapter 3, the QW emission includes two bands that were attributed to the excitonic recombination and to an acceptor-related transition ($e\text{-}A^0$), both at the QW. In this chapter, we investigate the characteristic time constants related to these two emissions from TR-PL measurements. This investigation was performed as

a function of the applied voltage, including the reverse and the forward conditions. Measurements were performed both at dark and using the pulsed laser excitation in order to deduct the continuous signals from the transient ones.

We have used a pulsed laser with energy (3.06 eV) larger than the GaAs band gap. We remark that as the laser is focused at the surface of the structure, carriers should be photo-created mainly at the top contact layer. However, in order to give rise to a QW PL signal under reverse bias, minority carriers should also be created at the QW or at the bottom GaAs contact layer. The later can take place if the laser beam spot is slightly larger than the diode, so that excitation photons are also directly absorbed at the GaAs mesa surface created by etching. Furthermore, direct excitation at the QW can also occur for this laser energy. This process should be relatively ineffective due to the small volume associated to the QW layer and to the strong laser absorption at the GaAs contact layers. Therefore, for bias voltages when the injection from the contacts is active, tunneling must dominate over direct excitation at the QW. However, under flat band condition when carriers are not injected in the QW, direct excitation at the QW should become the dominant process.

Figure 4-2 presents the total integrated QW emission, with and without the pulsed laser, as a function of the bias voltage for two different scale ranges. We also present in this figure the modulus of the current through the RTD. We observe a huge increase of the QW emission for voltages > 1.6, when the EL signal due to majority carriers tunneling into the QW clearly dominates the QW emission and the laser excitation only gives rise to a small variation of signal (figure 4-2 (a)). For smaller voltages, the QW emission is significantly smaller and can only be observed in the expanded scale of figure 4-2 (b). For those voltages, the EL signal without laser excitation becomes smaller than the detectable level and we only observe a QW emission under laser excitation (PL).

Note that the QW emission does not goes to zero at V_{FB}, when the electric field along the RTD should be null and carriers created at the contact layers are not injected into the QW. Therefore the residual signal at V_{FB} must come from carriers directly photocreated at the QW. The increased QW emission when the voltage becomes

slightly smaller than V_{FB} and an electric field is established along the RTD, must originate from tunneling of carriers photocreated at the contact layers. For larger reverse bias, i.e., smaller voltage values, the QW emission intensity tends to saturate and decrease, which must be associated to, respectively, the exhaustion of photocreated carriers and the tunneling of carriers out of the QW due to large electric fields.

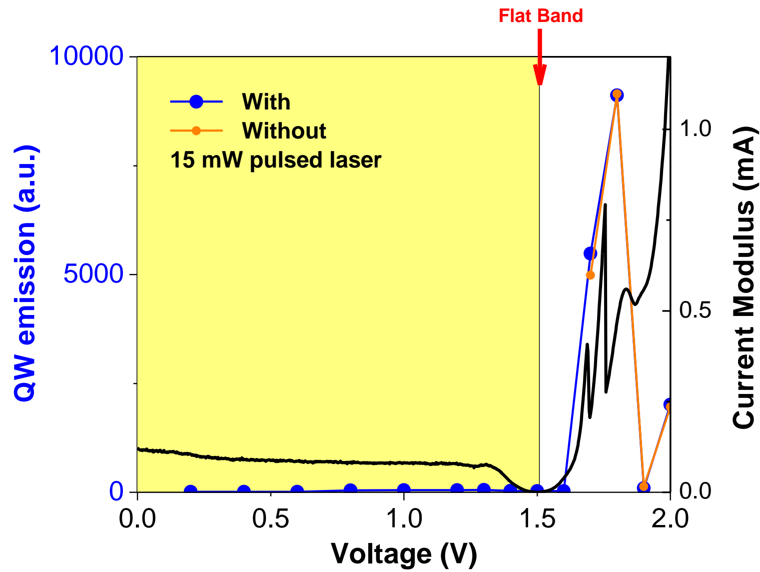

(a)

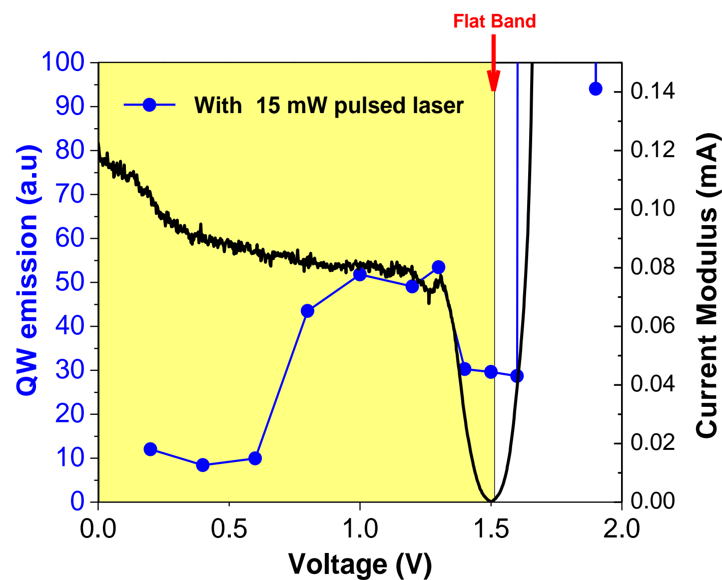

(b)

Figure 4-2 - Integrated intensity of QW emission (a) in dark and under a 15 mW pulsed laser excitation at 5K for whole bias range. (b) Detail of emission intensity for reversed bias under pulsed laser excitation. The flat-band condition and tunneling resonances are indicated on the graph.

Figure 4-3 presents the results of time-resolved PL measurements for our RTD structure when the EL emission is negligible and the QW emission is solely due to photocreated carriers by the pulsed laser that give rise to a time-dependent PL emission. The first column (figure 4-3 (a)) shows streak camera images from the QW emission for various bias voltages. The horizontal and vertical axes of the images correspond, respectively, to emission energy and time. The PL intensity is represented by a color scale. The PL spectra obtained for each image by integrating the signal for the full time range of the image is showed in the second column (figure 4-3 (b)). In the third column (figure 4-3 (c)) we present two additional spectra for each image obtained by integrating the PL emission for a short (0.5 to 1.0 ns) and a long (3.5 to 4.0 ns) time interval, where the time values correspond to the delay relative to the instant when the laser pulse strikes the sample. Each spectra is normalized relative to its maximum. Some spectra clearly comprise two emission bands separated by ~20 meV, as also observed in CW PL (chapter 2), labeled as e1 (cold line) and e2 (hot line) at the streak images, which were attributed to the e-A^0 and the e1-hh1 (excitonic) recombination at the QW, respectively.

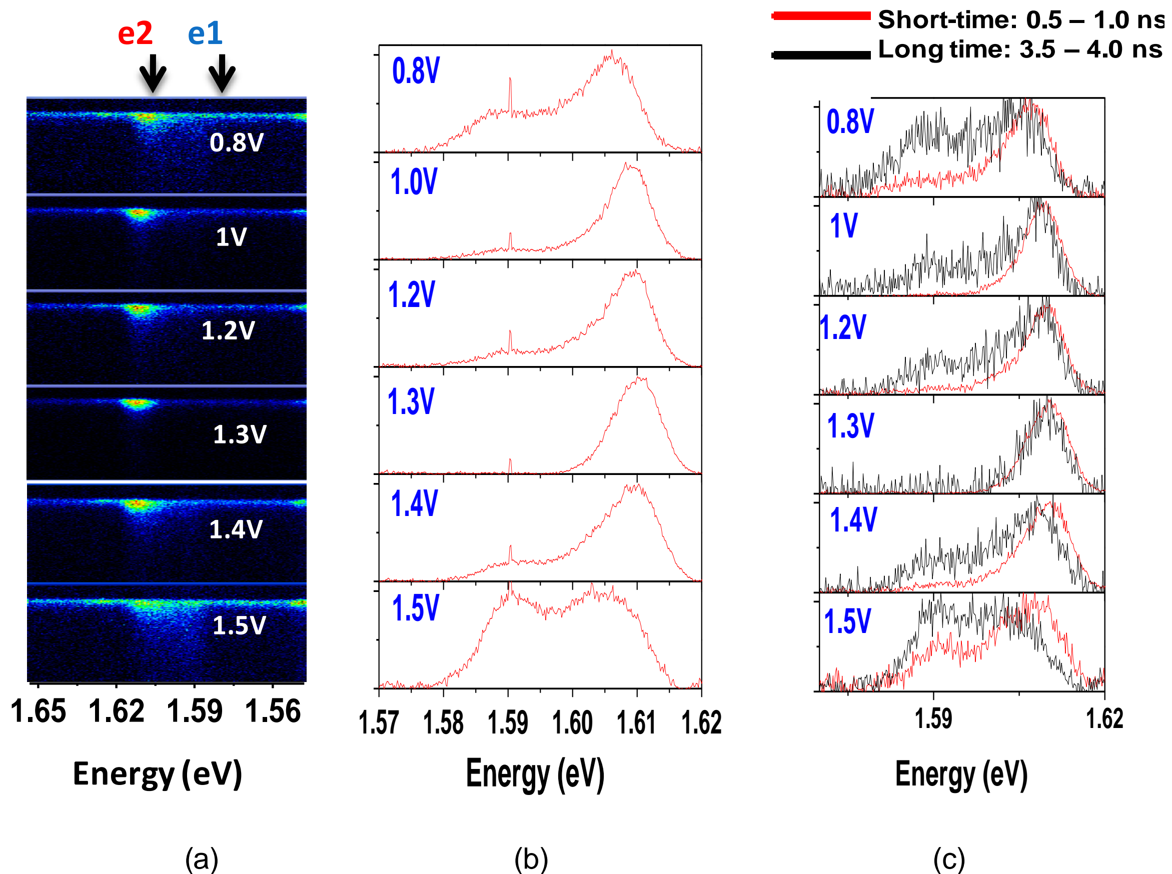

Figure 4-3 - (a) TRPL Images at T = 5K and P = 15mW for different voltages below the V_{FB}. (b) PL spectra obtained by integration of entire TRPL image and (c) Integrated PL spectra obtained by integration of different time windows at short and long times.

From the pair of spectra from figure 4-3 (c), it becomes evident that the e1 and e2 bands present different decay times. The normalized PL spectra show that for long delay times, the lower emission band (e1) becomes stronger relative to the higher energy band (e2). This result implies that the lower energy band associated to the acceptor-related QW emission has a longer decay time than the QW excitonic recombination.

In order to analyze the temporal decay of each band, we extracted two PL transients for each streak image, obtained by integrating the TRPL image at two separate wavelength windows centered at the e1 and the e2 emission, as shown in figure 4-4. At 1.3V we observe the absence of energy e1 and therefore the transient is also missing. Decay times (τ_d) were obtained for each emission (e1 and e2) as a bias

function by fitting the decaying part of the transients with a single exponential function (see solid line in the inset of fig. 4.4) (van Hoof, 1992 ; Romandi'c, 2000).

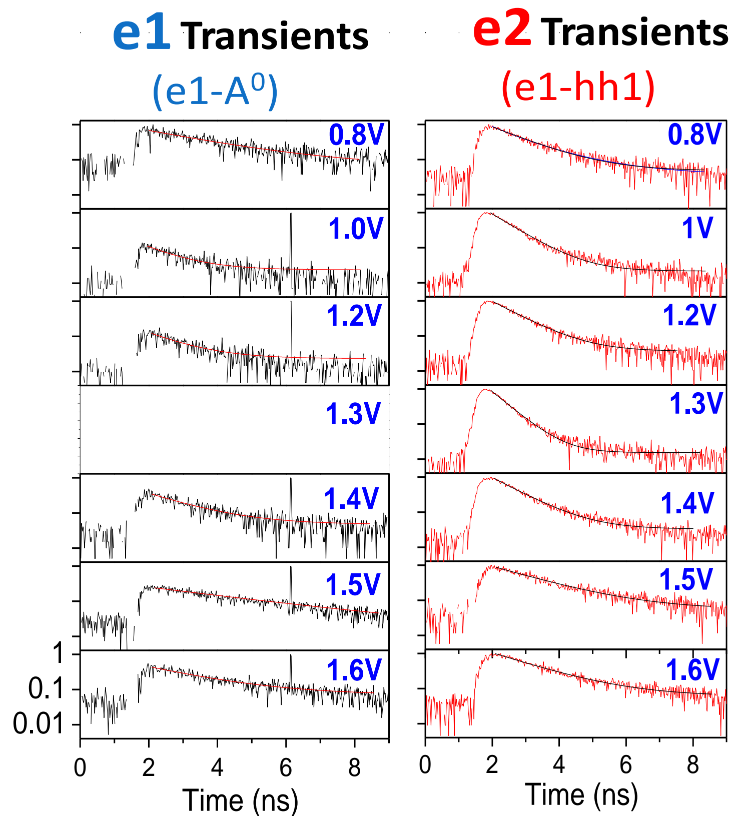

Figure 4-4 - PL transient obtained by integrating the PL signal for a wavelength interval of 1nm around each emission, correspond to the integrated intensity of the (a) lower energy (e1) and (b) higher energy (e2) of QW emission bands. A fitting of the PL transient was made to estimate the decay time values of each emission.

Figure 4-5 shows the τ_d values obtained for the transients of e1 and e2 QW emission bands as a function of the bias voltage. The decay time for both emission bands show a similar tendency with the bias voltages, however, τ_d values from the lower energy band (e1) associated to the e-A0 transition are always larger than those obtained from the excitonic band (e2). This result is in agreement with and corroborates the attribution of the lower energy band to a shallow-related transition. For bulk materials, these transitions usually present significantly longer decay times, however, it is expected that their decay times become somehow smaller in the case of impurities confined in a QW (Kundrotas, 2012; Harris, 1994; Godlewski ,1997). However, we still

expect that QW transitions involving an impurity level should present τ_d values longer than a QW excitonic transition, that should be <~ 1 ns, as obtained.

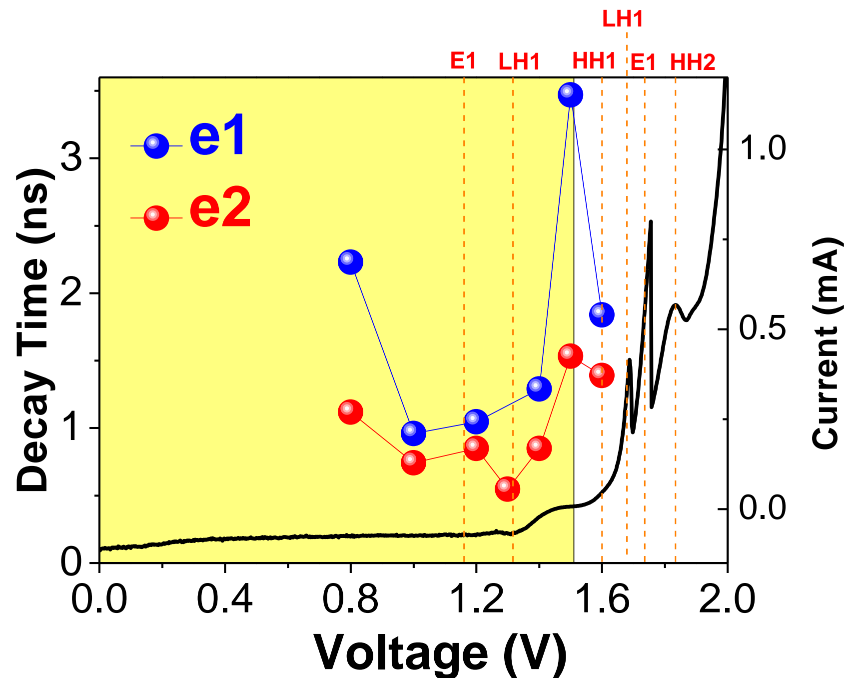

Figure 4-5 - PL characteristic time obtained by fitting the PL transient of each correspondent emission, lower energy (e1) and higher energy (e2) of QW PL bands.

We also note from figure 4-5 that as we go from V_{FB} to smaller voltages, the decay times for both emission bands become slightly smaller. This is a rather surprising result, as we would expect that the advent of tunneling photocreated carriers should somehow result in a delayed decay emission. A faster decay time with larger electric fields (smaller bias voltages) could be ascribed to the tunneling of carriers out of the QW. However, this should only occur for higher fields (smaller voltages) when the QW PL presented a decreased intensity. Here again we see a contradiction, as the decay times show increased values for the lowest voltage of figure 4-5. These contractions indicate that the small variation of τ_d with the applied bias should be dominated by a different effect, that may be, for instance, the concentration of carriers into the QW.

The variation of the carrier concentrations in the QW must also be the main effect that determines the relative intensity of the two emission bands on the PL spectra of figure 4-3. For bias values around the hh1 resonance (~1.3 V), the e1 intensity emission decreases to a negligible value and the PL spectra is dominated by the hot line associated to the excitonic recombination (e2). This result is in agreement with our previous EL analysis, which revealed that an increased acceptor-related QW emission band is directly related to an increased concentration of electrons on the QW. Indeed, the lower energy e2 band becomes relatively stronger at V_{FB} when electrons and holes are directly created in the QW with similar concentrations and for voltages < 1.3 V, when we are approaching the e1 resonance.

Figure 4-6 presents TR images from the QW emission for forward bias voltages ($V>V_{FB}$). We analyzed two different conditions: in dark, without optical excitation, when only EL emission is present; and under a pulsed laser excitation, when both EL and PL are present. In this way, we were able to analyze the effects of an increased density of carriers generated by the pulsed laser on the optical properties of the RTD. The EL emission was already discussed and it shows a strongly dependence on the applied bias. In general, the QW emission is dominated by the high energy peak (e2) associated to an excitonic transition, except for the voltage range of electron resonance, where the low energy band (e1) attributed to a shallow acceptor –related transition in the QW dominates. The pulsed laser usually gives rise to a small increase of the EL emission bands. However, under some critical bias values, the pulsed laser may give rise to a decrease of some EL band.

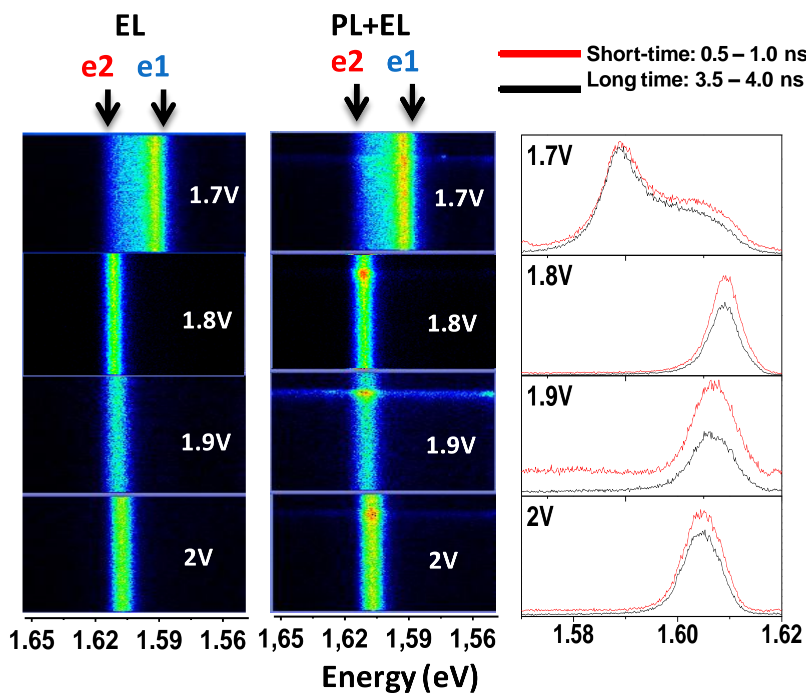

(a) (b) (c)

Figure 4-6 - TR Images at T = 5K and P = 15mW for different voltages at $V>V_{FB}$ (a) in dark, where only to EL is present, and (b) with pulsed laser excitation. (c) PL spectra obtained by integration of entire TRPL image.

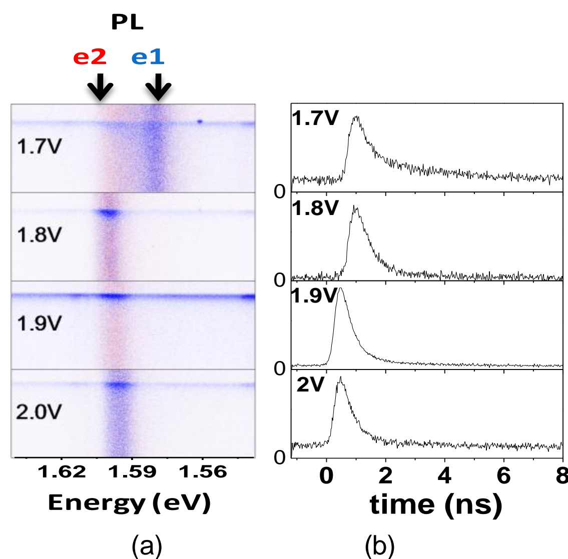

(a) (b)

Figure 4-7 - (a) TR Images obtained from subtraction of TR (EL) from TR (EL+PL) at T = 5K and P = 15mW, for different voltages at $V>V_{FB}$. The color scale indicate the intensity of signal after the subtraction procedure, where the blue color indicate positive values and red color indicates negative values.(b) Transients are obtained by integration of entire TRPL image.

In order to analyze the temporal decay of the QW under forward biases, we carried out a distinct procedure from when the RTD was reversed biased. Now, before analyzing the transients, we must compare the TR image obtained with and without the pulsed laser, as shown in figure 4-6 (a) and (b) for some bias voltages. The pairs of spectra obtained from those images, figure 4-6 (c) shows that the laser excitation gives rise to a very small variation of the QW emission. Figure 4-7(a) shows calculated images obtained by subtracting the images measured without the laser from those obtained with laser for the same bias voltages, so that we can focus on the effect of the pulsed excitation. The effect of the pulsed laser on those voltages results in an increase of both the e1 and the e2 QW emission bands, giving rise to normal transients, figure 4-8, similar to those obtained under reverse condition.

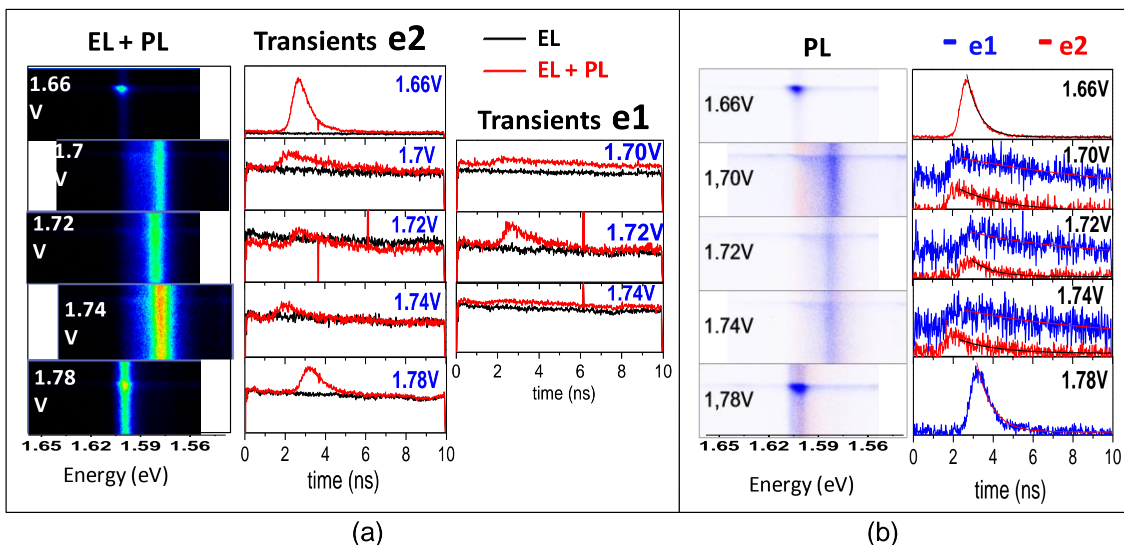

Figure 4-8 - (a) TR Images at T = 5K and P = 15mW for different voltages at $V>V_{FB}$ without (EL) and with (EL+PL) pulsed laser excitation. (b) PL transients obtained from the subtraction procedure explained in the text, by the wavelength integration for each QW emission (e1 and e2) and the correspondent exponential fitting of the transient decay is also shown on each transient.

In contrast, for some critical voltages we observed an opposite effect, where the QW emission decreases when the pulsed laser reach the RTD. In this case the subtracted images may present positive and negative signals, as shown in figure 4-7 for some critical voltages close to the onset and the peak of the e1 resonance and is shown by red color in PL streak images, figure 4-7(b). This effect becomes clear on the

transients of figure 4-9. In fact the laser excitation seems to give rise to two distinct effects: a constant shift of the intensity of a given QW emission band by a negative/positive value, and a positive transient on top of the new background intensity value. This behavior may be explained by a long-time effect, where the averaged laser excitation alters the charge distribution along the structure which alters the relative intensity of the two QW emission bands, so that one of the EL emission bands becomes smaller under laser excitation. Besides this long-time, the instantaneous additional carriers created by the pulse, gives rise to a usual positive transient. Therefore, in order to analyze those critical voltages, we added a positive constant to the subtracted transients with negative values, prior to its analysis. The obtained values are presented in the figure 4-10.

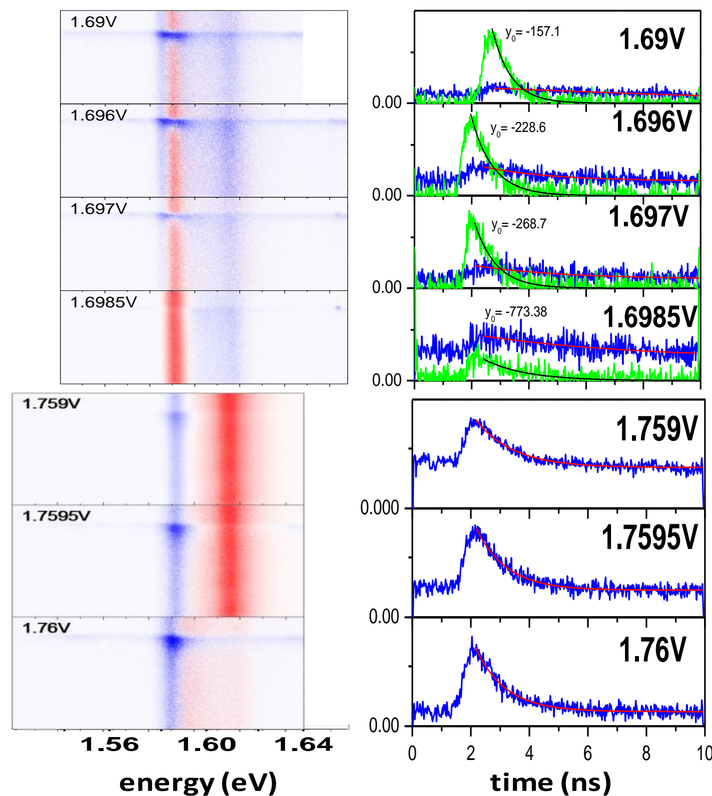

Figure 4-9- (a) TRPL Images at T = 5K and P = 15mW for different voltages at $V>V_{FB}$ obtained from images without excitation (dark) subtracted from images under pulsed laser excitation, here denominated Pure PL, where the blue color scale indicate positive, and red color, negative values of intensity. (b) Some critical bias transients close to e1 resonance present a decrease of the total luminescence (pure PL negative), here showed in green when is add a constant (y_0) in order to obtain the decay time.

The decay times obtained for forward bias (figure 4-10) present values with a magnitude similar to that obtained when the diode is reversed bias, where it is possible to observe a most significant increase around e1 resonance, since the decay times becomes larger when the concentration of electrons in the QW is high.

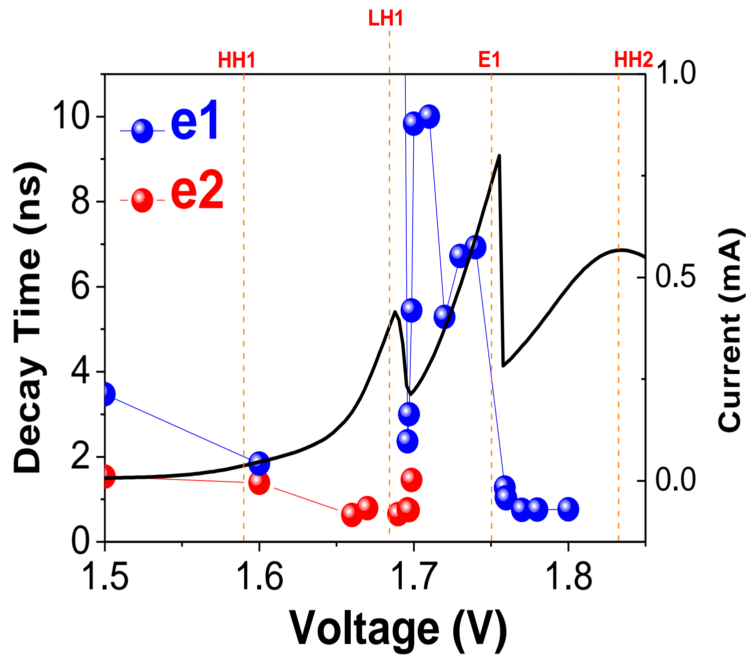

Figure 4-10 - PL decay time obtained by fitting the pure PL transients of each emission, lower energy (e1) and higher energy (e2) of QW PL bands, when the RTD is forward biased.

Another interesting effect observed at this sample is an abrupt variation of the EL when we analyze the TR images without laser excitation TREL. This effect occur at bias values close to NDR region, where a bi-stability is expected in the current of the diode and where it can present high frequency signal oscillations. The figure 4-11 present some streak images at corresponding bias values with their spectra and transients are also shown.

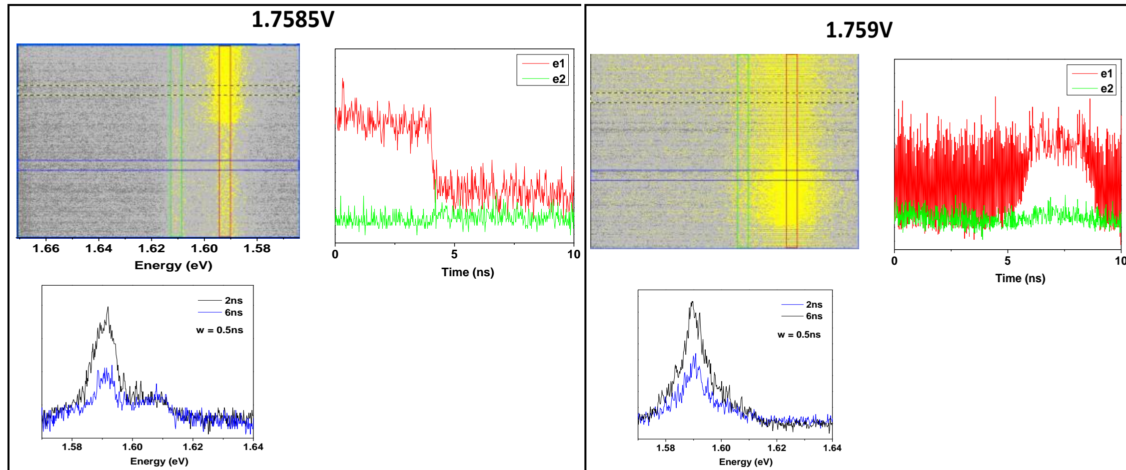

Figure 4-11 - PL transients obtained from streak images taken at two characteristic biases at NDR region, where an abrupt variation of EL intensity is observed.

In this type of measure (figure 4-11), differently of another TR data presented before, the signal integration is took only to one laser pulse. In this way, it is possible to follow a kind of “telegraphic noise” that must be related with the hysteresis in the electrons distribution in the structure, mainly at the negative resistance bias region. This effect could be useful for devices, since the system works like an oscillator between two emissions separated at 20 meV, which is a different effect observed in this kind of structure.

References:

- Romandi´c, I. et al. "Time-resolved photoluminescence spectroscopy of tunneling processes in a bipolar AlAs/GaAs resonant-tunneling structure" *Semicond. Sci. Technol.* 15, 665–675 (2000).
- Van Hoof, C. ; Borghs, G. ; Goovaerts, E. "Sequential hole tunneling in n-type AlAs/GaAs resonant-tunneling structures from time-resolved photoluminescence" *Phys. Rev. B* 46, 6982 (1992).
- Kundrotas, J. et al. "Light emission lifetimes in p-type δ-doped GaAs/AlAs multiple quantum wells near the Mott transition" *Appl. Phys.* 112, 043105 (2012).
- Harris, C.I. et al. "Exciton dynamics in GaAs/AlxGa1-xAs doped quantum wells" *Phys. Rev. B* 50, 18367 (1994).
- Godlewski, M. et al. " Interisland exciton migration and enhanced bound exciton recombination in an AlGaAs/GaAs quantum well structure grown by molecular beam epitaxy without growth interruptions at interfaces" *Semicond. Sci. Technol.* 12, 1416–1421 (1997).

Chapter 5 - Magneto-Transport and Magneto-Electroluminescence Studies in p-i-n resonant tunneling diodes.

In this chapter, we have investigated the magneto-transport and polarization resolved magneto-electroluminescence (EL) of p-i-n GaAs / AlAs double barrier structures.

Figure 5-1 shows typical I(V) characteristics curves of the device measured at T=2K for several magnetic fields. Pronounced electron- and hole-related resonant peaks are observed in the current-voltage characteristics, I(V). As explained previously resonant tunneling can occur from the alignment of two dimensional (2D) confined states at accumulation layers (Mizuta, et al., 1995) with QW resonant states (labeled E1, LH1, HH2 and etc). Particularly, three resonant peaks are observed in figure 5-1 which are associated to resonant tunneling through the LH1, E1 and HH2 confined stated in the QW. The results are similar to the observed results under B=0T (Chapter 3) Under high magnetic fields, additional features are observed after the main E1 resonance which is associated to the well known scattering-assisted resonant magneto-tunneling processes (Goodings, et al., 1994).

If the 2D gases (two dimensional hole gases (2DHG) or electron gases (2DEG)) formed in the accumulation layers have a preferential spin polarization they can act as spin polarized sources for carriers confined in the QW. Particularly, we have observed previously for p-type and n-type RTDs that this injection seems to be very efficient at low voltages (Santos, et al., 2011; Gobato, et al., 2011). However, under higher voltages, other effects that may affect the spin polarization of the carriers arise such as the formation of excitons (or trions) and additional scattering processes.

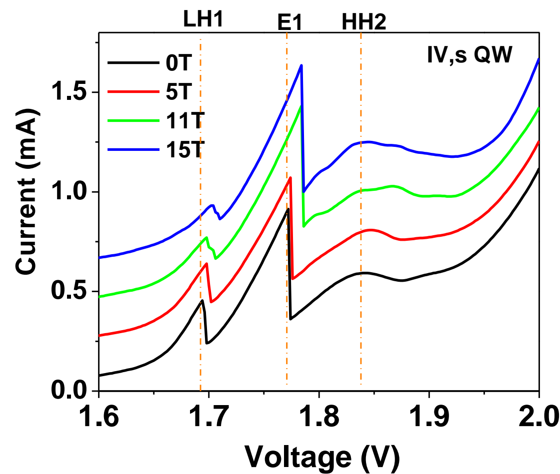

Figure 5-1 - I(V) characteristic curves for different magnetic fields at temperature T = 2K. Each IV curve is shifted 0.2mA upward.

In this work, we have investigated the spin polarization of carriers in a p-i-n RTD by analyzing the right (σ^+) and left (σ^-) circularly polarized electroluminescence (EL) from the contact layers and the QW as function of applied voltage and under magnetic fields up to 15T. As mentioned in the previous chapter, under applied voltages, electron-hole recombination processes may occur at different regions of the RTD. In fact, the electroluminescence (EL) spectrum shows many interesting features and consists of emission lines corresponding both to recombination at the QW and to recombination of electrons (holes) which tunnel through both barriers to recombine as minority carriers in the p-type (n-type) side contact layers. Figure 5-2 shows typical polarization-resolved EL spectra of the GaAs and QW contact layers under magnetic field for different applied voltages. As discussed previously (Chapter 3) the QW emission consists of two bands separated by about 21 meV. The higher energy peak corresponds to the recombination of electrons confined at the first electron level (E1) and holes confined at the first heavy hole level (HH1) (transition labeled E1-HH1) while the lower emission line corresponds to the recombination of electrons at the E1 level with neutral acceptors in the quantum well (labeled E1-A0). The intensity of these EL lines are strongly dependent on applied bias and usually show peaks at voltages corresponding to the electron and hole resonant tunneling condition. In general, these emissions are negatively polarized and

voltage dependent. In addition, the emission from the contact layers is also negatively-polarized and presents a complex shape including a band from the n-doped region and a band from the p-doped region and voltage dependent narrow peaks (labeled 2DEG-h) that will be discussed below.

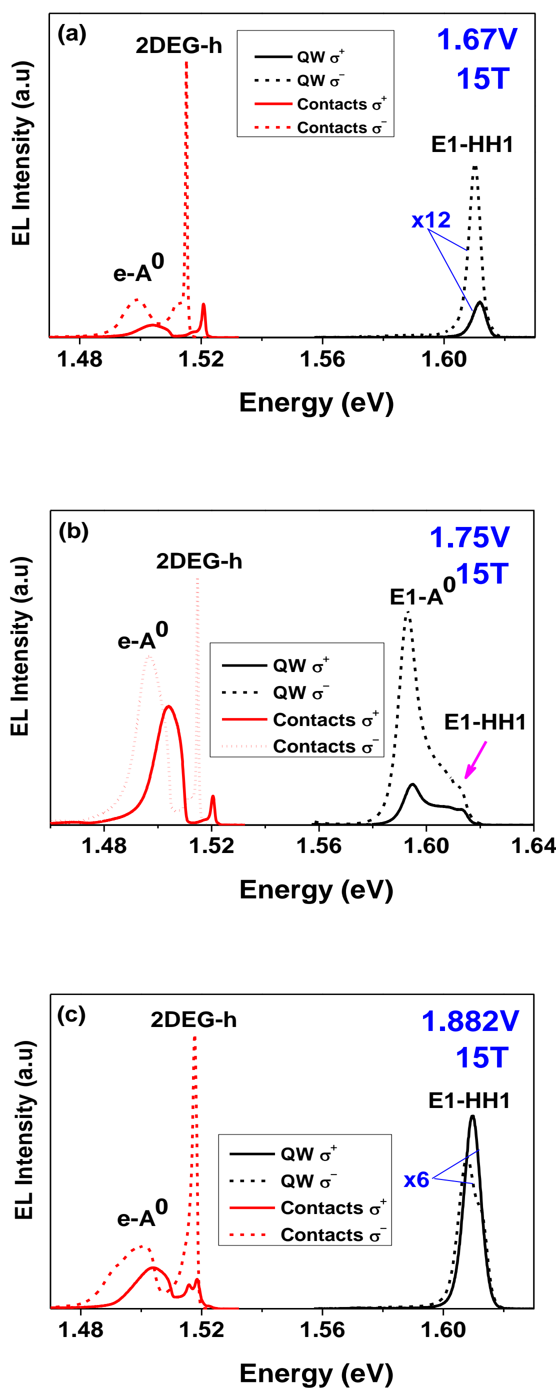

Figure 5-2 - Polarization resolved EL spectra σ^{+} and σ^{-} taken at different voltages for both QW and contact regions at 15T 2K.

Figure 5-3 shows the color-coded maps of the EL emission and the total integrated EL intensity (including energy bands from n-side and p-side contacts) of the contact emission as a function of the bias voltage for B = 8 and 15 T, on which we also included the I(V) characteristics curves. We observed that the total integrated EL intensity presents a good correlation with the I(V) characteristics curve. The emission bands are complex and are due to the emission from the n-type and p-type side contacts. The recombination of carriers from the undoped space-layer (bulk-exciton, BE) is also expected to be observed and its energy is in the same region of n-doped layers. This emission band remains basically constant in energy with increasing applied bias voltages, as expected. However, their intensities are clearly voltage dependent. For example, we observe that the acceptor band emission presents a stronger intensity around the electron resonance voltages and scattering assisted resonant tunneling conditions probably due to the increase of density of electrons arriving at the p-type side contact for those conditions. Furthermore, we observe additional EL sharp peaks which presents both the energy position and intensity clearly voltage dependent. Particularly, we remark that in the region of 1.8-1.9 volts these EL voltage dependent sharp peaks are only observed under high magnetic fields. We associate these peaks to spatially-indirect recombination between free carriers and carriers confined in 2D gases localized at the triangular like wells formed at the accumulation layers.

First, we focus on the EL band that emerges at voltages slightly larger than the flat band condition. This band presents a clearly marked red shift with increasing voltages. This characteristic is consistent with an emission involving a 2D gas formed at the accumulation layer by the applied voltage. At forward bias, we expect that 2DEG is already formed at the accumulation layers. We attribute the transition observed at the range of 1.5-1.7 Volts to the recombination between confined electrons at the 2DEG and free holes (2DEG-h). This attribution is based on the fact that optical transitions involving a 2DEG-h have been observed only under high magnetic field. This effect has

not been explained by a theoretical model yet, but is probably related to the different effective masses and mobilities of electrons and holes (Gobato, et al., 2011; Santos, et al., 2011).

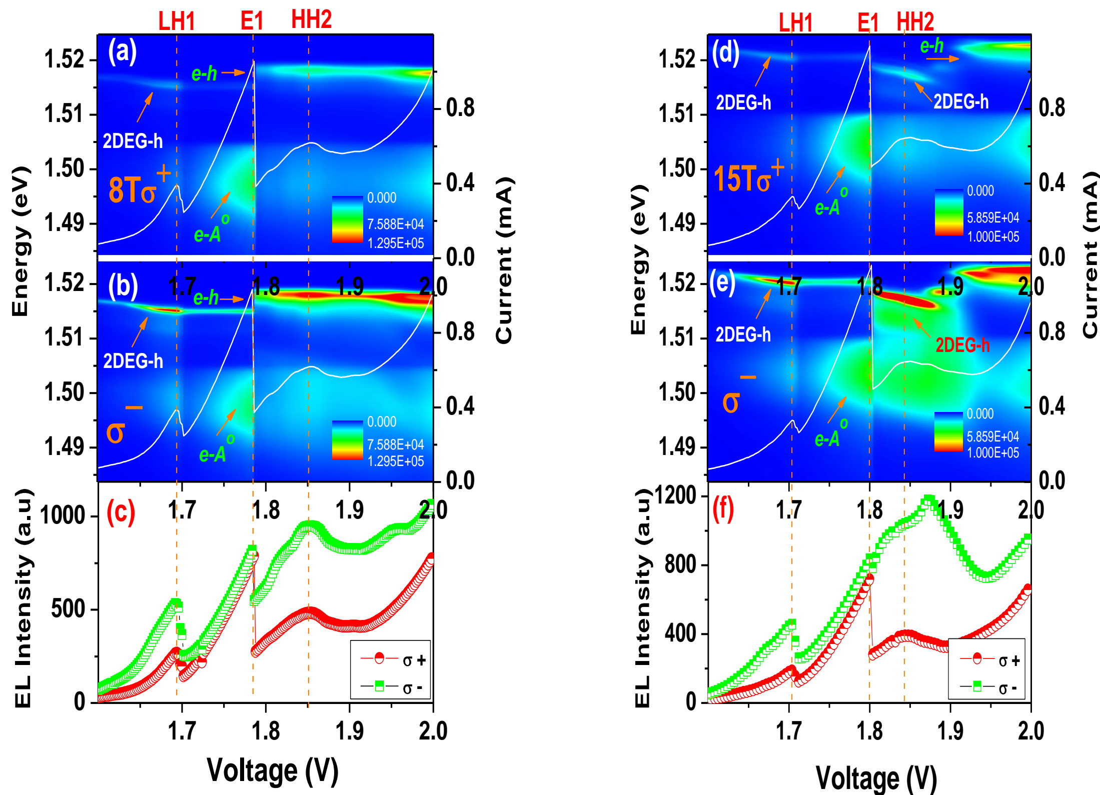

Figure 5-3 - Color coded maps of polarization resolved EL emission due to recombination in the GaAs contact region as a function of applied bias for different values of magnetic field 8T(a, b) and 15T(d, e) at T=2K. Polarization resolved EL intensity as a function of bias at 8T (c) and at 15T (f).

In addition, this voltage dependent emission is clearly highly σ- polarized. For higher magnetic fields (B=15T), we observe an additional voltage-dependent circularly polarized emission at higher applied voltages (V ≥ 1.8 Volt). Its rising is extremely abrupt and coincides with the vanishing of the bulk exciton (BE) transition. We associated this peak to the recombination between electrons of 2DEG and free holes (2DEG-h). This interpretation is consistent with the fact that this emission was not observed at zero magnetic field (Gobato, et al., 2011). In addition, the abrupt variation of intensity and energy position of this emission (~1.8 V) show an evident correlation

with the ceasing of electron resonance tunneling channels. Furthermore, abrupt transfers from the bulk exciton to a 2DEG-h transition were previously observed on high-quality modulation doped GaAs/AlGaAs heterojunctions as a function of a magnetic field and n-type resonant tunneling diodes as well (Santos, et al., 2011; Galeti, et al., 2012). It was previously established for modulation doped GaAs/AlGaAs heterojunctions that the 2DEG-h emission was only observed for filling factors $\nu<2$ (Ashkinadze, et al., 2002; Ashkinadze, et al., 2005; Van der Meulen, et al., 2004). Those results were explained by a simple phenomenological

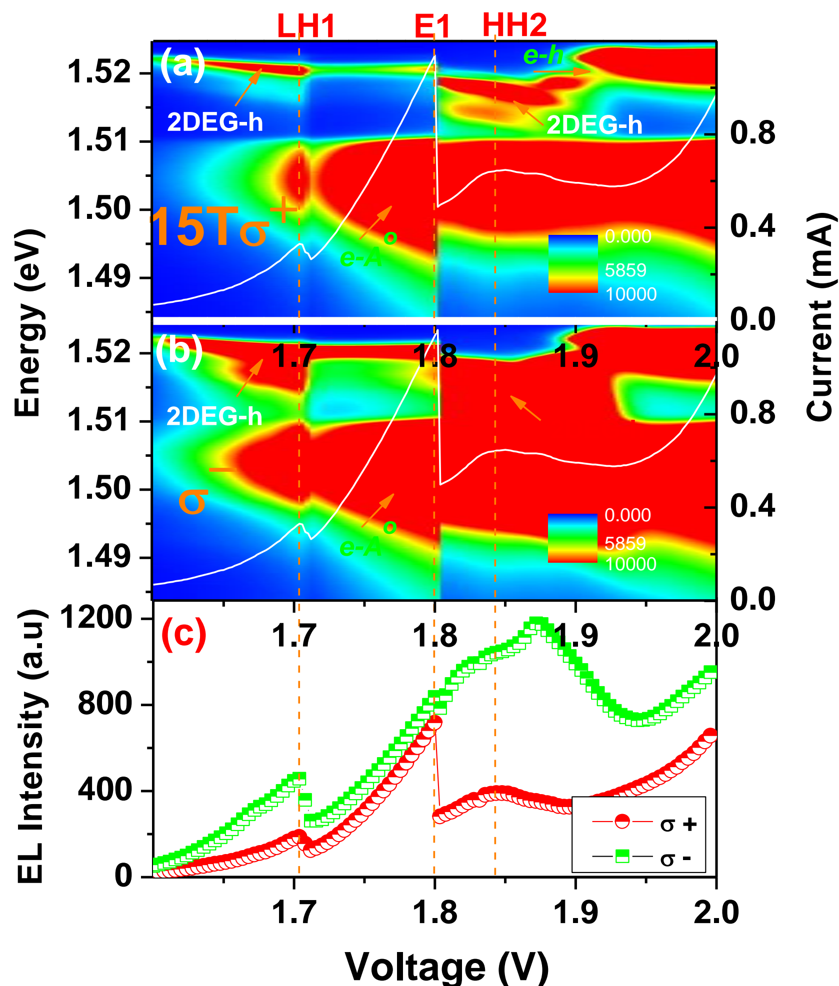

Figure 5-4 - (a) (b) are same results of figure 5-3 (d, e) in another color-coded scale and (c) Polarization resolved EL intensity as a function of bias.

model which considers the exciton generation far from the interface containing the 2DEG, followed by its diffusion and dissociation near the polarized 2DEG, which may give rise to the 2DEG-h transition. This exciton diffusion model cannot be directly applied for resonant tunneling diodes, as the free carriers attain the 2D gas regions preferentially by tunneling. However, we also observed an abrupt transfer from the bulk exciton to 2DEG-h peaks by varying the applied bias just after the electron resonance. The exception is the vanishing of the 2DEG-h peak at ~ 1.9 Volt for 15T, which may be probably associated to the $\nu<2$ observed limit. In fact, the increasing applied voltages and increasing electric fields along the structure, results in increasing carrier densities in the 2DEG formed at the accumulation layer. Consequently, the $\nu = 2$ condition may indeed be attained at ~1.9 Volts and 15T, which would explain the abrupt decreasing of the 2DEG-h emission intensity around this voltage. However, a quantitative analysis of these results requires the developing of another theoretical dynamical model for this very complex system.

We also remark that the 2DEG-h emission splits in two peaks at about 1.87 Volts which is probably due to another confined state from the 2DEG (figure 5-2 (c) and figure 5-3 (d) and (e)). Figure 5-4 and figure 5-5 illustrate these voltage dependent peaks in more details for 15T.

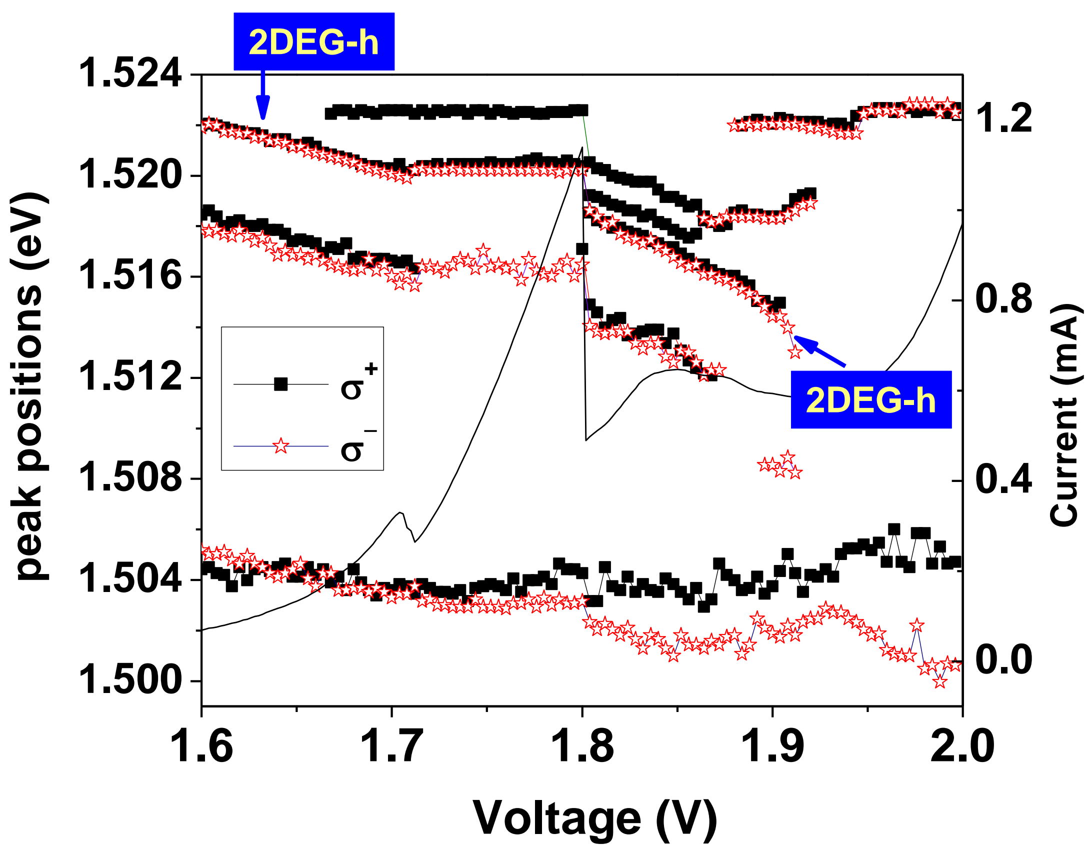

Figure 5-5 - Bias dependence of EL peak positions of contact emissions showing complex voltage dependent EL emission at contact layers under 15T at 2K.

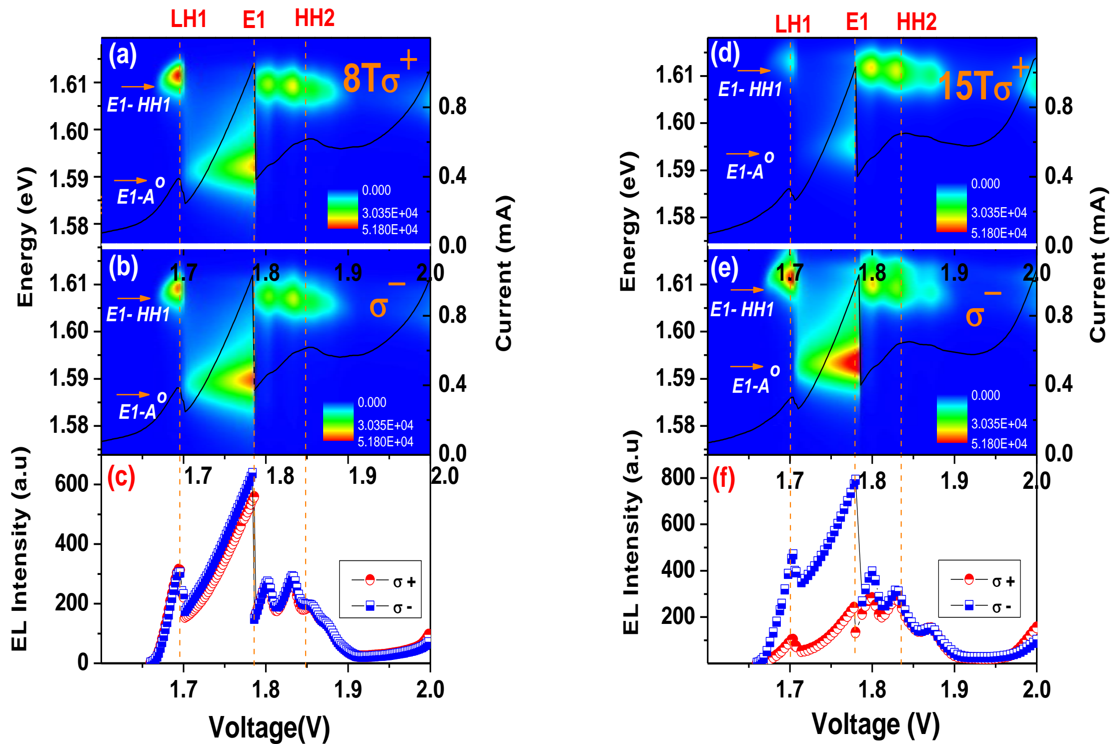

Figure 5-6 - I(V) characteristics curve and color coded maps of polarization resolved EL emission due to recombination in QW region as a function of applied bias for different values of magnetic field 8T (a, b) and 15T (d, e) at T=2K. Polarization resolved EL intensity as a function of bias (c, f).

Figure 5-6 presents the color-coded maps and the voltage dependence of the total QW EL integrated intensity for σ+ and σ- polarizations under two distinct magnetic fields B = 8T and B = 15T. The total QW EL presents intensity oscillations that correlates with the I(V) curve. The QW PL intensity should be proportional to the product of the densities of electrons and holes inside the QW. This explains the abrupt EL rising at the threshold of hole- tunneling into the QW, just after the LH1 resonance, as well as the EL intensity decreasing at higher voltages, due to the growing probability of carrier tunneling out of the QW. The results also clearly show that the QW emission is also strongly σ- polarized. In addition, similar to the case of B=0T (chapter 3) the QW emission presents two bands separated by about 21 meV. As discussed previously the higher energy peak was attributed to the E1-HH1, while the lower emission line corresponds to the electron recombination with neutral acceptors in the quantum well

(labeled E1-A0). Similar to the results obtained for B = 0T, the EL intensity shows an abrupt variation for both bands particularly for the threshold and I(V) peak associated to the E1 electron resonant tunneling. This effect will result in abrupt changes in the QW polarization degree which will be show in figure 5-7.

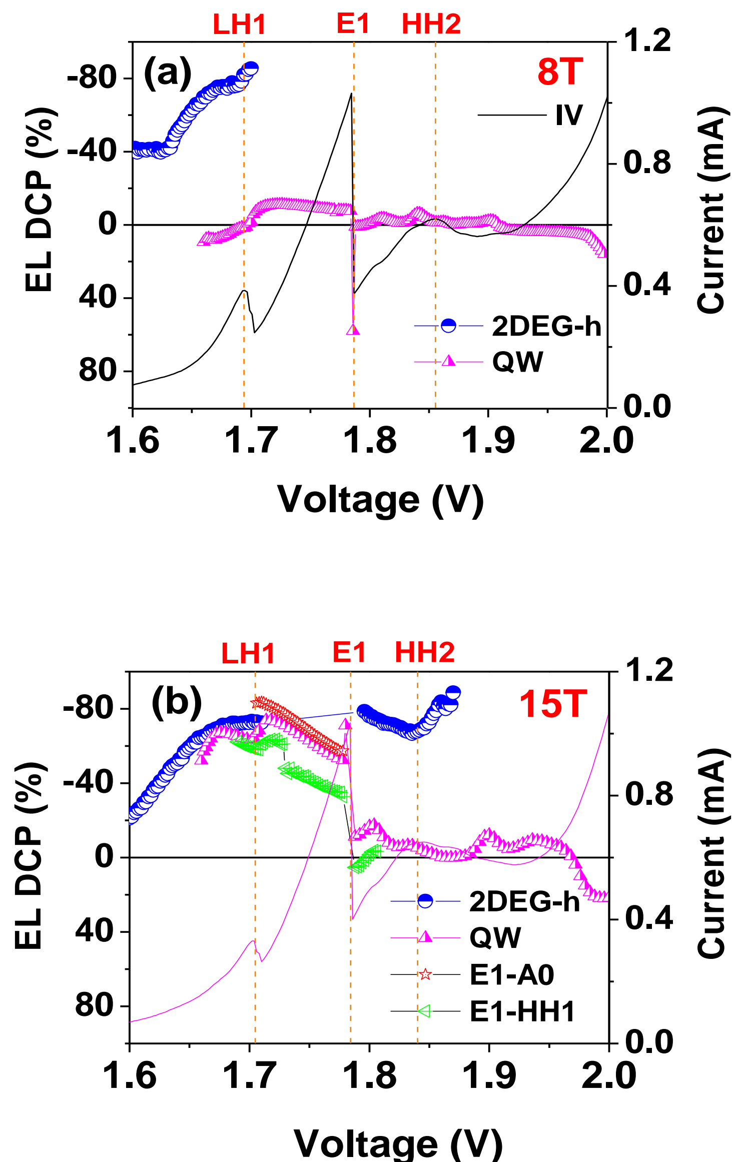

Figure 5-7 - Voltage dependence of the degree of circular polarization of EL for (a) the total QW emission and for the 2DEG-h emission under 8T 2K (b) Voltage dependence of polarization degree

for the 2DEG-h emission, for the total QW emission and for recombination lines E1-A0 (red symbols) and E1-HH1 (green symbols) under 15T and 2K.

Figure 5-7, presents the voltage dependence of the degree of circular polarization (DCP) obtained for the QW, 2DEG-h emission bands under 8 and 15T. The DCP was calculated by using the relation:

$$\mathrm{DCP} = (\mathrm{I}^{\sigma+} - \mathrm{I}^{\sigma-})/(\mathrm{I}^{\sigma+} + \mathrm{I}^{\sigma-})$$

where $\mathrm{I}^{\sigma+}$ and $\mathrm{I}^{\sigma-}$ are the integrated intensities of the right and left circularly-polarized emissions.

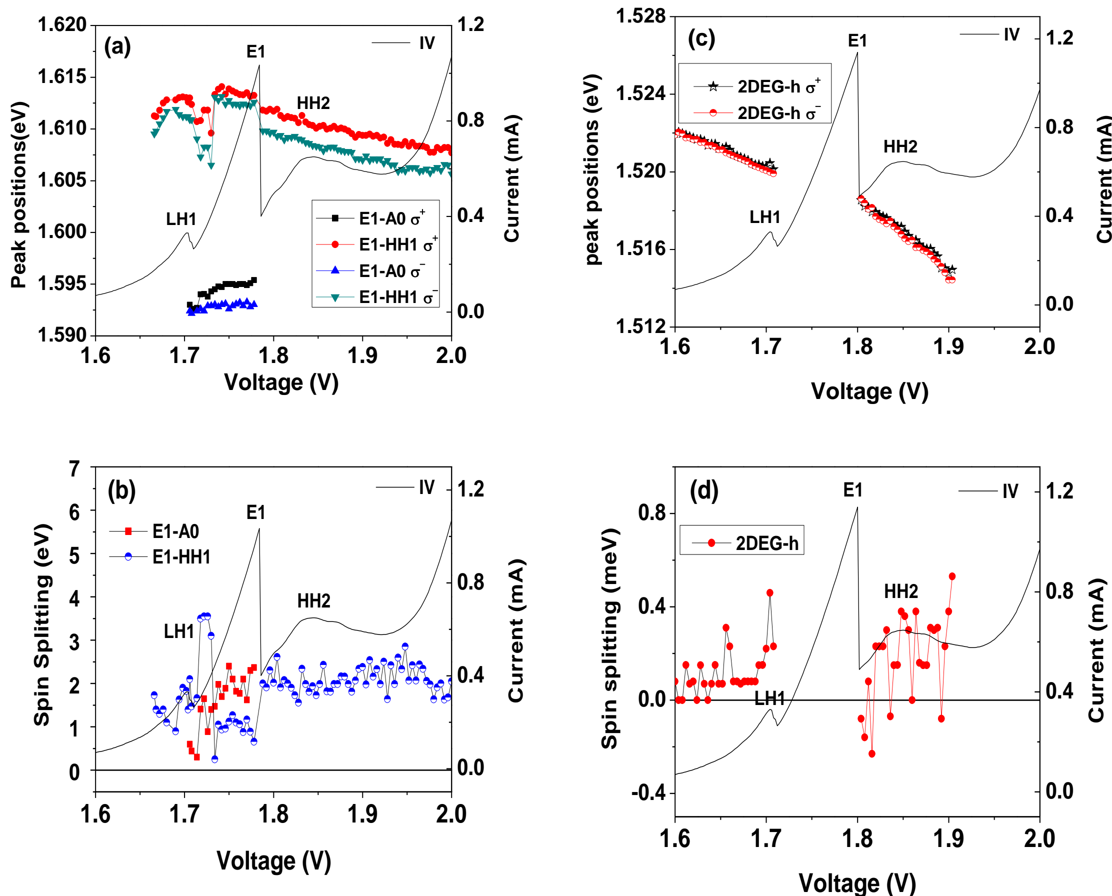

Figure 5-8 - Bias voltage dependence of (a) QW peak positions (b) QW spin splitting energy (c) 2DEG-h peak positions (d) 2DEG-h spin splitting energy under 15T and 2K.

Figure 5-8 (a) and (c) shows the voltage dependence of QW and 2DEG-h peak for both polarization and the spin-splitting (figure 5-8 (b) and (d)) under 15T. For both values of magnetic field, we observe that the QW DCP varies with the applied bias as shown in (figure 5-7 (a) and (b)), while the QW spin splitting remains mainly constant for all applied voltages as shown in Figure 5-8 (a).

Therefore, the QW polarization degree cannot be attributed solely to a thermal occupation effect. The QW spin-splitting may be partially responsible for the negative DCP, but it cannot explain the voltage variations, which seems to be related to the injection of carriers along the structure and to the nature of the emission bands (E1-HH1 or E1-A0).

We have also estimated the DCP for the 2DEG-h emission for the voltage ranges where they are observed. The 2DEG-h shows a strong voltage variation that may be associated to a 2DEG density variation, as in this voltage range the 2DEG density has just be formed and starts to be populated, and then decreases due to the onset of hole tunneling. The polarization degree of the 2DEG is voltage dependent and does not present important changes with the increase of the magnetic field for lower applied voltage. This voltage dependence seems to be correlated to the voltage dependence of the spin-splitting (Figure 5-8 (d)). In general, the g-factor from 2D carriers, and therefore the spin-polarization of the gas, is usually strongly dependent on the gas density. At the LH1 resonant peak and under 15T, the QW DCP seems to follow the 2DEG-h DCP, which could indicate that spin-polarized carriers from the 2DEG are injected and probed into the QW. However a different behavior is observed for different applied bias voltage. Particularly, for large voltages (after the electron resonant peak), when the 2DEG must have attained relatively high densities the QW emission presents lower values of DCP probably due to a very efficient scattering mechanism.

Figures 5-9 and 5-10 shows typical EL spectra for some critical voltages under 8T and 15T respectively. Under 8T, we observe a sign inversion for the polarization degree at about 1.7 Volts (figure 5-7 (a)). We remark that this inversion is due to the fact that the observed QW EL lines present different sign of polarization degree as illustrated in figure 5-9. We also observe another sign inversion at higher voltages (at about 1.9V)

which are related to the trion formation in the QW as illustrated in figure 5-9 (c) and 5-10 (c) and (d).

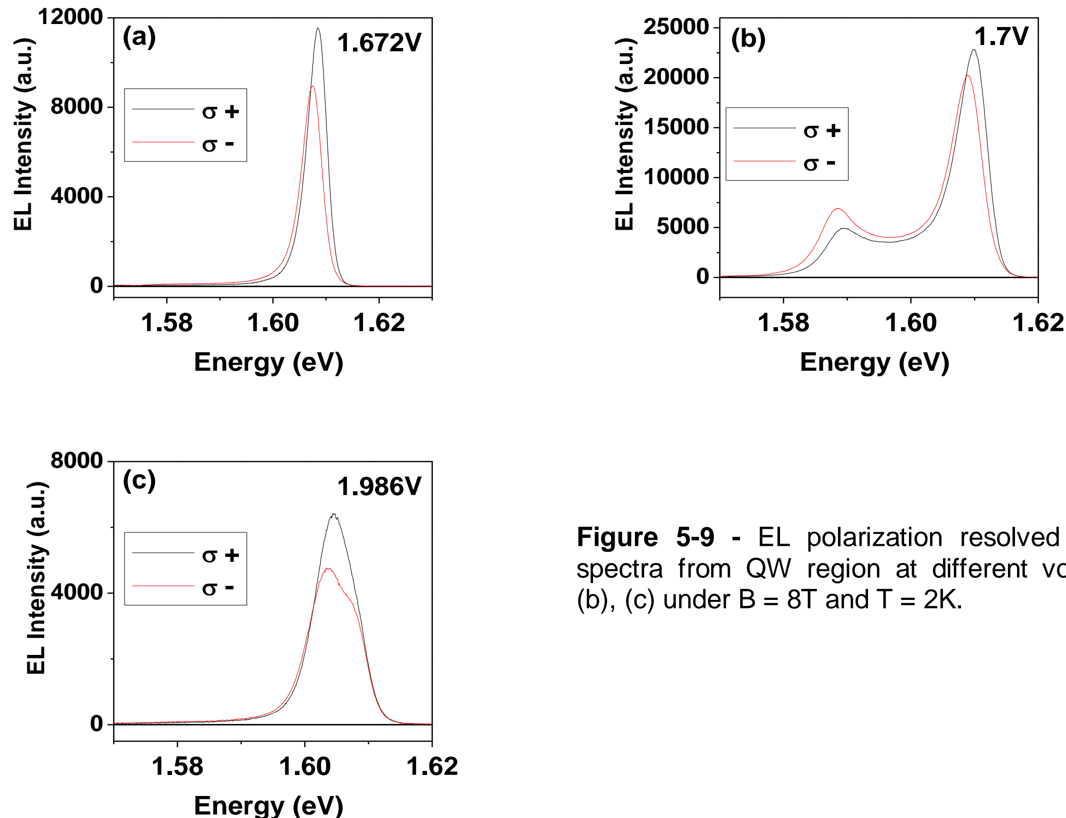

Figure 5-9 - EL polarization resolved emission spectra from QW region at different voltages(a), (b), (c) under B = 8T and T = 2K.

Under 15 T, we observe an important increase of the polarization degree in the voltage region of about 1.65-1.78 Volts. In addition, we remark that after LH1 resonance there is an oscillation of the polarization degree because at this critical region another band is observed as illustrated in figure 5-10. We remark that the polarization degree presents an abrupt reduction after the electron resonant peak which was associated to the observation of different emission lines at this critical voltage. We also observe a sign inversion at higher voltages (about 1.95V) which is associated to the observation of trion formation (Teran, et al., 2005; Joseph, 2005) in the QW as illustrated in figure 5-10 (c) and (d).

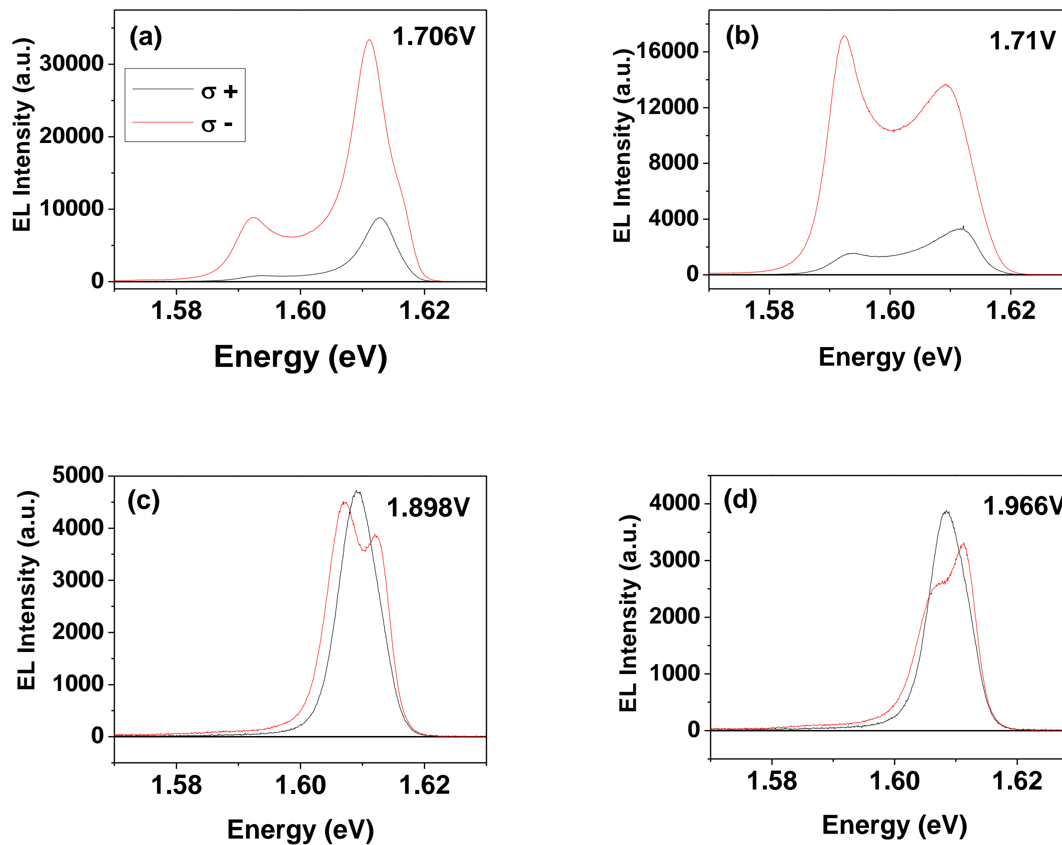

Figure 5-10 - EL polarization resolved emission spectra from QW region at different voltages (a), (b), (c), (d) under B = 15T and T = 2K.

In order to explain the observed experimental results, we could consider a simple model where the QW polarization degree is defined solely by the spin polarization of the injected carriers from the 2D gases at the accumulation layers. However, a quantitative analysis of the polarization degree is rather complex. If we consider the total spin-conservation for all tunneling processes, the two EL emissions, h-2DEG, and QW, should present the same degree of polarization. The fact that the QW shows a somehow smaller polarization as compared to the gas-related emission band indicates some spin polarization loss on the tunneling processes. However, a quantitative analysis of the QW polarization must also consider additional effects, including the thermal occupation of the QW levels and the loss/gain of spin polarization during the tunneling process and etc. In addition, the alignment between spin-split states at the

resonant condition and the observation of different emission lines are also an important issue to explain the observed oscillations of the QW DCP.

References:

- Ashkinadze, B M, et al. "Exciton to two-dimensional electron-hole photoluminescence transitions driven by the quantum Hall effect in photoexcited heterojunctions." *Phys. Rev. B* 72 (2005).

- Ashkinadze, B M, V Voznyy, E Cohen, Arza Ron, and V Umansky. "Condensation of bulk excitons on a magnetized two-dimensional electron gas in modulation-doped heterojunctions." *Phys. Rev. B* 65 (2002).

- Galeti, H V A, et al. "Magneto-optical investigation of two-dimensional gases in n-type resonant tunneling diodes." *Semiconduc. Sci. Technol* (IOP Publishing) 27 (2012).

- Gobato, Y Galvao, et al. "Spin injection from two-dimensional electron and hole gases in resonant tunneling diodes." *Applied Physics Letters* 99 (2011).

- Goodings, C J, H Mizuta, J R. A Cleaver, and H Ahmed. "Variable-area resonant tunneling diodes using implanted in-plane gates." *Journal of Applied Physics* 76, no. 2 (1994).

- Joseph, Israel Bar. "Trions in GaAs quantum wells." *Semicond. Sci. Technol* 20 (2005).

- Mizuta, Hiroshi, and Tomonori Tanoue. *The physics and applications of resonant tunnelling diodes.* 1995.

- Santos, Lara F dos, et al. "Circular polarization in a non-magnetic resonant tunneling device." 6 (2011).

- Teran, F J, et al. "Trion formation in narrow GaAs quantum well structures." *Phys. Rev. B* 71 (2005).

- Van der Meulen, H P, D Sarkar, and J M Calleja. "Free versus localized hole magnetophotoluminescence in semiconductor heterojunctions near." *PHYSICAL REVIEW B* 70 (2004).

CONCLUSION

In this thesis, we have investigated transport, optical and magneto-optical properties from a p-i-n GaAs-AlAs RTD using various experimental techniques such as Current voltage curves I(V), electroluminescence (EL) , photoluminescence (PL) and time-resolved photoluminescence (TR-PL). Three clear peaks were observed in the I(V) characteristics curve, corresponding to resonant tunneling to the LH1, E1 and HH2 states of the conduction and valence bands of the quantum well (QW). In addition, a weak HH1 shoulder was observed at lower bias from the differential conductance of the I(V) curve. The flat band condition was obtained when the p-i-n diode was forward biased with ~1.51 V (labeled V_{FB}).

Concerning the optical results, we observed two clearly separated EL peaks from the QW: a "hot" line centered at around 1.607 eV and a "cold" line with a peak around 1.586 eV. These lines are separated by ~21 meV and present a red shift with increasing applied bias voltage. The hot line was attributed to the excitonic recombination between fundamental confined states in the QW (labeled El -HH1), while the cold line was attributed to recombination involving holes bound to acceptors in the QW (E1-A_0 recombination). We also observed remarkably abrupt changes on the relative intensities of these two emission lines at critical voltages that correspond to the onset of electron resonant tunneling and to the resonant peak E1. Through a small variation of the applied bias, we can completely erase the cold/hot line independently,

abruptly switching the QW PL emission by ~21 meV. This effect can certainly be explored for practical optical devices.

The EL intensity is clearly correlated to the I(V) characteristics curves and present peaks for voltages corresponding to electron and hole resonant tunneling conditions. The EL emission from the contact layers show a complex shape including emissions from the n- and the p-doped layers, including peaks that do not vary and peaks that significantly depend on the applied bias voltage. The former are bulk-like GaAs transitions that originate from the GaAs areas with low electric fields, while the later were attributed to spatially-indirect transitions involving carriers confined at the triangular wells formed near the RTD barriers.

Under light excitation, the I(V) characteristics curves show a negative current flowing through the structure due to photo created carriers tunneling through the device. Additional resonant peaks were observed for reverse biases ($V < V_{FB}$) and were associated to resonant tunneling of photogenerated carriers through the E1 and LH1 states in the QW. The QW PL spectra under reverse bias also show the two emission lines discussed above, which intensities depend on the relative hole and electron densities in the QW, which are voltage controlled.

We have also investigated transport and polarization of the EL emission under a high magnetic field. In particular, we have investigated the spin polarization of the carriers by analyzing the right (σ^+) and left (σ^-) circularly-polarized EL emission from the contact layers and the QW as function of applied voltage under magnetic fields up to 15T. The I(V) curves have revealed additional features for biases larger than the E1

resonance which were attributed to the well known scattering-assisted resonant magneto-tunneling processes.

The correlation between the QW EL intensity and the I(V) characteristics curves, including the electron and hole resonant tunneling peaks, remains valid when a magnetic field is applied to the RTD. The QW EL emission is clearly negatively-polarized under high magnetic fields. In addition, the emission from the contact layers, including transitions from the n-doped region, the p-doped layers, and narrow peaks associated to the recombination of electrons from the 2DEG, also becomes negatively-polarized. Similarly to the results obtained for B = 0 T, the magneto-EL intensity shows remarkably abrupt variations at the threshold and at the peak of the E1 resonance. This effect is accompanied by abrupt changes of the QW polarization degree. Furthermore, an inversion of the polarization sign was observed for higher applied voltages and was associated to the formation of trions in the QW. The 2DEG-h emission intensity has showed a strong voltage variation that may be associated to the variation of the density of the 2DEG with the applied bias voltage. The QW emission shows an oscillation near the E1 resonance. In general, the value of the circularly-polarization degree obtained for the QW emission is somehow smaller than for the 2DEG-h emission, that may indicate some spin polarization loss on the tunneling processes. However, other effects should be considered for a quantitative analysis of the QW polarization. For instance, the QW polarization degree oscillation seems to have some correlation with the relative intensities of the different emission lines from the QW. Additional relevant effects were the presence of neutral acceptors in the QW and the thermal occupation of the QW levels. In addition, for critical voltages around the “negative-resistance edge” of the E1

resonance, we have observed an intriguing effect in the form of a telegraphic–random noise with abrupt inversions between the two main QW emission lines. A detailed explanation of this effect requires additional studies that should be performed in the future .

In conclusion, our investigation in p-i-n RTD devices revealed interesting results such as very abrupt voltage-controlled changes of the EL intensity and the spin-polarization of the injected carrier in the QW that may be useful for the development of future device applications.